



HAL
open science

Li isotope study of Yangtze River sediments : new constraints on climate, weathering and carbon cycle relationships

Chengfan Yang

► **To cite this version:**

Chengfan Yang. Li isotope study of Yangtze River sediments : new constraints on climate, weathering and carbon cycle relationships. Earth Sciences. Sorbonne Université; Tongji university (Shanghai, Chine), 2020. English. NNT : 2020SORUS433 . tel-03883685

HAL Id: tel-03883685

<https://theses.hal.science/tel-03883685>

Submitted on 4 Dec 2022

HAL is a multi-disciplinary open access archive for the deposit and dissemination of scientific research documents, whether they are published or not. The documents may come from teaching and research institutions in France or abroad, or from public or private research centers.

L'archive ouverte pluridisciplinaire **HAL**, est destinée au dépôt et à la diffusion de documents scientifiques de niveau recherche, publiés ou non, émanant des établissements d'enseignement et de recherche français ou étrangers, des laboratoires publics ou privés.



Sorbonne Université

Université de Tongji

Ecole doctorale 129

Le Laboratoire d'Océanographie de Villefranche ET

State Key Laboratory of Marine Geology



**Li isotope study of Yangtze River sediments : new
constraints on climate, weathering and carbon cycle
relationships**

Par Chengfan YANG

Thèse de doctorat de Sciences de l'Environnement

Dirigée par Nathalie VIGIER and Shouye YANG

Présentée et soutenue publiquement le 02/12/2020

Devant un jury composé de :

Chabaux, François, Professor, reviewer

Liu, Xiao-Ming, Assistant Professor, reviewer

Cardinal, Damien, Professor, examiner

Revel, Marie, Professor, examiner

Su, Ni, Associate Professor, examiner

Wei, Gangjian, Professor, examiner

Dédicace

Remerciements

After months' hard work and several rounds of revision, my doctoral thesis is finally finished. It's my honor to take this opportunity to express my special thanks to those who have helped me during the past five years. Without their support and encouragement, I can't complete my PhD studies successfully in Tongji and Sorbonne University.

I would like to first thank my Chinese supervisor Professor Shouye Yang who is a specialist on sedimentology and geochemistry. He also supervised my Master studies from 2012 to 2015 in Tongji University. In his group, I obtained excellent trainings on related aspects of scientific research. Under his guidance, I grow from a novice on scientific studies to a young researcher. His rigorous attitudes to academic studies impress me most, and I'm sure this will exert a positive influence on my future career. I gratefully acknowledge his help on my doctoral studies.

In 2017, I was granted by the China Scholarship Council with a two-year funding to continue my PhD studies in France. This is my first time to stay so long time overseas. I have to say I'm lucky that Professor Nathalie Vigier is my supervisor there. She tried her best to help me adjust myself to local life and laboratory work. In terms of my PhD studies, I benefited a lot from her optimistic attitude and clear guidance. At least in my opinion, she is the best one who is working on lithium isotopes. Thank you for her help with my PhD studies. I believe that the experience in LOV will benefit me forever.

Many thanks to the CMS (Continental Margin Sedimentology) group at Tongji and CHOC (Chemistry-Ocean-Climate) team at the LOV for their help with experiments and data discussions. Thanks to Alessandra, Amélie, Maryline, Thierry and those who have helped me in LOV. Besides, I'd like extend my thanks to all my Chinese friends in Nice, France. I spent the most joyful time with them.

At last, I would like to dedicate the thesis to my father. My doctoral career started in 2015 and will end in 2020. It's a honor that my doctoral diploma can be awarded by the Tongji and Sorbonne University both. However, the 5-year may be a long time for my father. I think he worried day and night about my study. I feel deeply gratitude to his support.

Sommaire

Remerciements	2
Sommaire	3
Chapter 1: Introduction	5
Chapter 2: Tracing continental weathering in the Changjiang (Yangtze River) basin : a review	12
2.1 River setting	12
2.2 The source of sediment transported by the Changjiang River into the East China Sea over different timescales	16
2.3 Chemical weathering studies in the Changjiang basin.....	20
2.4 Li isotope fractionation in river basins.....	25
2.5 Conclusion of this chapter.....	30
Chapter 3: Materials and Methods	31
3.1 Samples	32
3.2 Methods.....	36
3.2.1 Clay fraction (<2 µm) separation from bank and core sediments.....	36
3.2.2 Exchangeable phase extraction	37
3.2.3 Elemental concentration analyses	38
3.2.4 Mineralogical analyses.....	39
3.2.5 Nd isotope analyses.....	39
3.2.6 Li isotope analyses	40
Chapter 4: Progressive evolution of the Changjiang (Yangtze River) sediment weathering intensity since the Three Gorges Dam operation	43
4.1 Introduction	45
4.2 River setting	47
4.3 Materials and Methods	48
4.3.1 Sample collection	48
4.3.2 Major element analyses.....	49
4.3.3 Chemical weathering proxy	50
4.3.4 Monte-Carlo simulation	50
4.4 Results	51
4.5 Discussion	52
4.5.1 Larg Na depletion in fin-grained sediments.....	53
4.5.2 Stronger K leaching intensity after 2003.....	53
4.5.3 Significant impact of TGD on the sediment source-to-sink process.....	56
4.5.4 Possible mechanism responsible for downstream weathering signal variations.....	59
4.5.5 Implication for dissolved fluxes from the floodplain.....	64
4.6 Conclusions of this chapter	66
Chapter 5: Behavior of Li isotopes along a 2D transect in the Changjiang (Yangtze) Estuary.....	68
5.1 Introduction	69
5.2 Distribution of salinity, pH, temperature and SPM concentration.....	71
5.3 Mineralogy	71
5.4 Li concentration and isotope composition of dissolved, SPM and exchangeable phases	72
5.5 Conservative mixing of dissolved Li and $\delta^7\text{Li}$ in the estuary	74
5.5 Particulate Li and $\delta^7\text{Li}$ behavior in the Changjiang Estuary	77

5.6 Negligible influence of isotope exchange in the Changjiang Estuary	79
5.7 Conclusion and Implications	80
Chapter 6: Clay Li and Nd isotopes response to hydroclimate changes in the Changjiang (Yangtze River) basin over the past 14,000 years.....	82
6.1 Introduction	84
6.2 Regional background.....	85
6.3 Materials and Methods	87
6.3.1 Samples	87
6.3.2 Clay fraction (<2 µm) separation and Li isotope analyses	88
6.3.3 Al, Na and Li concentrations and Nd isotope analyses.....	89
6.4 Results	89
6.5 Discussion	90
6.5.1 Clay source discrimination and depositional environment changes	90
6.5.2 Grain size, lithological and diagenetic effects on clay Li isotopes	93
6.5.3 Possible links between chemical weathering and climatic change	95
6.5.4 Implications for the weathering-climate feedback	99
6.6 Conclusions of this chapter	99
Chapter 7: Conclusion and perspectives	101
7.1 Conclusions	101
7.2 Perspectives	102
Bibliographie.....	105
Table des illustrations.....	123
Table des tableaux	127

Chapter 1: Introduction

The average temperature across the Earth's surface is close to 15°C, which is mostly maintained by greenhouse gases, such as atmospheric carbon dioxide (CO₂). The natural CO₂ inputs to and outputs from the surface environment are predominantly related to the solid Earth (e.g. mid-ocean ridges and volcanoes) degassing, sulfide oxidation coupled to carbonate dissolution, continental weathering (chemical erosion) of rocks and soils, organic carbon oxidation and burial (Fig.1; Berner et al., 1983; Raymo and Ruddiman, 1992; Kump and Arthur, 1997; France-Lanord and Derry, 1997; Torres et al., 2014; Kasting, 2019). The combined surficial atmosphere-ocean-biosphere-soil reservoir contains about 3.4×10^{18} mol of carbon, which is smaller compared to that of the rock reservoir ($\sim 6300 \times 10^{18}$ mol, Berner et al., 1983). Thus, a mass balance for global carbon cycle is necessary for maintaining Earth's habitability, otherwise, the atmospheric CO₂ concentration would become excessively high or low after a few millions of years only (Goddéris and François, 1995; Berner and Caldeira, 1997).

There is a continuous input of about 10×10^{12} mol of carbon annually from the solid Earth to the atmosphere, mostly through mid-ocean ridge or other volcanic/metamorphic activities (Frings, 2019). This means that there must be a carbon sink which is needed to counteract solid Earth degassing. The most investigated mechanism is continental weathering coupled to carbonate formation in the ocean (Walker et al., 1981). On the Earth surface, atmospheric CO₂, in combination with rain water, interacts with plants and minerals from rocks and soils. This process leads to release chemical elements which are then transported by rivers to estuaries and sea. This process is linked to chemical erosion, and atmospheric CO₂ is ultimately sequestered. Rocks from continental crust can also react with sulfuric acid (i.e. product of sulfide oxidation), thus releasing dissolved elements to the sea with no related consumption of CO₂ (Torres et al., 2014). To our knowledge, $\sim 75\%$ area on the Earth surface is covered by sedimentary rocks, in which carbonate hosts nearly 85% of calcium (Holland, 1978). The CO₂ sequestered by carbonate weathering at Earth surface is generally considered as balanced by carbonate precipitation in deep-ocean itself on the million-year timescale. Thus, over long timescales (10^6 yr), silicate weathering with acidity coming from rainwater and high pCO₂ soil water is of particular importance in maintaining global climatic stabilization. Based on the compilation of river water chemistry at a global scale, Gaillardet et al. (1999a) estimated that the CO₂ consumed by silicate rocks (continental rocks and volcanic

arcs) is $\sim 11.7 \times 10^{12}$ mol/yr, which is of the same order of magnitude as the solid Earth degassing.

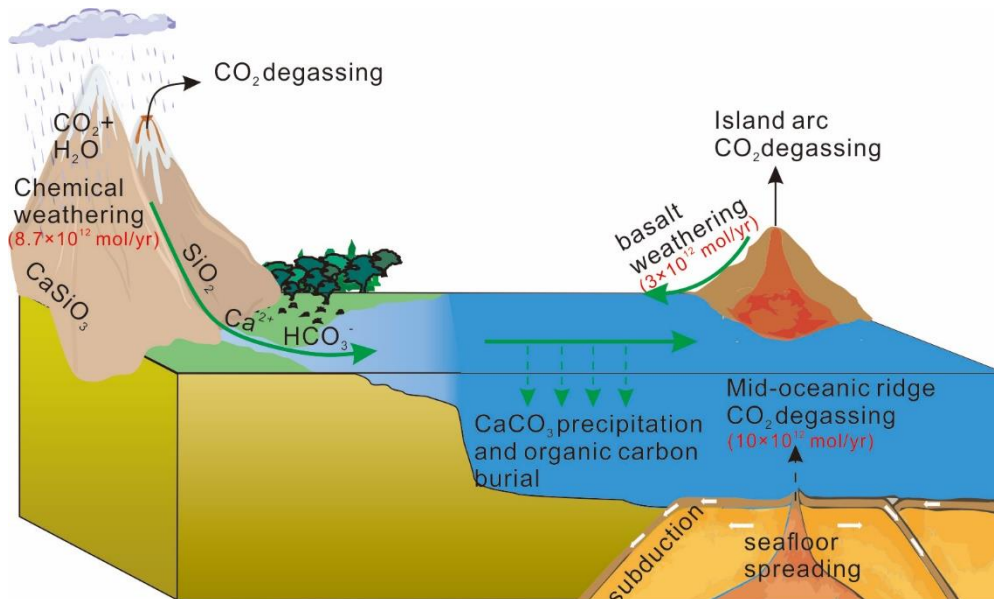


Figure 1 : Sketch map showing global carbon cycle. This figure is modified after Sarmiento and Gruber, (2006), Frings, (2019) and Kasting, (2019). The processes of carbon consumption are presented with green arrows, while carbon releases are presented with black arrow. The flux of carbon consumption and release are presented with red font, and data cited from Gaillardet et al., 1999a and Frings, 2019

Over the last 60 Myr, global climate has experienced significant cooling. Seawater $\delta^{18}\text{O}$ recorded by benthic foraminifera show a trend of positive shift during this period (Fig. 2; Miller et al., 1987), while this proxy is sensitive to ocean temperature and ice formation (Zachos et al., 2001). The deep-ocean temperature in the early Eocene (a ice-free world) was estimated to be $\sim 12^\circ\text{C}$ warmer than present (Zachos et al., 2001, 2008). The corresponding estimations globally for atmospheric CO_2 display that the concentration decreased from 1000 – 1500 ppm at the middle to late Eocene ($\sim 45 - 34$ Ma) to about 280 ppm during the pre-industrial period (Fig. 2; Pagani et al., 2005, 2009; Rubino et al., 2013). Long-term declines of global temperature is associated to the appearance of ice sheets in Antarctic at ~ 34 Myr ago. The decline of temperature continued with time, and the Antarctic was gradually covered by ice sheets. Because of the global anti-correlation between CO_2 and foraminifera $\delta^{18}\text{O}$, it is generally believed that decreasing atmospheric CO_2 concentration is the primary factor affecting the long-term global cooling.

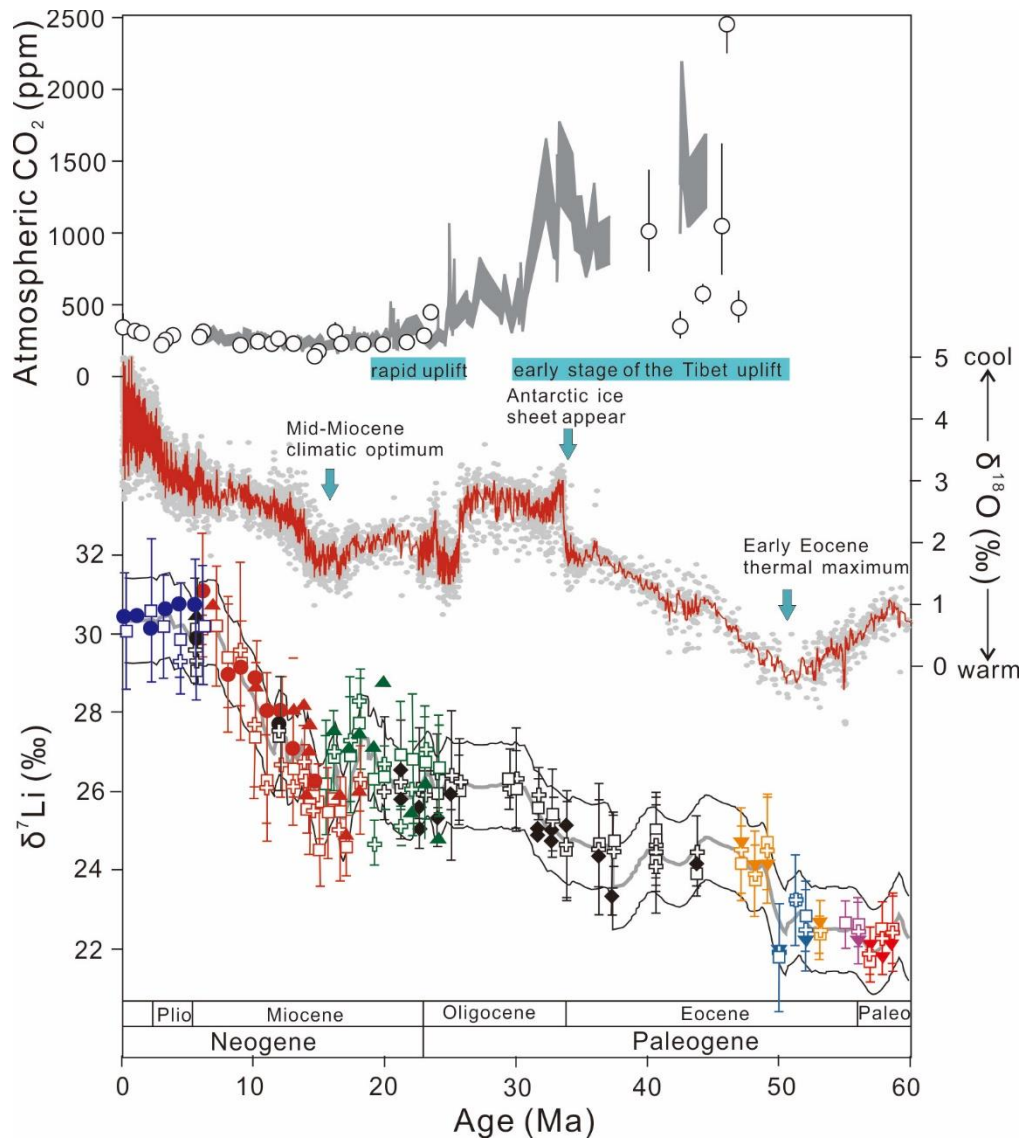


Figure 2 : Global deep-sea lithium and oxygen isotope records and atmospheric CO₂ concentration over the past 60 Myr. Modified from Zachos et al. (2001); Pagani et al. (2009) and Misra and Froelich (2012). Seawater δ⁷Li were estimated from measurements in planktonic foraminifera tests, assuming no isotope fractionation during their formation.

Li is mostly derived from silicate weathering (Huh et al., 1998; K1sakürek et al., 2005), and is not affected by redox state (only +1 charge). Large Li isotope fractionation can be expected on the Earth surface (compared to in the deep mantle). Therefore, lithium isotopes were thought to be one of the most powerful indexes of chemical weathering. Over the Cenozoic era, associated with the long-term temperature cooling, a ~9‰ increase of seawater δ⁷Li was recorded by planktonic foraminifera (Fig. 2). Misra and Froelich (2012) suggested tectonic activity (i.e. uplift) shifted the continental weathering regime from transport-limited (congruent) to weathering-limited (incongruent). Consequently, riverine δ⁷Li over the last 60 Ma increased by nearly 20‰, which results in the increase of seawater δ⁷Li. The simulation

results of Li and West (2014) showed that ~13 ‰ increase of riverine $\delta^7\text{Li}$ was more reasonable, and meanwhile, more dissolved Li was absorbed by autogenetic clay minerals due to the increased flux of degraded continental material delivered to the oceans. In contrast, Vigier and Godderis (2015) indicated that the changes of riverine Li flux can totally solve the seawater $\delta^7\text{Li}$ increase without a significant change of river $\delta^7\text{Li}$. This could be explained if, at the warmth Eocene, nearly 100% of Li was preserved in the soil, while present-day solid phase only account for ~80% of Li flux. Additionally, Caves Rügenstein et al. (2019) suggested long-term cooling during the Neogene reflects a change in the partitioning of denudation between weathering and erosion, that is seawater $\delta^7\text{Li}$ increase during this period indicate intensified incongruent weathering.

To date, although the mechanism for seawater $\delta^7\text{Li}$ increase over the Cenozoic era is still debated, the long-term cooling induced by chemical weathering has prevailed for couples of years. Raymo and Ruddiman (1992) indicated that the uplift of the Tibetan Plateau supplied more fresh materials and possibly induced greater monsoonal rainfall, which ultimately led to CO_2 drawdown via chemical weathering. As mentioned above, a slight disequilibrium between uptake and release of CO_2 can easily exhaust all of atmospheric CO_2 within a few million years. A negative feedback is required to balance the net consumption of atmospheric CO_2 . The decrease of organic carbon burial in the deep ocean was first proposed (Raymo and Ruddiman, 1992). However, recent work has shown that up to 90% of organic carbon burial occurs in continental margin sediments. Due to the rapid erosion in the Ganga-Brahmaputra rivers, net burial of organic carbon in the Himalayas was suggested to increase over the Neogene (France-Lanord and Derry, 1997). Model result also indicated that organic carbon burial during the Cenozoic was insufficient to balance the enhanced chemical weathering (Li and Elderfield, 2013). Another mechanism was attributed to enhanced sulfide oxidation coupled to carbonate dissolution (Torres et al., 2014). With the uplift of the Tibetan Plateau, rapid erosion not only produced fresh silicate materials but also exposed organic-rich sedimentary rocks. The enhanced sulfide oxidation potentially balances the excess CO_2 drawdown. However, this solution was questioned by Caves Rügenstein et al. (2019) who observed a minimal effect of pyrite oxidation on the ocean-atmosphere carbon budget according to their model results. Some other scientists proposed that the feedback most likely operates via the climate system itself (Frings, 2019). Kump and Arthur (1997) suggested that the weathering-limited regions were the place for balancing enhanced CO_2 consumption over the Cenozoic era because weathering-limited regions are sensitive to climate changes. Li and Elderfield (2013) further indicated that the long-term decline of island basalt weathering in

response to global temperature cooling played an important role in stabilizing the long-term carbon cycle. Taken together, in order to better understand the mechanism for the Cenozoic cooling, the weathering-climate feedback need to be further investigated at the global scale.

Compared to million-year timescales, glacial-interglacial cycles ($10^4 - 10^5$ years) are recent enough that high resolution sediment records are easily accessible. On this timescale, tectonic activities on global scale are dormant, and climate is the major external force for chemical weathering. However, the interpretation of weathering proxies for studying weathering-climate feedback is not straightforward. The changes of chemical weathering response to climate variation can be damped or even modified during sediment transport as a result of natural processes or human activities. First, the sediment records can respond to erosional patterns changes within the basin or are sensitive to water circulation changes during sediment transport, rather than reflecting the average chemical weathering (Wan et al., 2017; Bi et al., 2017; Zhao et al., 2018). Secondly, in large river systems, long sediment residence time in the well-developed flood/alluvial plains may buffer any trace of chemical weathering changes caused by climate changes (Li et al., 2016; Romans et al., 2016). Thirdly, due to the difference in ionic strength, pH and temperature between river and seawater, chemical compositions of river sediment can be modified in the estuary by adsorption-desorption, particle dissolution and/or ongoing weathering processes (Gislason et al., 2006; Jeandel and Oelkers, 2015).

The large river basins cover significant proportions of continental crust and various climatic regimes, and thus give advantages of studying weathering on a global scale (e.g. Gaillardet et al., 1999a, 1999b). Recently, the rivers around the Himalayas received more concerns on the studies of weathering-climate feedback. For instance, Lupker et al. (2013) interpreted the Bay of Bengal record as reflecting enhanced weathering intensity since ~21 ka, in response to more favorable Holocene climate than in the Last Glacial Maximum. Similar studies were also carried out in the Changjiang (Yangtze) Delta (Wang and Yang, 2013; Bi et al., 2017). On one hand, these rivers historically transported at least 20% of global sediment flux to the marginal sea (Fig. 3; Milliman and Farnsworth, 2013). These sediments provide suitable and high-resolution materials for recording paleoclimate and weathering in the geologic past. On the other hand, the uplift of the Tibetan Plateau likely contributed to the Cenozoic cooling (Raymo and Ruddiman, 1992; Kump and Arthur, 1997). The weathering studies in the river basins around the Himalayas are helpful to understand the role of the Tibet uplift played in regulating global climate. Additionally, strong human activities within these river basins, such as dam constructions, largely altered sediment transport patterns, which

show potentially influences on chemical weathering studies in the future. For instance, dams artificially separate sediment connection between upper mountainous area and lower floodplain region (Dynesius and Nilsson, 1994; Syvitski et al., 2005; Grill et al., 2019; Yang et al., 2019).

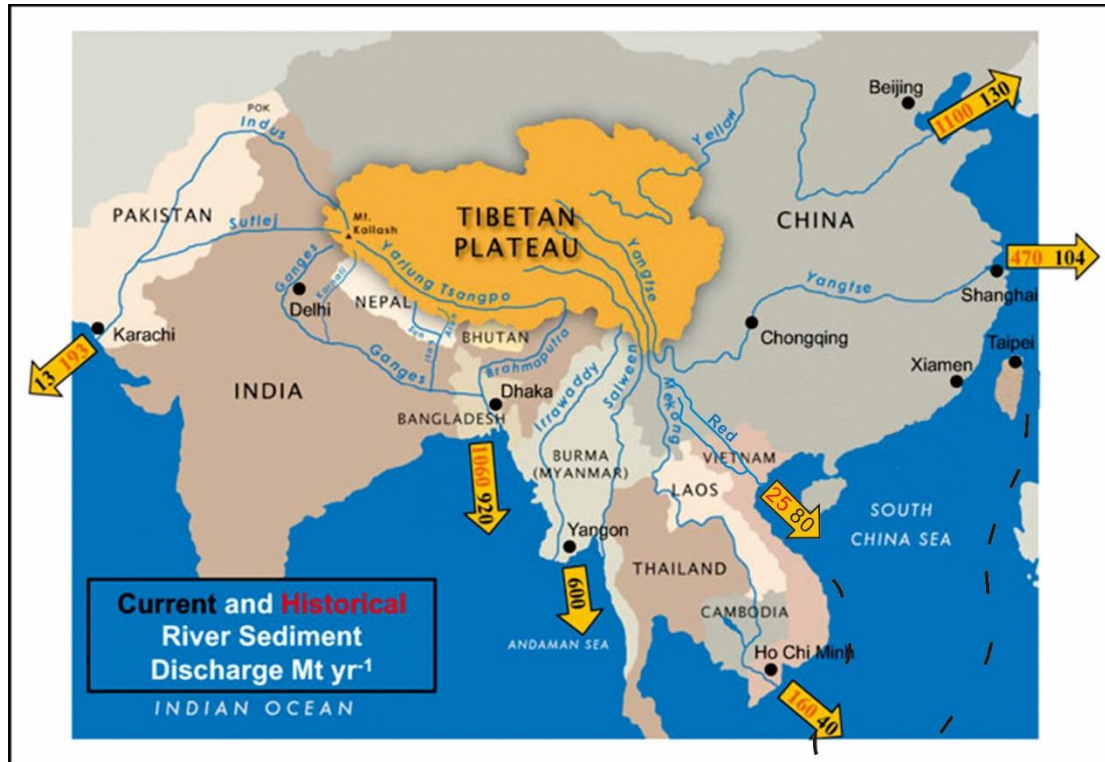


Figure 3 : Current and historical sediment flux of Asia’s Mega rivers originated from the Tibetan Plateau. Modified after Kuehl et al. (2020)

Recently, Li isotopes were also used to decipher weathering-climate feedback during specific hydroclimate events, which suggest distinct response to climate change. Bastian et al. (2017) observed higher clay $\delta^7\text{Li}$ values during lower insolation periods for the last 30 kyr in the Nile Delta. The increase of $\delta^7\text{Li}$ values in the middle-upper Datangpo Formation (Guizhou province, China) also reflects initiation of global cooling before the Marinoan glaciation (Wei et al., 2020). Although these studies implicitly or explicitly assumed negligible influence of estuarine process on Li isotope compositions, the behavior of Li isotopes in estuary did not reach consensus until now. For instance, Pogge von Strandamann et al. (2008) observed increased Li concentration and $\delta^7\text{Li}$ of particulate materials collected in the estuary of an Iceland river, which is ascribed to ongoing weathering during particles interaction with seawater. However, few other studies concerning dissolved Li in estuaries suggested a conservative behavior (Stoffyn-Egli, 1982; Colten and Hanor, 1984; Brunskill et al., 2003).

Clearly, there is a lack of studies of Li isotopes in the mixing zones, in particular for large basins with large discharge to the ocean.

For my PhD studies, the ultimate goal is to better understand how chemical weathering respond to climate variations. In the Chapter 1, the study background was briefly introduced. The Chapter 2 summarized the the basic information of the Changjiang (Yangtze) basin, including studies of natural background, sediment source, chemical weathering. The Li isotope fractionation in river basins were also reviewed. The Chapter 3 introduced samples collected and measurement used in the studies. In Chapter 4, in order to verify if the dam construction has altered the chemistry of downstream sediment, the temporal variations of elemental compositions of suspended particulate matter (SPM), river-bed sand (RBS), bank sediments and core samples collected downstream of the Three Gorges Dam were investigated. In Chapter 5, Li and its isotope compositions of suspended and dissolved load collected in the Changjiang Estuary were investigated, in aim to determine the impact of estuarine processes on the $\delta^7\text{Li}$ signature during materials delivered to the ocean. In Chapter 6, with the aim of determining weathering-climate feedback, clay Li and Nd isotopes and element concentrations in core CM97 recovered from the Changjiang Delta and in modern river bank sediments were investigated. Finally, the conclusions and perspectives were summarized in Chapter 7.

Chapter 2: Tracing continental weathering in the Changjiang (Yangtze River) basin : a review

The Changjiang (Yangtze) is the largest river in Asia and the third longest river in the world. It originates from the Tibetan Plateau, and flows eastward into the East China Sea. The study of weathering and erosion processes in the Changjiang catchment is of great significance for better understanding continental weathering and material cycling from a global perspective. However, the studies related to weathering-climate feedback in the Changjiang basin are rare. Additionally, the Changjiang basin is one of the most populated areas in the world. It also provides an ideal environment for studying the influence of human activities on geochemical compositions of sediments. Previous studies have shown that dam constructions in the Changjiang basin have largely disturbed the natural sediment “source-to-sink” systems. Sediment-transport patterns in the downstream of the Three Gorges Dam have changed from transport-deposition balance to net riverbed erosion (Yang et al., 2006; Chen et al., 2010; Luo et al., 2012; Lai et al., 2017). This physical pattern changes may also affect sediment geochemical composition, but this is poorly known.

In this chapter, the background of the Changjiang basin will be first introduced. Then, sediment source changes over different timescales and chemical weathering studies in the Changjiang basin are briefly summarized based on compilation of published articles. The use of Li isotopes to trace chemical weathering in the Changjiang basin is rare and mainly focused on the dissolved load (Wang et al., 2015; Ma et al., 2020). Thus, I will briefly review Li isotope fractionation in river basins worldwide reported previously.

2.1 River setting

The Changjiang River is more than 6,300 km long, and has a catchment area of 1.8×10^6 km². Its catchment host nearly 400 million people, ~6.6% of the world’s population, and provides ~42% of China’s Gross Domestic Product. In terms of water discharge and sediment flux, the Changjiang River transports nearly 900 km³/yr and 470 Mt/yr to the East China Sea (Yang et al., 2006). This value represents ca. 2.5% of the present-day estimate for the global sediment flux (19000 Mt/yr, Milliman and Farnsworth, 2013). The Changjiang drainage basin is primarily located in the South China Block, which is composed of the Yangtze Craton and

the Cathaysia Block (Fig. 4). It is bounded by the Qinling-Dabie orogenic belt to the north and by the Songpan-Garze terrain to its northwest.

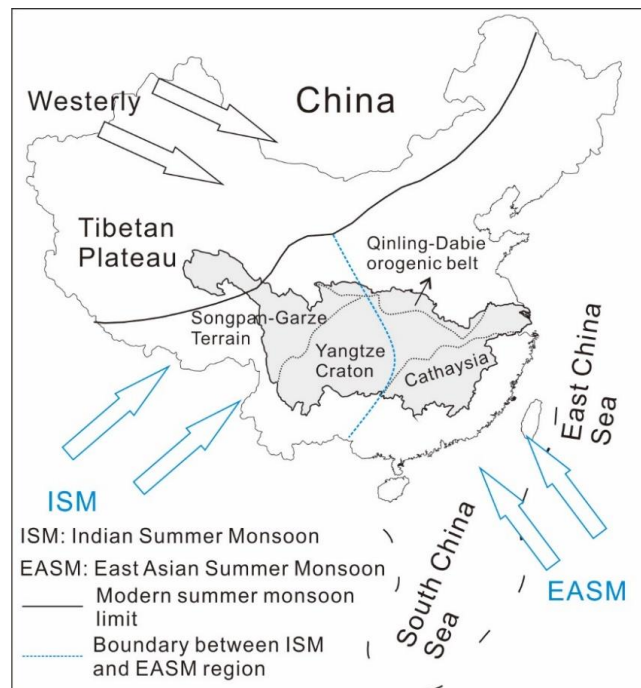


Figure 4 : Sketch map showing monsoon systems in China and the tectonic units in the Changjiang basin. The Indian Summer Monsoon (ISM) dominates climate variation in the upper Changjiang basin, while the climate changes in the mid-lower basin are subject to East Asian Summer Monsoon (EASM). The line indicating modern summer monsoon limit is drawn according to precipitation (4 mm/day isochrone)

The Changjiang catchment is strongly affected by the humid sub-tropical Asian monsoon climate, that is warm and humid in summer and cold but arid in winter. Generally, the upper basin is subject to the Indian Summer Monsoon (ISM), while the East Asian Summer Monsoon (EASM) dominates climatic changes in the mid-lower basin (Fig. 4). At present, the mean annual precipitation over the whole basin is ~1,100 mm, ranging from 150 mm to 1000 mm in the upper basin and averaging 1200 mm in the mid-lower basin. More than 60% of the annual precipitation falls during the wet season from May to October. Correspondingly, the period from May to October accounts for more than 70% of annual water discharge, with a peak mostly in July. Spatially, the annual precipitation increases eastward, from < 400 mm/yr in east Tibet, to about 700 mm/yr in Sichuan basin and > 2,000 mm/yr in lower reaches. Except for the cold climate (below 4°C) in the Himalayan river source area, the mean annual temperature in the mid-lower basin is about 16 – 18°C.

According to hydrological and geographic settings, the Changjiang drainage basin is generally divided into three sections (Fig. 5A). The upper reaches indicate the portion from

the headwater to Yichang city with 4,500 km in channel length. This section can be subdivided into two parts, in which Jinshajiang River is from the headwater to Yibin city and Chuanjiang River is from Yibin city to Yichang city. The upper Changjiang basin is made up of various tributaries, such as Yalongjiang, Daduhe, Minjiang, Tuojiang, Jialingjiang and Wujiang. The Three Gorges Dam (TGD), one of the largest hydroelectric engineering projects in the world, started to be constructed in 1994 and was completed in 2009. The TGD is located 40 km upstream of Yichang city. Currently, the Three Gorges Reservoir covers upstream river channel over distance of 660 km (Fig. 5A). The storage capacity of the reservoir is designed to be 39.3 km³, and the water level within the reservoir fluctuates seasonally by 30 m between 145 m and 175 m for flood control (Yang et al., 2014). The middle reaches are 950 km long, running from Yichang to Hukou city. The lower reaches extend from Hukou to the river mouth with a length of about 850 km. The Dongting and Poyang Lakes are two major tributaries of the Changjiang River in the middle basin.

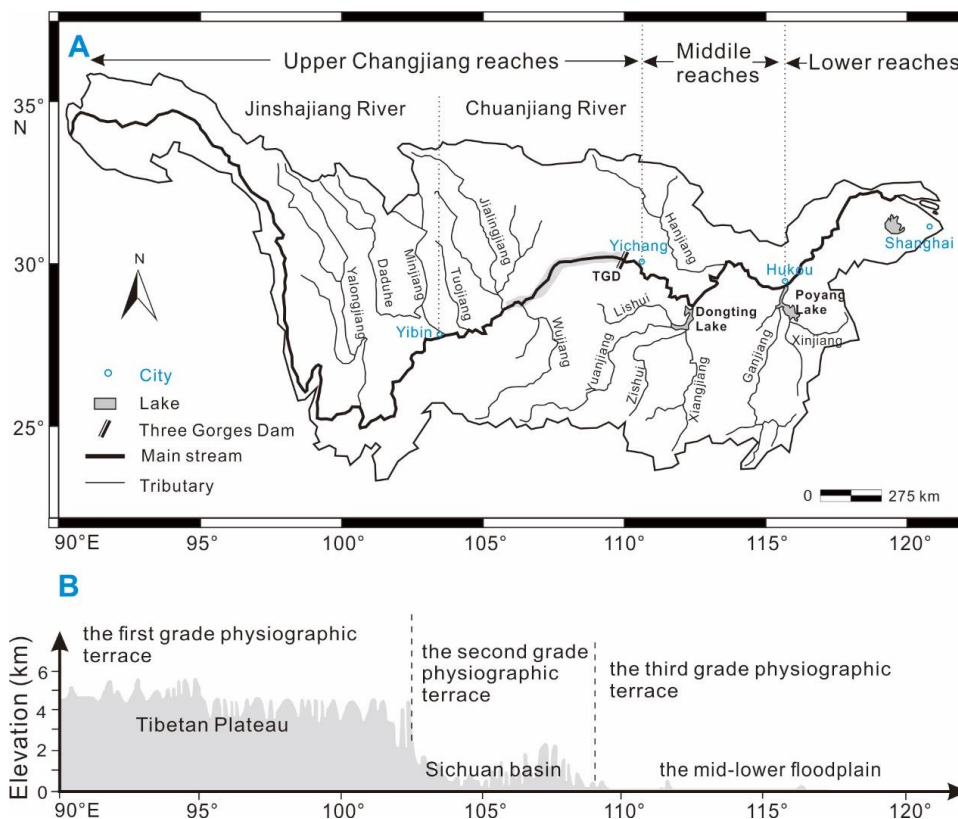


Figure 5 : (A) Sketch map showing the drainage and (B) the topography in the Changjiang basin. TGD means the Three Gorges Dam

Geographically, the Changjiang basin spans three-grade physiographic terraces in China, with average elevations of 3,000 – 5,000 m, 500 – 2,000 m and less than 500 m respectively (Fig. 5B). The upper watershed features active tectonics and steep mountains,

especially in the Jinshajiang valley, with an elevation above 3,500 m. This section is mostly located on the first-grade physiographic terrace. With river flowing eastward, the topography changes dramatically. The Chuanjiang River is mostly located on the second-grade physiographic terrace, with an elevation ranging from 500 – 2,000 m. The elevations of middle and lower reaches are mostly below 500 m (third-grade physiographic terrace). The floodplain and alluvial plains are well developed here, occupying about 44% of the total basin area.

Geologically, the Changjiang basin is covered by complex rock types (Fig. 6). Along the river flowing direction, source region is dominantly composed of clastic sedimentary rocks, igneous rocks and metamorphic rocks. The Permian Emeishan large igneous province is distributed along the western margin of the Yangtze Craton, with an area of $\sim 2.5 \times 10^5 \text{ km}^2$, representing an important basalt provenance in upper basin. In the following section, Paleozoic clastic rocks and carbonate are widely exposed, and Mesozoic intermediate-acidic igneous rocks and Triassic low-grade metamorphic rocks distribute sporadically (Wu et al., 2011). The exposed rocks in Sichuan basin are mainly Jurassic red sandstone, and Paleozoic carbonate rock occupies the segment from City Wanzhou to Yichang (Fig. 6). In the mid-lower basin, the basement rocks of the Yangtze Craton are rarely exposed. The lithology here is characterized by Paleozoic low-grade meta-sedimentary rocks, Mesozoic acidic igneous rocks and Quaternary fluvial-lacustrine sediments (Yang et al., 2009).

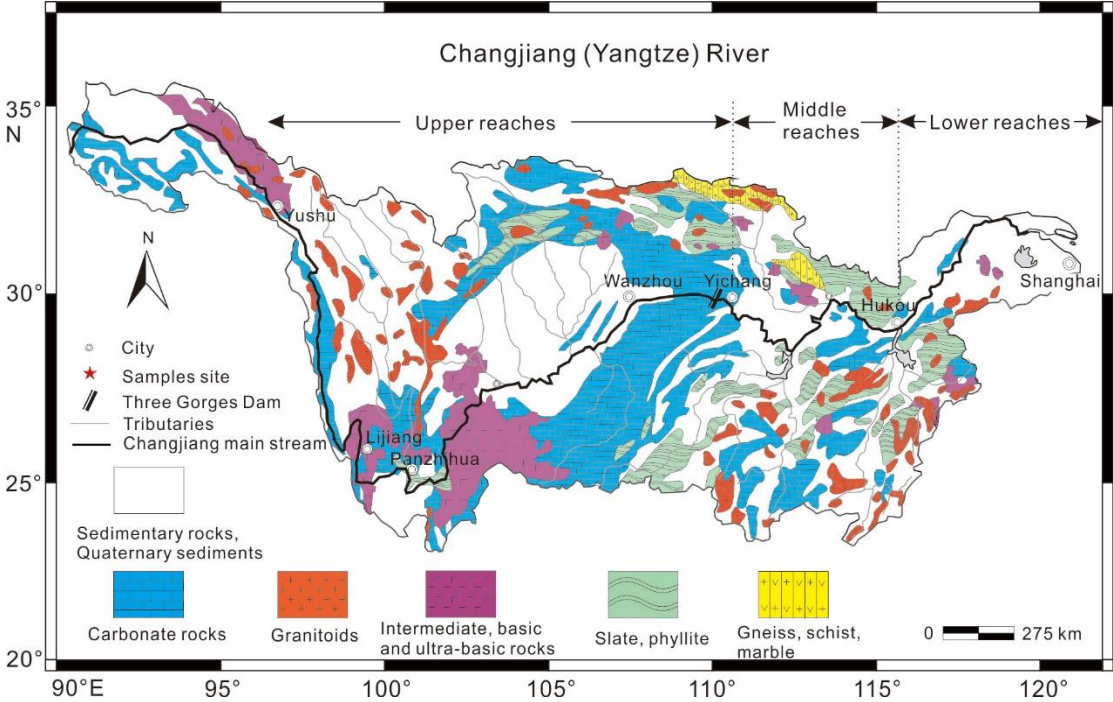


Figure 6 : Sketch map showing the bedrock lithology in the Changjiang basin. Modified after Yang et al. (2009)

2.2 The source of sediment transported by the Changjiang River into the East China Sea over different timescales

Sediment source discrimination is the prerequisite for investigating chemical weathering and past climate registered in the sedimentary records. During the chemical weathering and sediment transport, some specific elements or minerals can be delivered conservatively from the source to sink, and then reflect the geochemical information of bedrock in the source area. The studies concerning sediment source in the Changjiang basin can date back to 1980s – 1990s in China (Zhao, 1983; Zhao and Yan, 1992, 1994). During the past decades, different kinds of methods have been applied to investigate the characteristic of bedrock in each sub-basin and sediment distribution in the East China sea, including elements, Sr-Nd isotopes, mineralogy and thermochronology (Fan et al., 2012 ; Yang et al., 2015). Overall, the Himalayan intermediate-acid igneous rocks and Permian basalt are widely distributed in the upper basin, while silicate rocks in the mid-lower basin are characterized by sedimentary rocks, low-grade metamorphic rocks and acid igneous rocks. Consequently, compared to the downstream sediments, the upstream-derived sediments contain more mafic components and have slightly higher $^{143}\text{Nd}/^{144}\text{Nd}$ (Yang et al., 2007; Chatelat et al., 2013; Bi et al., 2015). The average ϵNd of sediment derived from the Dongting and Poyang Lakes are -13.7 ± 1.1 , while it is -11.0 ± 1.0 for upstream sediments (Yang et al., 2007; He et al., 2015).

As suggested by Barbour (1936), the paleo-Changjiang River once flowed into the South China Sea along the paleo-Red River channel (Fig. 7). With the uplift of the Tibetan Plateau and tectonic subsidence in the Eastern China, the paleo-Changjiang River eventually flowed eastward into the East China Sea by river capture and reversal. Although a large number of studies have been conducted in some key areas, the age of the Yangtze River flowing eastward is still strongly debated, with estimation ranging from ~ 0.75 Ma to 40 – 45 Ma (Fan et al., 2004; Yang et al., 2006; Xiang et al., 2006; Wang and Li, 2009; Zhang et al., 2013). For instance, based on the geochemical compositions and monazite crystallization ages of the sediment from core PD in the Changjiang delta, the sediment source of samples in the Changjiang delta significantly changed in the early Quaternary, and since then, the sediment source is characterized by modern pattern (Fan et al., 2004; Yang et al., 2006). In contrast, Zheng et al. (2013) suggested that the modern Changjiang river was established before ~ 23 Ma, according to $^{40}\text{Ar}/^{39}\text{Ar}$ ages from basalts in together with detrital zircon U-Pb ages. Despite disagreement on the timing of modern river system establishment, a conclusion can

be drawn that the source changes of sediments into the East China Sea since the late Pleistocene were less affected to tectonic activities at global scales.

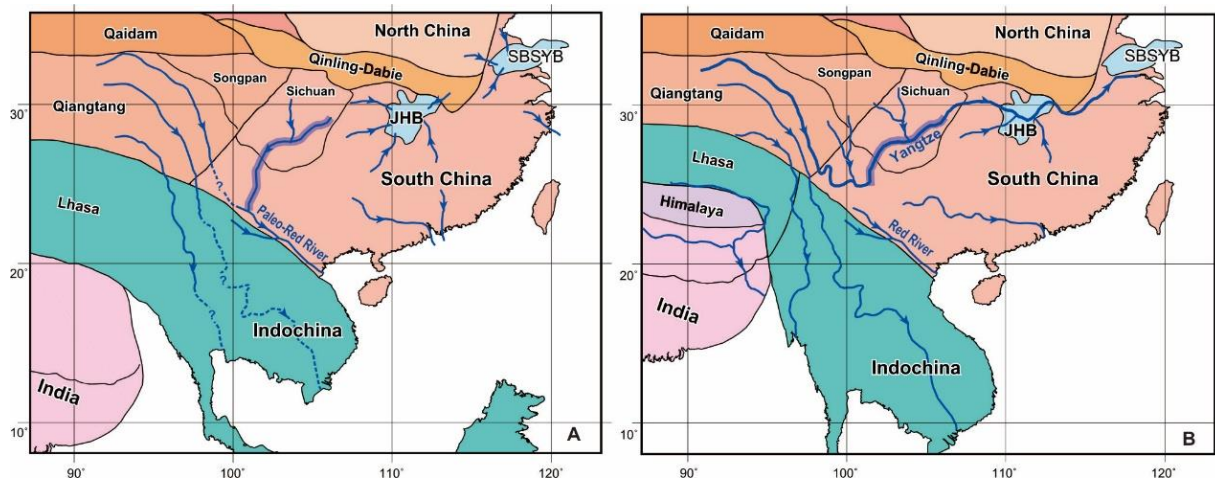


Figure 7 : Simplified maps showing the development of the Changjiang River in response to tectonic evolution in East Asia. Modified after Zheng et al. (2013). (A) the Paleochangjiang River flowed into the South China Sea along the paleo-Red River channel at ~32 Ma suggested by Zheng et al. (2013). (B) the modern Changjiang River formed at least since the late Pleistocene (Yang et al., 2006). JHB: Jiangnan basin; SBSYB: Subei-South Yellow Sea Basin.

Since then, monsoon climate dominates sediment source changes in the Changjiang basin over sub-orbital or much shorter timescales. At the Last Glacial Maximum (LGM), the upstream-derived sediment possibly deposited *in situ* due to weak monsoon, and the sediment into the East China Sea at that time mainly came from the mid-lower basin (Wang and Fan, 2013). Based on the Sr-Nd isotopes of bulk sediments in core CM97 (the core I studied during my PhD), Bi et al. (2017) indicated that the sediment source changed from the upper Changjiang basin at the early Holocene to the mid-lower basin during the mid-late Holocene in response to asynchronous evolution of the Indian and the East Asian summer monsoon. Similarly, the seasonal variation of sediment source in response to rainfall belt shift was observed in the modern Changjiang River (Shao and Yang, 2012; Yang et al., 2013). Compared to the dry season, the riverine suspended particulate matter during the flood season (May – October) have higher ratios of illite/kaolinite (~5) and $^{143}\text{Nd}/^{144}\text{Nd}$ values (-11.24 – -10.55), indicating much stronger physical erosion and sediment contribution from the upper basin (Mao et al., 2010, 2011).

Based on long-term (1951 – 2002) hydrological observations, the upper basin accounts for 85 – 90% of sediments transported by the Changjiang River into the East China Sea (Changjiang Water Resources Commission, 2002). The sediments contribution from the Jinshajiang and Jialingjiang River was estimated to be 47% and 24% accounting for the

upstream-derived sediment flux (Fig. 8A; Yang et al., 2006). However, the sediment source traced by mineralogical method leads to contradictory results. The clay mineral assemblages indicated that the Yalongjiang, Daduhe, Minjiang and Jialingjiang River in the upper basin accounts for the major sediment sources (Fig. 8B; He et al., 2013). The detrital zircon U-Pb ages suggested sand fraction of the Changjiang bank sediment mainly derived from Hanjiang, Xiangjiang, Jialingjiang and Jinshajiang River (Fig. 8C; He et al., 2014). However, the $^{40}\text{Ar}/^{39}\text{Ar}$ ages of detrital muscovites showed that the main contributor to the Changjiang delta sands is the Minjiang River (Sun et al., 2016). To our knowledge, the contents of detrital zircon in different tributaries are different, which can mask the contribution of rivers with low zircon contents. The muscovite can be abraded into much smaller grain size during transport, possibly resulting in incomplete analyses of the sample population if only sand fractions are analyzed. Thus, Vezzoli et al. (2016) suggested that provenance studies based on single-mineral species bear large uncertainty. According to high-resolution petrographic and heavy mineral analyses, they demonstrated that the Jinshajiang, Minjiang and Hanjiang River supplied most of the sand reaching the East China Sea (Fig. 8D). The inconsistent major sediment sources determined by different methods can be potentially caused by hydrodynamic sorting during sediment transport. The sediment source for samples with different grain size may be different. For instance, Mao et al. (2010) suggested that the grain size of upstream-derived sediment is coarser than those derived from the mid-lower basin. During sediment transport, coarse-grained particles preferentially deposit. Luo et al. (2012) suggested that the upper Changjiang basin contributed more particulates to bottom water layer. Another explanation is that the sand fraction has potentially long transport times. The coarse-grained zircon and muscovite provenance may reflect paleo-erosion patterns (He et al., 2014; Sun et al., 2016). For instance, the heavy mineral assemblages and detrital zircon U-Pb ages both indicate the Hanjiang River is one of the major sources of sediment into the East China Sea (Figs. 8C and 8D; He et al., 2014; Vezzoli et al., 2016). However, with the Danjiangkou Dam construction in 1968, the hydrological observation shows that no more than 20 Mt/yr of sediment flux is exported by the Hanjiang River into the Changjiang mainstream (Changjiang Water Resources Commission, 2002). Apparently, the Hanjiang River is not the major sediment contributor to the present-day Changjiang River.

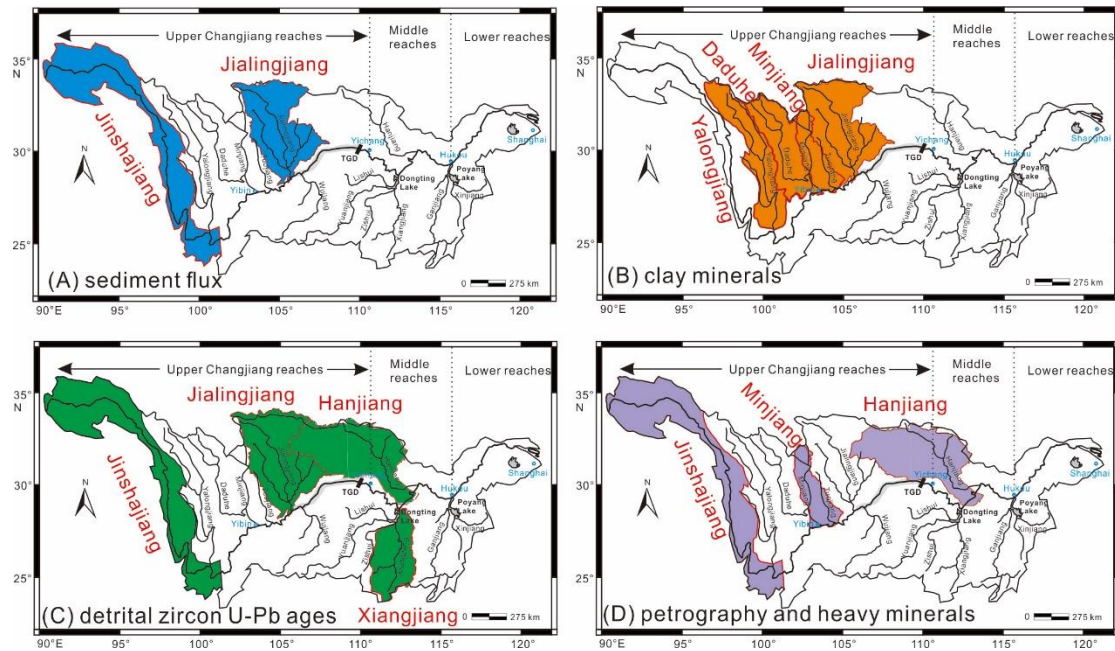


Figure 8 : Schematic maps showing the major sources of sediments into the East China Sea determined by different methods. (A) sediment flux (Yang et al., 2006), (B) clay minerals (He et al., 2013), (C) detrital zircon U-Pb ages (He et al., 2014), (D) petrography and heavy minerals (Vezzoli et al., 2016).

Apart from natural processes, human activities can also affect the source of sediment into the East China Sea. Based on the hydrological observation at Datong gauging station since 1950, the water discharge transported by the Changjiang River remained stable with time, while sediment flux decreased systematically. As shown in Figure 9, during the last 65 years, water discharge mostly ranged from 800 km³/yr to 1000 km³/yr, and sediment flux decreased from ~490 Mt/yr at 1951 – 1968 to ~150 Mt/yr at 2003 – 2015. The decrease of sediment flux is mainly caused by dam constructions (Yang et al., 2006). The Three Gorges Dam (TGD), the world’s largest hydroelectric engineering project, was initially constructed in 1994, and fully completed in 2009. Since the operation of the TGD in 2003, nearly 80% of upstream-derived sediment (~110 Mt/yr) was retained in its reservoir (Changjiang Water Resources Commission, 2002 – 2015; Yang et al., 2018). Note that the upper Changjiang basin is not the major source of sediment into the East China Sea since then. With the flux decline of upstream-derived sediments, the sediment previously deposited in the mid-lower river floor and bank started to be resuspended (Chen et al., 2010; Luo et al., 2012; Lai et al., 2017). The average erosion depth in the segment between Yichang and Zhicheng City was up to ~3.7 m (Xu and Milliman, 2009; Lai et al., 2017). Since then, the resuspended sediments in the mid-lower basin became the dominant source of sediment into the East China Sea (Yang et al., 2006; Dai and Liu, 2013; Yang et al., 2018).

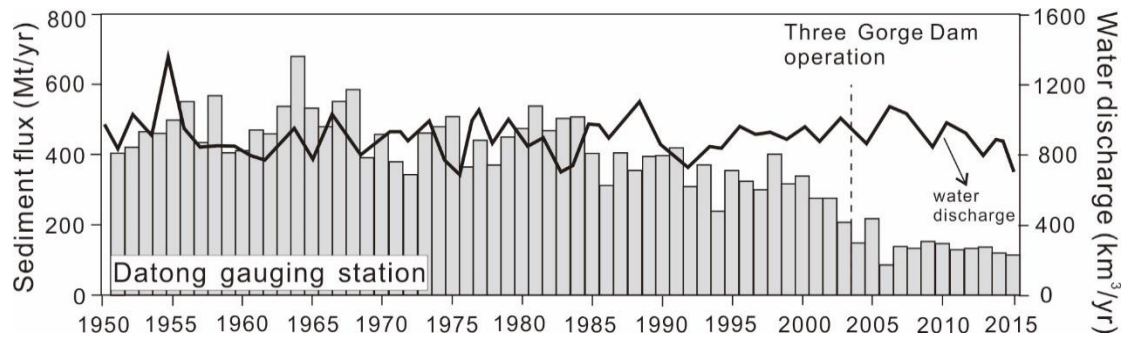


Figure 9 : the water discharge (black line) and sediment flux (grey bars) transported by the Changjiang River into the East China Sea recorded at Datong gauging station. The data of water discharge and sediment flux were collected from the Changjiang Water Resources Commission website: <http://www.cjw.com.cn/>.

2.3 Chemical weathering studies in the Changjiang basin

Chemical weathering is thought to be one of the most important mechanisms for modulating global climate (Walker et al., 1981; Raymo and Ruddiman, 1992). To date, the studies related to the interactions among climate, erosion and chemical weathering rate have been carried out for over 100 years. However, the identification of the dominant control on chemical weathering remains unclear (Chamberlin, 1999; Goudie and Viles, 2012). Some advocate that climate (i.e. temperature and runoff) is the critical factor, which process follows the Arrhenius rate law (Bernier et al., 1983; White and Blum, 1995; Kump et al., 2000; Gislason et al., 2009). In contrast, others propose that orogenic erosion can supply fresh materials, which is the major process favoring chemical weathering (Raymo and Ruddiman, 1992; Riebe et al., 2001, 2004). Based on a compilation of chemical and physical erosion rates in small catchments, West et al. (2005) indicated that chemical weathering rates are not governed by any single parameter. In the transport-limited regimes, physical erosion rate is low, and the chemical weathering rate is directly proportional to the supply of fresh materials (Fig. 10A). In the kinetic-limited regimes, there is abundant fresh materials for chemical weathering but climatic parameters limit the production of silicate cations. With the increase of denudation rate ($10^3 - 10^4$ t/km²/yr), chemical weathering rate reaches plateau or even decrease (Fig. 10A). The watersheds with regolith thickness of 0.5 m was suggested to produce the greatest solute flux (Fig. 10B; Gabet and Mudd, 2009). The upper Changjiang basin is mountainous, with physical erosion rate mostly higher than 10^2 t/km²/yr. This part is characterized by weathering-limited regime (Wu et al., 2008; Li et al., 2019). In contrast, the mid-lower basin is covered by well-developed flood/alluvial plains. The weak physical

erosion (generally $<10^2$ t/km²/yr) and favorable climate there feature it as a transport-limited regime (Yang et al., 2004; Li et al., 2019).

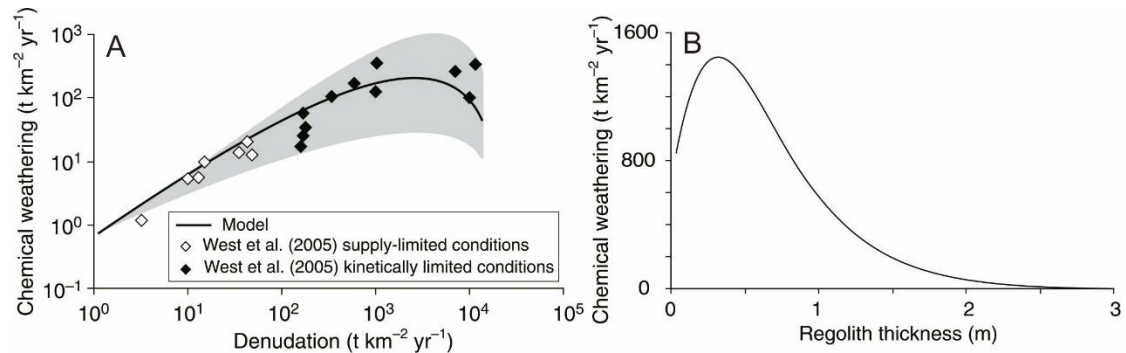


Figure 10 : (A) model results showing the relationship between denudation and chemical weathering rate and (B) the relationship between regolith thickness and chemical weathering. Denudation rate is the sum of chemical weathering rate and physical erosion rate. After Gabet and Mudd (2009).

Generally, the flux of dissolved load is of particular importance for estimating the rate of chemical weathering and atmospheric CO₂ consumption (Gaillardet et al., 1999a; Moon et al., 2014). The studies of river water chemistry in the Changjiang basin can date back to 1980s, but remain scarce at that time. For instance, based on 3 samples collected in the middle reaches, Hu et al. (1982) suggested that the Changjiang River accounts for over 5% of the flux of Mg²⁺, Ca²⁺, Cl⁻, SO₄⁴⁻ and HCO₃⁻ to the ocean. A case study in the estuary revealed that the dissolved load transported by the Changjiang River mainly come from the weathering of carbonates and silicates (Zhang et al., 1990). It is worthy noting that the systematic investigation started at the beginning of this century, which was largely supported by the Ministry of Water Resources of the People's Republic of China. Based on the measurement of major ions concentration at 191 gauging stations across the Changjiang basin, Chen et al. (2002) demonstrated that the average total dissolved solid (TDS) concentration of the Changjiang River was 209.5 mg/l, and the annually flux was 154×10^6 tons. This value is slightly higher than the estimate conducted by Gaillardet et al. (1999a) who proposed a mean value of $\sim 118 \times 10^6$ tons/yr. Generally, the dissolved load in the Changjiang River is mainly derived from the weathering of carbonates. HCO₃⁻ accounts for about 80% of the total anions, while Ca²⁺ accounts for 60 – 75% of the total cations (Chen et al., 2002; Wang et al., 2007). Inverse model results indicated that carbonate accounts for nearly 40 – 60% of cationic TDS (Chetelat et al., 2008), while the weathering of silicates contributes $\sim 10 – 20\%$ to the TDS (Fig. 11). Nevertheless, the river water chemistry in the headwater indicates significant differences from the downstream. As shown in Figure 11, the contribution of evaporite is up

to 50% in the Jinshajiang River. Also, evaporite dissolution accounts for 45 – 83% of the total cations and nearly 100% of Li concentration in the headwater (Wu et al., 2008a; Ma et al., 2020). Additionally, the Changjiang basin is one of the most populated area in the world. Several lines of evidences have demonstrated that human activities have storngly altered river water chemistry. For instance, the abrupt increase of SO_4^- concentrations in the Chongqing-Guiyang region was caused by severe acid rainfall in response to coal burning. Overall, the contribution of anthropogenic input to the TDS was estimated to be 15 – 20% in the Changjiang basin (Fig. 11; Chetelat et al., 2008).

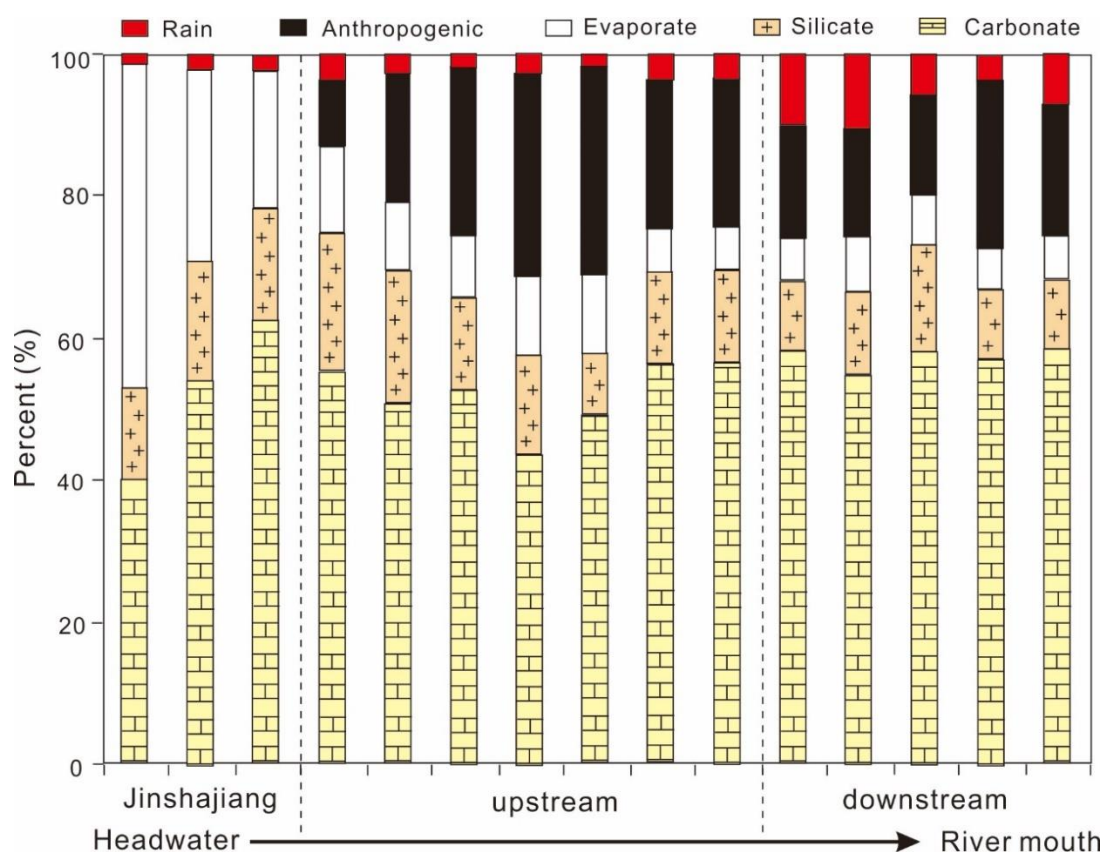


Figure 11 : Calculated contribution of different reservoirs to the cationic total dissolved solid for the Changjiang mainstream. The detailed method of calculation can refer to Chetelat et al. (2008). The graph is also modified after Chetelat et al. (2008).

Based on the analysis of river water chemistry, the overall chemical weathering rate (silicate and carbonate) in the Changjiang basin was estimated to be about $16.4 \text{ ton/km}^2/\text{yr}$, however, silicate weathering rate across the whole basin only range from $1.7 \pm 0.3 \text{ ton/km}^2/\text{yr}$ to $3.3 \pm 0.3 \text{ ton/km}^2/\text{yr}$ (Chetelat et al., 2008). The Changjiang River consumes $\sim 1.91 \times 10^{11} \text{ mol/yr}$ of atmospheric CO_2 by silicate weathering, which only accounts for $\sim 2\%$ of global CO_2 consumption annually by silicate weathering (Fig. 12; Chetelat et al., 2008). The Himalayan rivers account for only about 10% of the global CO_2 consumption by silicate

weathering, which likely implies a lesser role of the Himalayas played in long-term global cooling (Fig. 12; Raymo and Ruddiman, 1992; Wu et al., 2008b; Manaka et al., 2015). Water chemistry in the major rivers originating from the Himalayas were widely investigated. The results indicated that the Ganges River consumes the largest amount of atmospheric CO₂ annually, two times higher than the Changjiang River (Fig. 12). The carbonate weathering rate estimated for the Changjiang River is the highest among Himalayan-sourced rivers (Fig. 12).

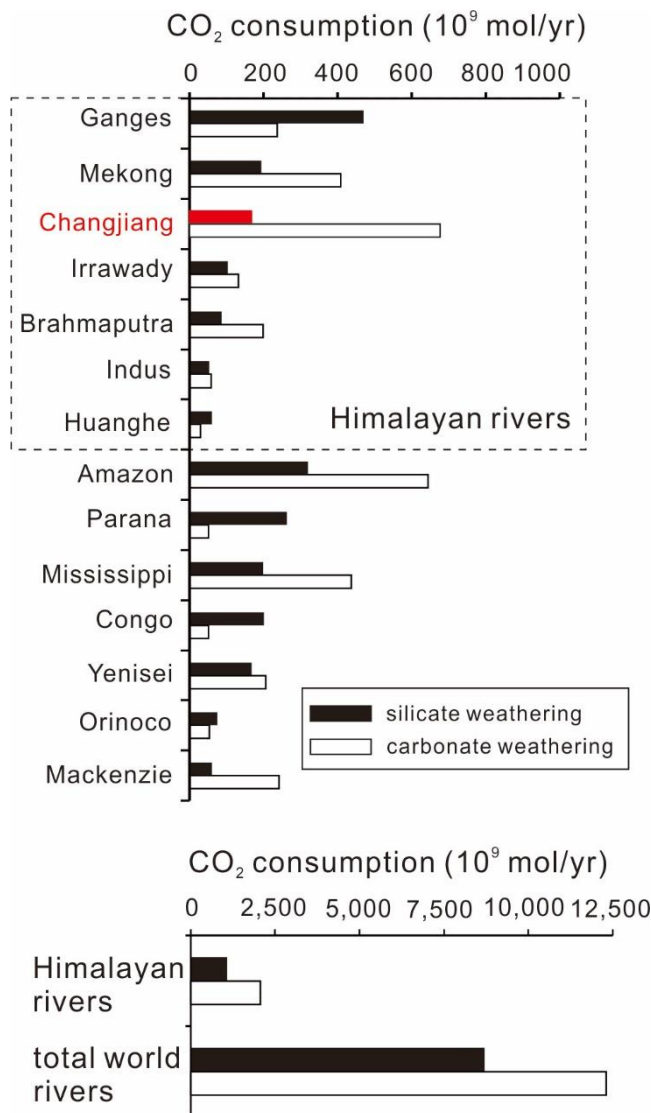


Figure 12 : CO₂ consumption by chemical weathering of silicates and carbonates in major world rivers. The data are mostly from Gaillardet et al. (1999a). The data in the Changjiang River are from Chetelat et al. (2008). The data in the Irramady River are from Manaka et al. (2015). This graph is modified after Manaka et al. (2015).

During chemical weathering, residual solids and newly formed phases form weathering profile *in situ*, or experience erosion, transportation and finally deposit in the sediment sink, which give insight into weathering and climate over the geological past (Gaillardet et al., 1999b; Lupker et al., 2013). The weathering intensity can refer to the extent of mobile elements leaching out of the bedrock, or the fraction of total denudation

accomplished chemically (Dellinger et al., 2015; Frings et al., 2019). The weathering intensity increases with the increasing of mobile elements leaching. Overall, the weathering intensity of sediments in the Changjiang basin is intermediate. Na and Ca are largely leached, while K is mostly hosted in K-feldspar and illite (Yang et al., 2004, 2013; Zhou et al., 2015). The clay mineral assemblages in the mainstream bank sediments are dominated by illite, with relative content of 60 – 70%. The subsequent clay minerals are kaolinite and chlorite (10 – 20%), and smectite has extremely low content (He et al., 2013; Zhao et al., 2018). The factor controlling chemical weathering in the eastern China was thought to be climatic parameters based on modern river samples (Yang et al., 2004; Bi et al., 2015). The warm and humid climate is in favor of chemical weathering. This is also the reason for higher weathering intensity in the mid-lower basin compared to that in the upper basin. For seasonal variation, Shao and Yang (2012) observed lower chemical index of alteration (CIA) values of SPM (suspended particulate matters) samples (CIA=76) during the flood season relative to that in dry season (CIA=79), which likely implied weaker weathering intensity. However, the detail investigation on grain size and mineral assemblages suggested that this was caused by sediment source changes. Indeed, heavy rainfall results in strong physical erosion in the upper basin during the flood season (Mao et al., 2010; Shao and Yang, 2012). During the flood season, SPM samples are coarser and have higher illite/kaolinite ratios. Based on the investigation of sediment core located in the Changjiang Delta, the variation of detrital clay components over the last 14 kyr was likely caused by chemical weathering changes within the basin in response to the Asian Summer Monsoon evolution (Wang and Yang, 2013).

Additionally, as a result of dam constructions, geochemical compositions of sediment and dissolved load downstream of the TGD may have largely been altered. Based on the analysis of river water chemistry in one hydrological year, Wang et al. (2018) observed an increase of dissolved Si flux transported by the Changjiang River into the East China Sea. It is suggested that the dissolution of particulate biogenic silica downstream of the TGD is the major cause. Zhao et al. (2018) investigated clay mineral assemblage in the bank sediments before and after the dam operation, and found that relative content of kaolinite increases due to more sediment contributions from the Dongting and Poyang Lakes in the mid-lower basin. However, these effects still need to be more precisely quantified.

2.4 Li isotope fractionation in river basins

During my PhD, I mostly used lithium isotopes to trace continental weathering and its variations in the Changjinag Basin. Lithium (Li) is a moderately incompatible element, and owns two isotopes, ^6Li and ^7Li , with respective abundance of 7.52% and 92.48%. In the catchments, dissolved Li is mostly derived from the weathering of silicates, even in a carbonate-dominant basin (Huh et al., 1998; Kısakürek et al., 2005). In soils, Li is mostly hosted in the phyllosilicate octahedral sites, while less parts are adsorbed onto the particle surface, interlayer sites and the pseudo-hexagonal sites (Fig. 13; Vigier et al., 2008; Hindshaw et al., 2019; Pogge von Strandmann et al., 2019). Up to now, case studies related to Li isotopes have been widely carried out worldwide, such as in the Amazon River, the Changjiang River, the Mackenzie River and the Iceland rivers (Huh et al., 1998; Vigier et al., 2009; Pogge von Strandmann et al., 2010; Dellinger et al., 2014, 2015, 2017; Pogge von Strandmann and Henderson, 2015; Wang et al., 2015; Gou et al., 2019; Maffre et al., 2020). Several review papers were also published by Chinese and international scientists (Tomascak, 2004; Wang et al., 2006; Tang et al., 2007; Tang et al., 2009; Burton and Vigier, 2012; Penniston-Dorland et al., 2017; Gou et al., 2017; Yang et al., 2018).

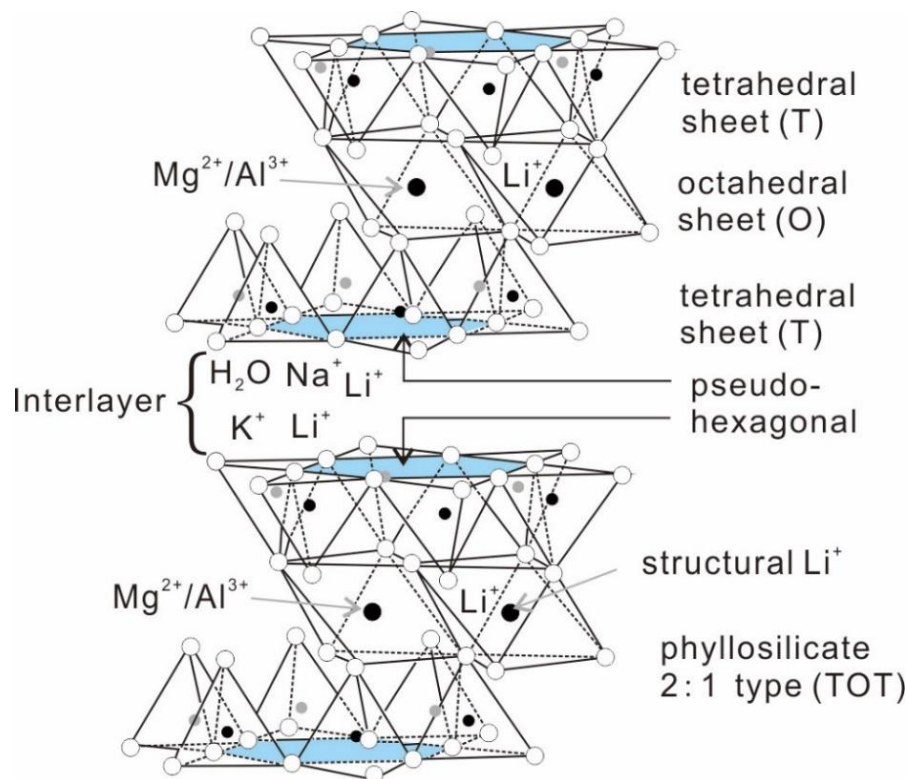


Figure 13 : Schematic diagram showing the location of Li in a 2:1 type phyllosilicate. Li^+ can be incorporated into the octahedral site or pseudo-hexagonal sites in tetrahedral sheet, or be adsorbed onto the surface, interlayer sites. This diagram is modified from Vigier et al. (2008).

Similar to other stable isotopes, Li isotope compositions ($\delta^7\text{Li}$) are reported as delta values, representing $^7\text{Li}/^6\text{Li}$ ratios of samples deviated from an international standard. It can be expressed as following:

$$\delta^7\text{Li} = \left[\frac{(^7\text{Li}/^6\text{Li})_{\text{sample}}}{(^7\text{Li}/^6\text{Li})_{\text{L-SVEC}}} - 1 \right] \times 1000$$

The standard is generally the U.S. National Institute of Standards and Technology (NIST) high-purified Li_2CO_3 reference material L-SVEC, which has $^7\text{Li}/^6\text{Li}$ ratio of 12.02 ± 0.03 .

As an important input end-member of global Li cycle, the average riverine dissolved Li flux was estimated to be $8 - 12 \times 10^9$ mol/yr, with concentration and isotope composition ($\delta^7\text{Li}$) of $1.5 \mu\text{g/l}$ and $+23\text{‰}$, respectively (Huh et al., 1998). Based on the compilation of reported data, the dissolved Li concentrations in rivers mostly range from $0 \mu\text{g/l}$ to $5 \mu\text{g/l}$ (Fig. 14A). The seawater Li concentration is $\sim 182 \mu\text{g/l}$ ($26 \mu\text{M}$, Chan and Edmond., 1983). In contrast, the Li concentrations of SPM samples vary significantly, but are mostly concentrated in the range of $30 - 60 \mu\text{g/g}$ (Fig. 14B). This indicates that solid phase, other than dissolved phase, is the major host for Li at large scale (Millot et al., 2010; Dellinger et al., 2015). Indeed, field observations have suggested that approximately 80% of Li in the modern river basins is carried by particulate materials (Millot et al., 2010; Dellinger et al., 2015). Due to Li isotope fractionations, dissolved $\delta^7\text{Li}$ values show a large variation, from $+1.3\text{‰}$ to $+43.7\text{‰}$ (Tomascak, 2004; Burton and Vigier, 2012; Penniston-Dorland et al., 2017). The lowest value was observed in the Negro River, where the dissolution of secondary minerals results in bedrock-like dissolved Li isotope compositions (Dellinger et al., 2015). As shown in Figure 14C, the dissolved $\delta^7\text{Li}$ values are mostly concentrated in the range of $+10 - +22\text{‰}$. The world-wide average Li isotope compositions of river water is about $+23\text{‰}$, significantly lower than the homogenous composition of seawater ($+31.2\text{‰}$, Chan and Edmond., 1983). Compared to the large variation of dissolved $\delta^7\text{Li}$, Li isotope compositions in SPM samples show narrow changes. The variation ranges from -4‰ to $+4\text{‰}$, close to the average $\delta^7\text{Li}$ of the upper continental crust ($0 \pm 2\text{‰}$; Teng et al., 2004; Sauzeat et al., 2015). This likely indicates that SPM samples contain not only secondary minerals but also large amount of primary minerals, and lithology has a great influence on Li isotope compositions of particulate materials.

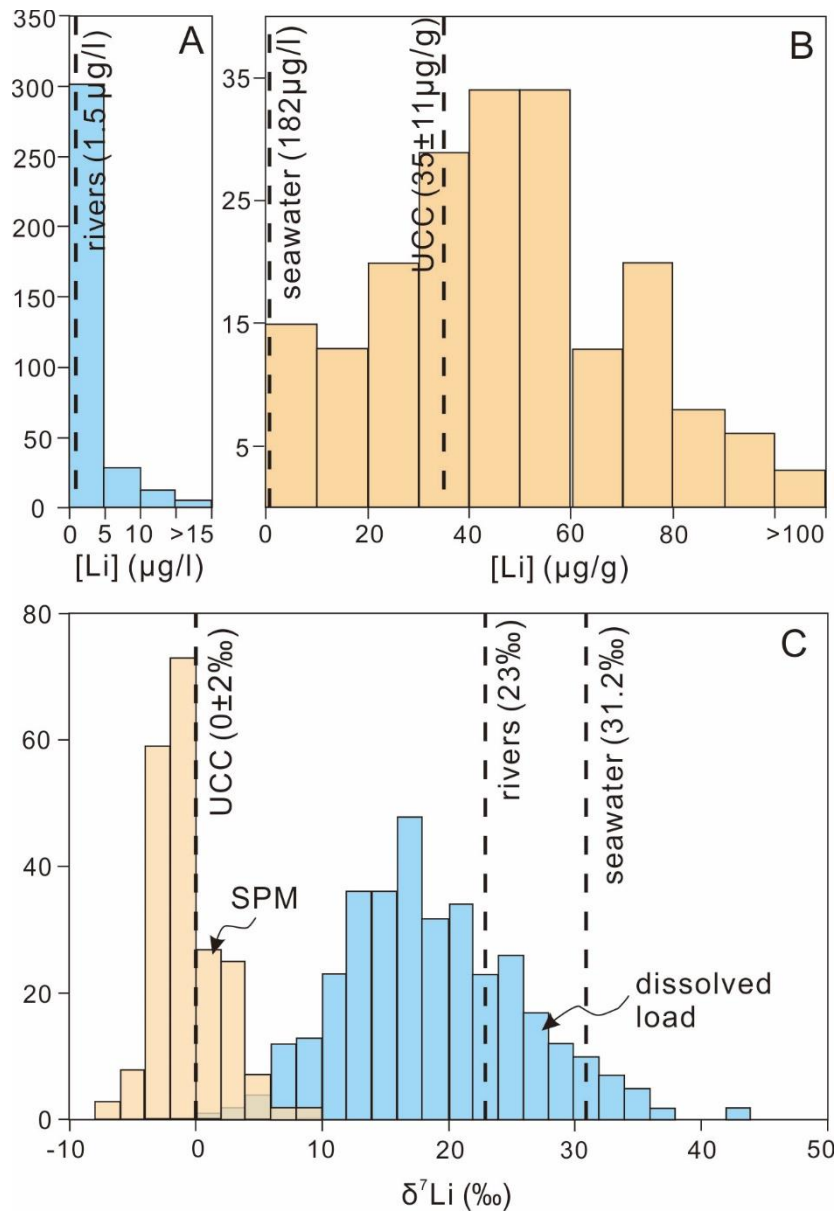


Figure 14 : (A) the Li concentration in river water and (B) in suspended particulate matter and (C) their Li isotope compositions. Data source: Kısakürek et al., 2005; Pogge von Strandmann et al., 2006, 2010, 2017; Vigier et al., 2009; Lemarchand et al., 2010; Millot et al., 2010; Wimpenny et al., 2010b; Bagard et al., 2015; Dellinger et al., 2014, 2015; Liu et al., 2015; Pogge von Strandmann and Henderson, 2015; Wang et al., 2015; Henchiri et al., 2016; Manaka et al., 2017; Bastian et al., 2019; Gou et al., 2019. The river and seawater lines are from Huh et al. (1998) and Chan and Edmond, (1988), and the upper continental crust line is from Teng et al. (2004).

Due in part to the large mass difference between ${}^6\text{Li}$ and ${}^7\text{Li}$, Li isotope fractionation is significant during the chemical weathering. Based on modeling approaches and observations, Li isotope compositions mainly depends on the fraction of secondary minerals formation relative to the primary mineral dissolution. During the primary mineral dissolution, no significant Li isotope fractionation occurs, which has been identified by laboratory

experiments (Pistiner and Henderson, 2003; Wimpenny et al., 2010; Verney-Carron et al., 2011) and by field studies (Ryu et al., 2015). The secondary mineral formation is the major process responsible for Li isotope fractionation, with fractionation ranging from -11‰ to -21‰ (Vigier et al., 2008; Millot et al., 2010; Dellinger et al., 2014). However, in natural environments, the dissolved Li isotope compositions are affected by many other factors, such as atmospheric input, carbonate and evaporite dissolution, hydrothermal Li-rich fluids, and anthropogenic activities which may disturb the environment and Li sources. This makes the indication of Li isotopes to weathering intensity particularly ambiguous. For instance, nearly 80 – 100% of dissolved Li in the Changjiang headwater is derived from evaporite dissolution (Ma et al., 2020), and the relative contribution of evaporite decreases to ~ 55% in the Jinshajiang River (Liu et al., 2013; Wang et al., 2015). In the Changjiang basin, the Li contribution from carbonate weathering is generally lower than 4 %, while the anthropogenic inputs may account for 0% – 15% of the dissolved Li flux (Wang et al., 2015).

Interestingly, even after correction of factors mentioned above, dissolved $\delta^7\text{Li}$ values still display a non-linear correlation with weathering intensity (Fig. 15). The dissolved $\delta^7\text{Li}$ values do not increase positively and persistently with the increasing of weathering intensity, as it was early anticipated (Huh et al., 2001; Pogge von Strandmann et al., 2006, 2010; Millot et al., 2010; Wang et al., 2015; Pogger von Strandmann and Henderson, 2015). For easily understanding, the ratio (W/D) between the silicate weathering rate (W) and the total denudation rate (D) was defined to represent the weathering intensity (Bouchez et al., 2014). The very low and high weathering intensity were set to < 0.01 and > 0.1 by Dellinger et al. (2015). Low dissolved $\delta^7\text{Li}$ values can be observed in river systems with very low or high weathering intensity (Fig. 15). At very low weathering intensity, physical erosion produces large amounts of fresh material for dissolution, but generally no secondary minerals form due to less water-rock reaction time. In contrast, at very high weathering intensity, the climate and long resident time favor the dissolution of secondary minerals. Higher dissolved $\delta^7\text{Li}$ values only occurs at intermediate weathering intensity that most ^6Li partitions into the secondary minerals (Pogge von Strandmann and Henderson, 2015). As shown in Figure 15, the Changjiang mainstream samples are mostly distributed in the left side, indicating low to intermediate weathering intensity. The weathering intensity is consistent with the result determined by elemental compositions of mainstream sediments (Yang et al., 2004, Shao and Yang, 2012).

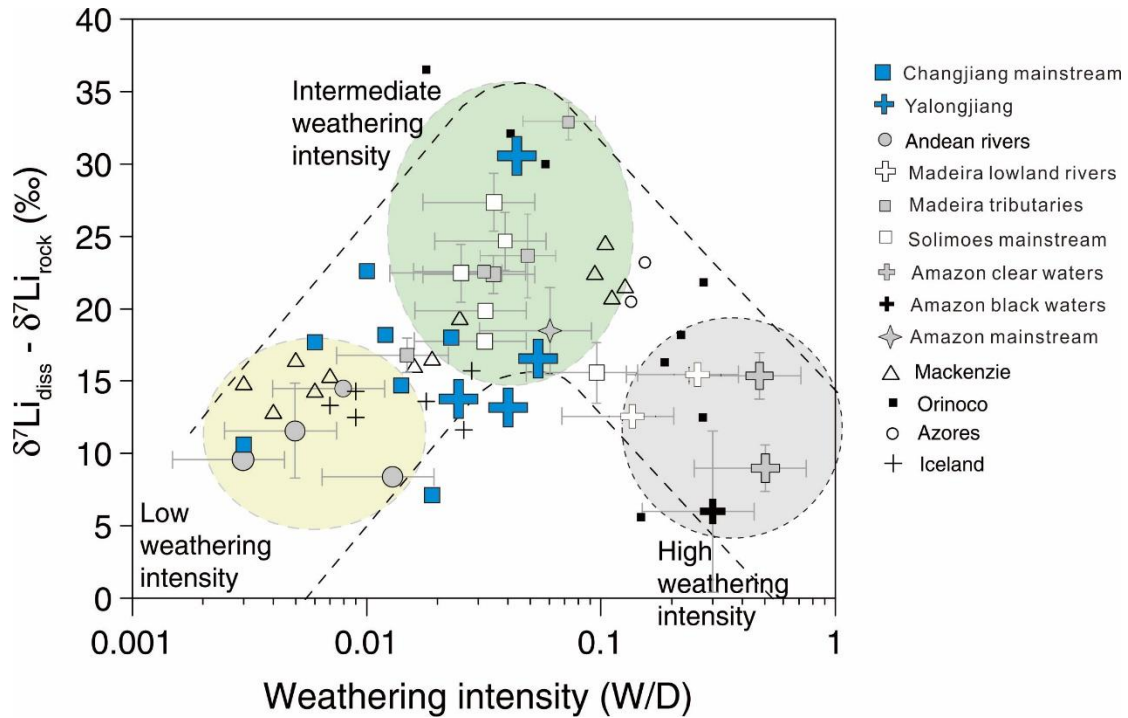


Figure 15 : Dissolved Li isotope composition corrected from the composition of the bedrock ($\delta^7\text{Li}_{\text{diss}} - \delta^7\text{Li}_{\text{rock}}$) vs. silicate weathering intensity (W/D). W represents silicate weathering rate, and D is total denudation rate. Lithium isotope data are from Huh et al. (2001), Pogge von Strandmann et al. (2006, 2010), Vigier et al. (2009), Millot et al. (2010b), Wang et al. (2015), Ma et al. (2020). This graph is modified after Dellinger et al. (2015).

Relative to the dissolved load, the Li behavior observed in particulate materials is less explored. Indeed, the riverine SPM samples can be considered as a mixture of different primary lithologies (igneous rocks, metamorphic rocks and sedimentary rocks) and their respective weathering products (Dellinger et al., 2014). Based on the compilation of literature data, the average $\delta^7\text{Li}$ values of bedrocks are $4.3 \pm 0.9\text{‰}$ of mid-oceanic basalt, $0 \pm 1.6\text{‰}$ of igneous rocks, $-0.5 \pm 1\text{‰}$ of shale, $0 \pm 2\text{‰}$ of metamorphic rocks (Chan et al., 1983; Teng et al., 2004; Dellinger et al., 2014). As shown in Fig. 14C, there is a large overlap of $\delta^7\text{Li}$ values between SPM samples and the bedrocks. This implies that SPM samples contain parts of unweathered rock fragments, and the influence of lithology on $\delta^7\text{Li}$ should be corrected first for the chemical weathering investigation (Dellinger et al., 2017). During sediment transport, hydrodynamic sorting separates coarse-grained quartz, feldspar and fine-grained clays into different parts (Lupker et al., 2012; Bouchez et al., 2012; Guo et al., 2018). Consequently, Li isotope compositions of SPM samples from the floodplain rivers are generally more negative than the bedload. In contrast, there is less difference in mountainous areas. Thus, the comparison of $\delta^7\text{Li}$ in different grain size should be cautious. With the correction of lithology and grain size, particle $\delta^7\text{Li}$ values define a negative relationship with the W/D, as suggested

by Dellinger et al. (2017). Relative to the mainstream samples, corrected $\delta^7\text{Li}$ values of sediments in the Changjiang lowlands are lower (Fig. 16), demonstrating stronger weathering intensity there.

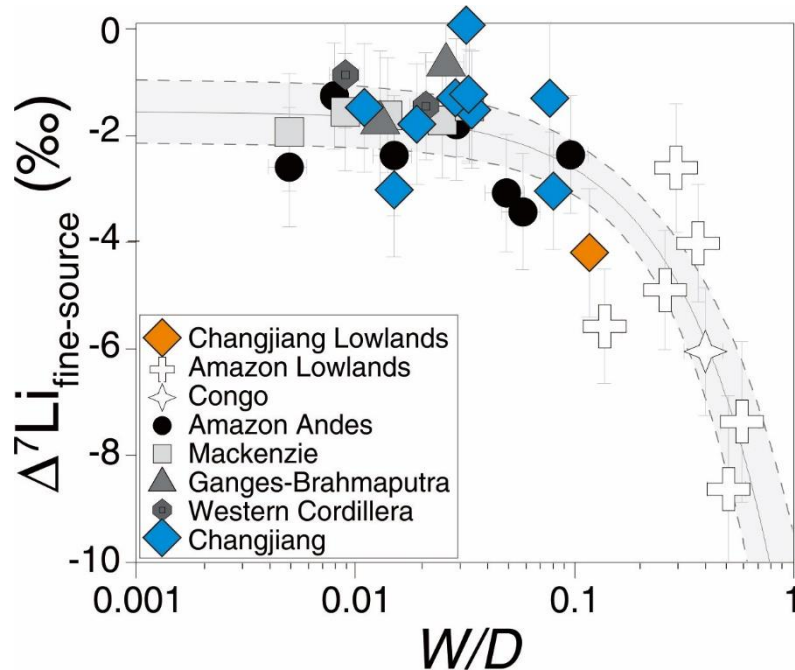


Figure 16 : Li isotope composition of fine-grained sediments corrected from the source rock ($\Delta\delta^7\text{Li}_{\text{fine-source}}$) vs. silicate weathering intensity (W/D). Modified after Dellinger et al. (2017).

2.5 Conclusion of this chapter

In this chapter, I reviewed the source of sediment transported by the Changjiang River into the East China Sea, chemical weathering studies in the Changjiang basin over different timescales and how Li isotopes were used in the literature for tracing chemical weathering. Apparently, chemical weathering studies in the Changjiang basin are complex, in term of lithology, climate and human activities. The influence of sediment source changes on sediment geochemical compositions need to be first investigated. For instance, the sediment geochemical compositions downstream of the TGD can be either caused by sediment source changes or by floodplain weathering. Over millennium or sub-orbital timescales, chemical weathering intensity variations resulting from monsoon climate oscillations need to be further studied, because it can be caused by erosional pattern change within the basin as well. Finally, Li isotopes studies in the Changjiang basin, especially in its estuary, are rare. The geochemical composition changes of sediments passing through the mixing zone question the reliability of sedimentary archives in terms of past weathering and paleoclimate.

Chapter 3: Materials and Methods

In this chapter, the samples and methods are introduced. Briefly, nearly 200 samples were collected in the Changjiang basin by myself or my colleagues since 1997. These samples include bank sediments, river bed sands, suspended particulate matters (SPM), sediment core and water samples, which cover the Changjiang mainstream, major downstream tributaries and estuary (Fig. 17). The bank sediments (red stars in Fig. 17), river bed sands (black square in Fig. 17), SPM samples (blue stars in Fig. 17) and core LGZ (purple star in Fig. 17) were used to investigate the influence of the TGD on the downstream sediment geochemical composition. Only major elements (i.e. Na, K, Mg, Ca and Si) were measured for these samples. The sediment core CM97 (green star in Fig. 17) was used to study the feedback between chemical weathering and climate over the last 14 kyr in the Changjiang basin. Clay fractions ($<2 \mu\text{m}$) were separated first from the bulk sediments, and then elemental concentrations (i.e. Li, Al and Na) and Li-Nd isotope compositions were analyzed. SPM and water samples collected in the Changjiang estuary (red cycles in Fig. 17) were used to investigate Li isotopic behavior during land-sea interaction. Elemental concentrations (i.e. Li, Na, Ca, Si and Al), Li isotope compositions and mineral assemblages were analyzed for the three phases (SPM, waters and exchangeable fractions). This chapter relates all the corresponding methods used for these various works.

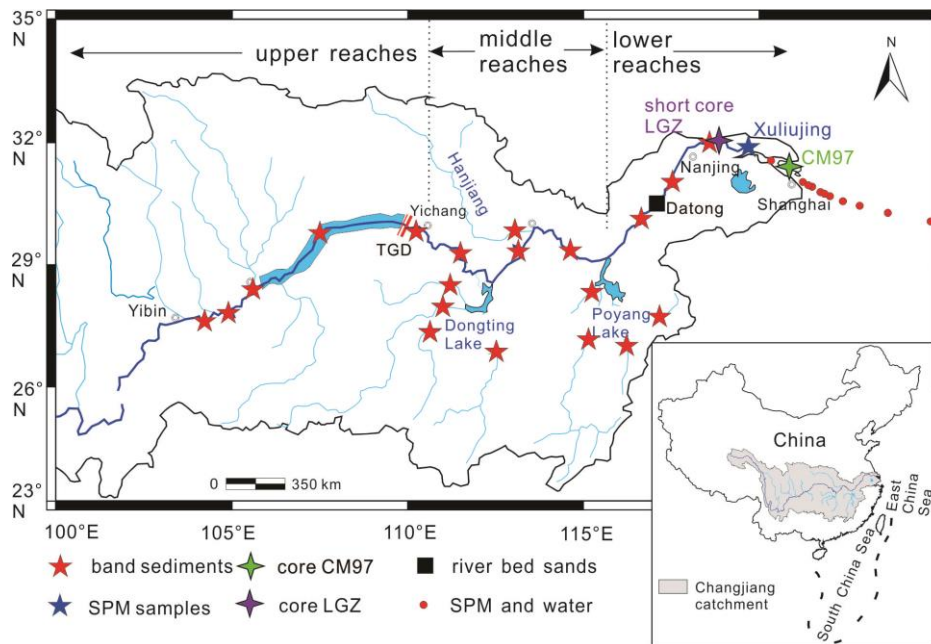


Figure 17 : Sketch map showing location of all samples collected for this study. SPM means suspended particulate matters, and TGD represents the Three Gorges Dam. SPM samples were collected in water column with different depths.

3.1 Samples

A total of 5 river-bed sand (RBS) samples were collected by ship-based grab sampler in 2010 and 2011 at Datong gauging station (black square in Fig. 3.1), 600 km landward of the river mouth. The river bank samples within the upper Changjiang basin were collected in May, 2018. These samples were collected from the mainstream (Fig. 17 and Table 1). For the mid-lower basin, the river bank sediment samples were collected in July 2018, including 7 from the Changjiang mainstream, 3 from the Dongting Lake tributaries, 7 from the Poyang Lake tributaries and 1 from the Hanjiang river (Fig. 17 and Table 1).

Table 1: Basic information for the river bank samples collected and analyzed in this study

Sample ID		Location	Longitude	Latitude	Date
CQ		Chongqing	106.5196	29.4228	2018.07
HJ		Hejiang	105.8258	28.8248	2018.07
LZ	Upper reaches	Luzhou	105.3709	28.8546	2018.07
WZ		Wanzhou	108.4267	30.7615	2018.07
YZ18YC		Yichang	111.2742	30.7047	2018.07
YE18-JLX		Jianli	113.2144	29.5575	2018.05
YZ18-JY	Middle reaches	Jiayu	114.0003	30.0533	2018.05
YZ18-HS		Huangshi	115.3725	29.9948	2018.05
YJCD18		Changde	111.5201	28.9361	2018.05
ZS18	Dongting Lake	Yiyang	112.2147	28.5961	2018.05
LS18-S		Lixian	111.7229	29.6205	2018.05
YTXJ18		Shangrao	116.8014	28.4763	2018.05
NCGJ		Nanchang	116.0165	28.8342	2018.05
CH18		Poyangxian	116.7143	28.9811	2018.05
FH18	Poyang Lake	Jinxian	116.1704	28.1872	2018.05
YXXS18		Yongxiu	115.8156	29.0330	2018.05
BH18		Raoshan	116.5905	29.0471	2018.05
YTXJ18		Shangrao	116.8014	28.4763	2018.05
HJ18	Hanjiang River	Zhongxiang	112.6017	31.0731	2018.05
YZ18-WH		Wuhu	118.2831	31.2939	2018.05
YZ18AQ	Lower reaches	Anqing	116.9567	30.4478	2018.05
YZ18-ZJ		Zhenjiang	119.3108	32.2011	2018.05
YZ18NT		Nantong	120.5689	32.0458	2018.05

Generally, a wooden spade is used to collect bank sediments at the field, and I usually took sediments at 10 cm below the surface and mix several kilograms of different aliquots, directly on the field, in order to get a representative sample. Once at the laboratory, these samples were dried to constant weight at 60°C temperature, and were reserved in plastic sealing bags. The field work mentioned above were completed by my colleagues Chao Li, Xiangtong Huang, Ergang Lian and Yalong Li from Tongji University.

18 suspended particulate matter (SPM) samples were collected during the wet season (i.e. June, August, and October) in 2014 at the Xuliujing gauging station (Fig. 17), approximately 100 km upstream of the river mouth. More detail information is reported in Table 2. The average water depth at Xuliujing during the sampling period was 50 m. For each month, 6 SPM samples were collected along a vertical profile from 0 to 50 m in depth, with a sampling interval of 10 m. Because the sampling site is in the central of river channel, about 50 L river water was collected first by staffs of Xuliujing gauging station, and then I filtered the water on-site using a 0.45 μm membrane of cellulose acetate to collect particulate matter. In the laboratory, SPM samples were washed from the membrane using Milli-Q water, and all these samples were dried to constant weight at 40°C temperature for storage.

Table 2: Basic information corresponding to the suspended particulate matters (SPM) collected along depth profiles at the Xuliujing station

ID	Location	Longitude (E)	Latitude (N)	Sampling depth (m)	Sampling date	Suspended load (mg/l)
S370	Xuliujing	120.9647	31.7919	0	2014.06	26
S371	Xuliujing	120.9647	31.7919	10	2014.06	102
S372	Xuliujing	120.9647	31.7919	20	2014.06	88
S373	Xuliujing	120.9647	31.7919	30	2014.06	91
S374	Xuliujing	120.9647	31.7919	40	2014.06	165
S375	Xuliujing	120.9647	31.7919	50	2014.06	165
S424	Xuliujing	120.9647	31.7919	0	2014.08	84
S425	Xuliujing	120.9647	31.7919	10	2014.08	77
S426	Xuliujing	120.9647	31.7919	20	2014.08	95
S427	Xuliujing	120.9647	31.7919	30	2014.08	114
S428	Xuliujing	120.9647	31.7919	40	2014.08	108
S429	Xuliujing	120.9647	31.7919	50	2014.08	109
S472	Xuliujing	120.9647	31.7919	0	2014.10	65
S473	Xuliujing	120.9647	31.7919	10	2014.10	75
S474	Xuliujing	120.9647	31.7919	20	2014.10	84
S475	Xuliujing	120.9647	31.7919	30	2014.10	100
S476	Xuliujing	120.9647	31.7919	40	2014.10	98
S477	Xuliujing	120.9647	31.7919	50	2014.10	128

For completing the work about the impact of the TGD (described in chapter 4), a small continental core (core LGZ), 2 m long, was collected in the central bar at the lower Changjiang mainstream in 2008 (33°18'393 N, 119°45'218 E), about 150 km upstream of the river mouth (purple star in Fig. 3.1). The core was split and subsampled at 2-cm intervals, and stored in the State Key Laboratory of Marine Geology since 2008. The depositional age of bottom sediments can date back to about 150 years ago, based on the ^{210}Pb geochronology (Zhan et al., 2010). This work was done by my colleague Wan Zhan in 2010. During my

Ph.D., 16 samples were taken throughout core LGZ for major-element analyses, with an estimated average temporal resolution of ~10 years.

The water and SPM samples in the Changjiang Estuary were collected during the KECES (Key Elements Cycling in the Changjiang-Estuary-Shelf Transect) cruise from 28 August to 4 September, 2019. This cruise was organized by the State Key Laboratory of Marine Geology, and led by Prof. Shouye Yang (Tongji University). Water samples were first collected using a 60 L bottle, and filtered on-site immediately through 0.45 μm cellulose acetate membranes after the sampling. Then, about 50 ml of the filtered samples were acidified to $\text{pH} < 2$ with concentrated HNO_3 , and stored in pre-cleaned centrifuge tubes. These acidified samples were used for measurement of cations and Li isotope ratios. Their basic information are reported in Table 3. These samples were collected by myself and my colleague Zheng Lai from the Tongji University (Fig. 18).

Table 3: Basic information of suspended particulate matters and water samples collected in the Changjiang Estuary

	Longitude $^{\circ}\text{E}$	Latitude $^{\circ}\text{N}$	Depth m	Salinity ‰	pH	T $^{\circ}\text{C}$	SSC mg/l
C1S	121.0561	31.7805	-1	0.1	7.8	28.9	44.7
C1B	121.0561	31.7805	-10	0.1	7.8	28.9	58.4
C5S	121.7494	31.2883	-1	0.1	7.8	28.9	198.9
C5B	121.7494	31.2883	-16	0.1	7.8	29.1	279.8
C6S	121.9116	31.1529	-1	0.2	8.0		575.1
C6B	121.9116	31.1529	-7	0.2	7.9		
C6-1S	121.9674	31.0939	-1	1.0	7.8	28.1	
C6-1B	121.9674	31.0939	-6	3.2	7.8	27.7	1517.2
C6-2S	121.9860	31.0852	-1	2.7	7.8	27.8	384.1
C6-2B	121.9860	31.0852	-6	6.2	7.8	27.4	2078.5
C6-3S	121.9850	31.0843	-1	9.1	7.8	26.9	478.9
C6-3B	121.9850	31.0843	-6	9.1	7.8		1541.3
C8S	122.2495	31.0217	-1	14.4	7.8	27.5	
C8B	122.2495	31.0217	-6	14.8	7.8	27.5	609.2
C9S	122.3643	31.0019	-1	18.6	7.8	27.1	
C9B	122.3643	31.0019	-10	20.0	7.8	26.8	837.7
C18S	124.9874	29.8646	-1	32.1	8.2	29.4	5.1
C18B	124.9874	29.8646	-62	34.6	7.9	21.9	26.5



Figure 18 : A photo showing all the members involved in the KECES cruise sampling the Changjiang Estuary.

The deltaic core CM97 (~70 m in depth) used for paleo-weathering study (described in chapter 6) was drilled at the modern Changjiang River mouth (31°370' N, 121°230' E) in 1997. The AMS ^{14}C dating on molluscan and/or snail shells was reported by Hori et al. (2001), and then the age model was gained using linear interpolation (Fig. 19). Core CM97 thus recorded the depositional history over past ~14,000 years (Fig. 19), and the sedimentary sequence primarily consists of fluvial and floodplain facies at the bottom (70 – 60.3 m in depth), estuarine to shallow marine facies in the middle part (60.3 – 20.1 m), and deltaic facies at the top (20.1 – 0 m). The average sedimentation rate of core CM97 was 10.1 m/kyr at 13 – 11 ka, and then decreased to 6.6 m/kyr at 11 – 9 ka (Fig. 19). During the middle and early late Holocene, the sedimentation rate of core CM97 was the lowest, with an average of 1.1 m/kyr. During the last 2 kyr, the sedimentation rate abruptly increased to 13.6 m/kyr (Fig. 19). During my Ph.D., a total of 61 samples were selected from core CM97 for geochemical measurements.

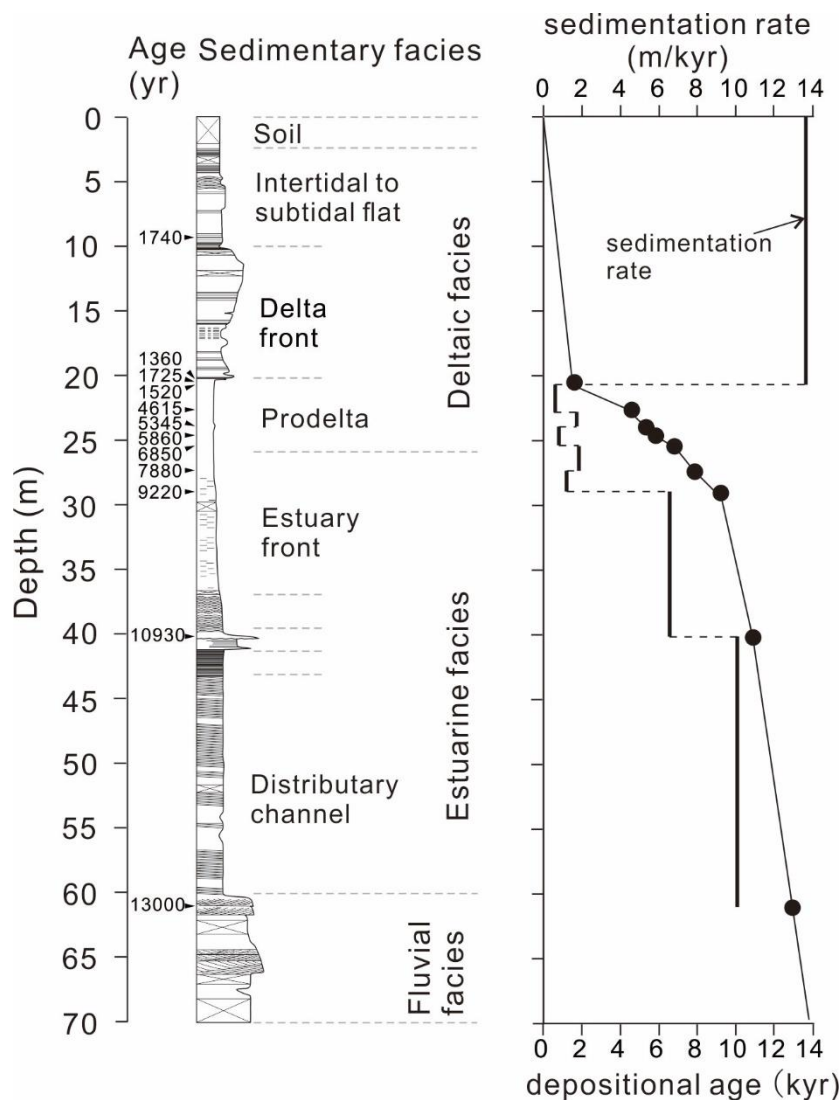


Figure 19 : Sedimentary facies, sedimentation rate and depositional age of core CM97. The ^{14}C ages are shown with a black arrow on the left (Hori et al., 2001).

3.2 Methods

3.2.1 Clay fraction (<2 μm) separation from bank and core sediments

After mixing, about 1 g bulk sediment was first split in two distinct groups (i.e. > 63 μm sand fraction and < 63 μm fine-grained fraction) using a wet sieving method (Fig. 20). The fine-grained fraction (<63 μm) was immersed into 20 ml 1N HCl for twenty minutes to remove carbonates at room temperature. The carbonate content of downstream bank sediments in the Changjiang basin is about 6% (Yang et al., 2002), so this method is effective enough for carbonate removal. After the leaching, the residue was washed three or four times with Milli-Q water until the supernatant pH gets to neutral. Afterwards, the fine-grained sediments were mixed with 50 ml Milli-Q, and shook to make them mix homogeneously.

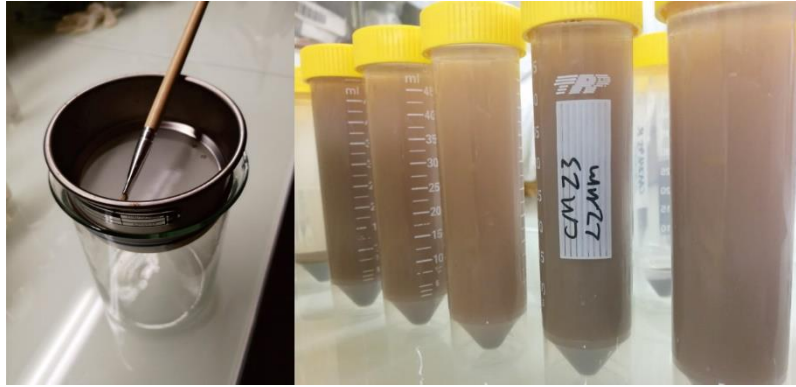


Figure 20 : photos showing the instrument used for clay fraction separation

The velocity of particle deposition (v) can be calculated based on the Stoke's Law at room temperature:

$$v = \frac{\rho_P - \rho_w}{18\mu} g d^2$$

Where ρ_P and ρ_w represent density of particles and water, μ is dynamic viscosity of water, g represents acceleration of gravity and d is particle diameter. The parameters are listed in Table 4.

Table 4: parameters used to calculate velocity of particle deposition

ID	symbol	value	unite
deposition velocity	v		m/s
particle density	ρ_P	1800	kg/m ³
water density	ρ_w	1000	kg/m ³
dynamic viscosity of water	μ	0.001	Pa.s
acceleration of gravity	g	9.81	m/s ²
particle diameter	d	2×10^{-6}	m

In our experiment, 25 ml turbid liquid (~4 cm) was extracted using pipette after 6h22 standing. After centrifuging, clay fraction was freeze-dried.

3.2.2 Exchangeable phase extraction

I expect that the exchangeable phase includes all the Li absorbed onto the mineral surface and/or in the interlayer position (Fig. 13). In this study, the exchangeable phase extraction was conducted for SPM samples collected in the Changjiang Estuary, following the established procedures by Vigier et al. (2008). Briefly, 10 ml of 1 N ammonium chloride (NH₄Cl) was added to the pre-cleaned tube, mixing with about 0.1 g SPM samples. Then, these tubes were placed on a rotary shaker to ensure the full reaction (Fig. 21). After 1h

mixing, the slurry was then centrifuged at 4000 rpm and finally the supernatant was decanted. In order to extract quantitatively all the Li absorbed onto the mineral surface and/or in the interlayer position, the SPM samples had to be saturated twice using with NH_4Cl solution. Note that the NH_4Cl solution is weakly acidic, and parts of carbonate were possibly dissolved.



Figure 21 : A photo showing the rotating shaker used during the exchangeable phase extraction ($2 \times 1\text{h}$).

3.2.3 Elemental concentration analyses

In this study, the SPM and RBS samples were analyzed for major elements by Inductively Coupled Plasma-Optical Emission Spectrometers (ICP-OES, model: IRIS Advantage), and the bank sediment and core samples were analyzed by X-ray fluorescence (XRF, model: AXIOSmAX). The instrument precisions are better than 1% for XRF and 0.5% for ICP-OES. The Li concentration was measured by Inductively Coupled Plasma Mass Spectrometry (ICP-MS, model: Agilent 7900). All of these analyses were conducted in the State Key Laboratory of Marine Geology at Tongji University.

About 50 mg of each sample was ground in an agate mortar, and then ignited in a muffle furnace at 600°C in order to weigh loss of ignition (LOI) and remove organic matter before acid digestion. In order to verify a potential bias related to the sample pre-treatment, I selected 6 SPM samples and treated them with 1M HCl following the method of Bi et al. (2015), while all other data come from untreated samples. The objective of the 1M HCl

treatment was to remove the carbonate fraction. For the ICP-OES measurement, about 50 mg powder samples were dissolved with a mixture of 1:1 concentrated HNO₃ and HF in a tightly closed Teflon vessel for at least 48 h at 190°C. After drying, samples were re-dissolved in HNO₃ to remove any fluorides. Finally, samples were re-digested in 2 ml 30% HNO₃ at 190°C. The Si concentration was obtained by assuming the total content of major oxide and trace elements in the residues is 100%, following the calculation method of Guo Y et al. (2018). The errors of calculated Si concentration are less than 8%. For the XRF method, the powder samples were directly fused with lithium tetraborate (Li₂B₄O₇) at 1050°C to make a glass disk for the XRF measurement. The analytic precision and accuracy were monitored by the simultaneously processed standards of BCR-2 for ICP-OES and GSR-3 for XRF (Table 5). The results showed that the accuracy of major element is generally better than 5% and the precision (one standard deviation) is better than 1%.

Table 5: Major element concentrations of rock reference materials

Sample ID	SiO ₂ %	Al ₂ O ₃ %	CaO %	K ₂ O %	MgO %	Na ₂ O %
BCR-2		11.7	6.8	1.7	3.0	3.2
		13.2	6.8	1.8	3.5	3.3
		13.6	6.8	1.8	3.7	3.3
		13.3	6.9	1.8	3.6	3.3
		13.4 ^a	7.2 ^a	1.8 ^a	3.6 ^a	3.1 ^a
GSR-3	45.0	14.4	8.8	2.3	7.6	3.6
	44.9	14.5	8.8	2.3	7.6	3.6
	44.6 ^a	13.8 ^a	8.8 ^a	2.3 ^a	7.8 ^a	3.4 ^a

Note: 'a' represents data compiled from previous studies (<http://georem.mpch-mainz.gwdg.de/>). The BCR-2 was analyzed by Inductively Coupled Plasma-Optical Emission Spectrometers (ICP-OES), and the GSR-3 was measured by AXIOSmAX X-ray fluorescence (XRF)

3.2.4 Mineralogical analyses

The mineral compositions of SPM samples were carried out by the X-ray diffraction (XRD) using a PANalytical X'Pert PRO diffractometer at the State Key Laboratory of Marine Geology, Tongji University. About 1.5 g SPM samples were first ground to <200 mesh in an agate mortar. Then, the powder was pressed into sample holder for XRD measurement. Mineral identification was made by Siroquant software.

3.2.5 Nd isotope analyses

The Nd purification was conducted with a two-step method. The Rare Earth Elements (REE) were first separated using 2.5 N HCl elution on an ion-exchange column filled with

Bio-Rad AG50W-X12, 200-400 mesh resin. Then, the Nd was separated from the REE solution using 0.25 N HCl elution. Finally, the Nd isotope ratios were determined using a MC-ICP-MS Neptune plus at the State Key Laboratory of Marine Geology, Tongji University. The standard reference material JNdi-1 was used to correct the instrumental signal drift. The accuracy of the isotopic measurements was monitored by analyzing basaltic rock reference BCR-2, with average of 0.512632 ± 0.000023 (2SD, n=18). This value is close to the published data of 0.512635 ± 0.000029 shown in GeoReM website (http://georem.mpch-mainz.gwdg.de/sample_query_pref.asp) (Fig. 22). In this study, Nd isotope values are reported as ϵNd , which is equal to $[(^{143}\text{Nd}/^{144}\text{Nd})_{\text{samples}} / (^{143}\text{Nd}/^{144}\text{Nd})_{\text{CHUR}} - 1] \times 10^4$. The CHUR represents Chondritic Uniform Reservoir, with a value of 0.512638.

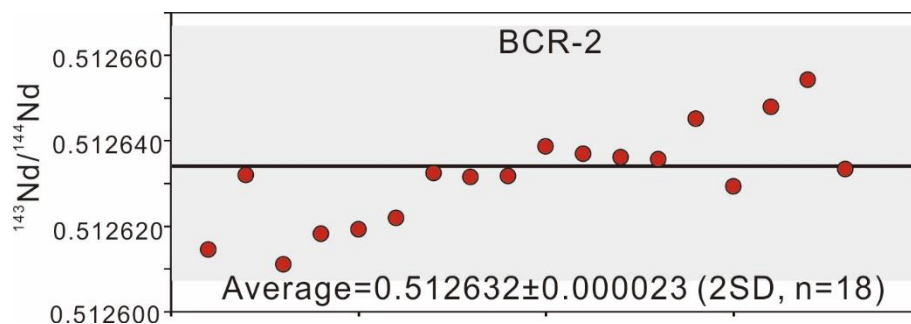


Figure 22 : The measured $^{143}\text{Nd}/^{144}\text{Nd}$ ratios during my PhD for the international o basaltic reference BCR-2. The black line and grey bar represent the compiled data of BCR-2, with average of 0.512635 ± 0.000029 .

3.2.6 Li isotope analyses

About 10 mg samples were ground to <200 mesh in an agate mortar and then were digested first using 3:1 HF/HNO₃ solution at 70°C for several hours. Afterwards, the solution was evaporated and re-dissolved with concentrated HNO₃ several times. The sample was then re-digested with 3:1 HCl/HNO₃ solution. Finally, the solution was evaporated and re-dissolved in 1 N HCl (Fig. 23A). At this stage, the solution is systematically centrifuged to ensure the lack of any solid residue. The Li purification was performed on a cationic resin column (Fig. 23B), following the method described in Vigier et al. (2008). In this method, 1 N HCl was used as eluent to purify Li. For each batch of column chemistry, one blank and one inhouse standard reference (i.e. basaltic reference BE-N or carbonate reference 7Li-N) were involved. All these experiments described above were conducted at Laboratory of Oceanography of Villefranche-sur-Mer (LOV), Sorbonne University.

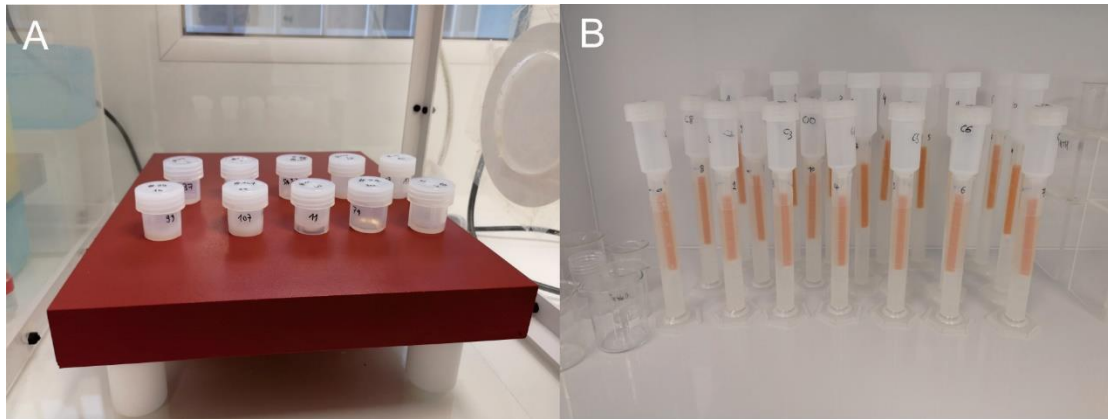


Figure 23 : Photos showing (A) the acid attack process and (B) resin columns used for Li purification.

Li isotopes measurement were performed using a Multi-collector inductively coupled plasma mass spectrometry (MC-ICP-MS) Neptune plus (ThermoFisher) at the Ecole Normale Supérieure de Lyon (National Facilities). The Neptune plus is equipped with 7 ion counters and 9 Faraday cups. All the Faraday cups are equipped with $10^{11} \Omega$ resistors. The distance between two farthest Faraday cups (L4 and H4) equal a relative mass dispersion of $\sim 17\%$, which is theoretically able to simultaneously analyze ${}^6\text{Li}$ and ${}^7\text{Li}$. However, two ion counters on the corresponding cups obstruct the movement, thus, zoom optics were applied to make the simultaneous analysis of ${}^6\text{Li}$ and ${}^7\text{Li}$. The sample solution was introduced using membrane de-solvation system (Aridus II). Within the introduction system, the newly designed X skimmer cone and Jet sampler cone were applied. The operating parameters of MC-ICP-MS for Li isotope analyses are listed as follow (Table 6):

Table 6: Major element concentrations of rock reference materials

Instrument	Neptune Plus
RF Power	1200 W
Guard electrode	On
Cool gas	15 l/min Ar
Auxiliary gas	0.76 l/min Ar
Sample gas	1-1.16 l/min Ar
Resolution setting	Low
Cycles/Blocks	30 cycles/1 block
Vacuum-ICP	$\sim 2 \times 10^{-7}$ mbar
Vacuum-analyzer	$\sim 5 \times 10^{-9}$ mbar
Cup configuration	L4 (${}^6\text{Li}$) and H4 (${}^7\text{Li}$)
Cones	X skimmer cone and Jet sampler cone
Sensitivity	~ 1 V for ${}^7\text{Li}$ at 1 ng/g
background (2% HNO_3)	60 mv

Generally, a mean ${}^7\text{Li}$ signal of about 1 V per ng/g Li could be obtained. During the measurement, the initial ${}^7\text{Li}$ instrumental background is generally 60 mv, and this value could increase to ~90 mv after 2 days working. The signal intensity of blank samples after column chemistry cannot be distinguished from this instrumental background. The samples and standard L-SVEC solution were generally diluted to ~4 ppb for instrumental test. The determination of ${}^7\text{Li}/{}^6\text{Li}$ ratio is implemented by a sample-standard bracketing (SSB) method, with analysis sequence of Blank1-LSVEC1-Blank2-Sample-Blank3-LSVEC2-Blank4. The SSB method can correct the instrumental signal drift and background, which is helpful for analyses accurately and precisely. The correction equation is as follow:

$$\delta {}^7\text{Li} = \left[\frac{\left(\frac{{}^7\text{Li}_{\text{sample}} - ({}^7\text{Li}_{\text{Blank2}} + {}^7\text{Li}_{\text{Blank3}})/2}{({}^6\text{Li}_{\text{sample}} - ({}^6\text{Li}_{\text{Blank2}} + {}^6\text{Li}_{\text{Blank3}})/2)} \right)}{\left(\frac{{}^7\text{Li}_{\text{LSVEC1}} - ({}^7\text{Li}_{\text{Blank1}} + {}^7\text{Li}_{\text{Blank2}})/2}{({}^6\text{Li}_{\text{LSVEC1}} - ({}^6\text{Li}_{\text{Blank1}} + {}^6\text{Li}_{\text{Blank2}})/2)} + \frac{{}^7\text{Li}_{\text{LSVEC2}} - ({}^7\text{Li}_{\text{Blank3}} + {}^7\text{Li}_{\text{Blank4}})/2}{({}^6\text{Li}_{\text{LSVEC2}} - ({}^6\text{Li}_{\text{Blank3}} + {}^6\text{Li}_{\text{Blank4}})/2)} \right)/2} - 1 \right] \times 1000$$

Without separation chemistry, the mean value was $+30.3 \pm 0.1\%$ (2SE, n=26) for Li7-N pure Li solutions, which compare well with published values of $+30.2 \pm 0.3\%$ (Carignan et al., 2007). The accuracy of the isotopic measurements was monitored by analyzing BE-N basaltic rocks. Repeated measurements yielded mean $\delta {}^7\text{Li}$ value of $+5.0 \pm 0.4\%$ (2SD), which is slightly higher than published value of $+4.6 \pm 0.2\%$. In addition, three samples were processed repeatedly using the same but independent chemical procedure, yielding values of $-1.9 \pm 0.4\%$ (2SD), $-1.5 \pm 0.4\%$ (2SD) and $-1.3 \pm 0.2\%$ (2SD), respectively (Fig. 24).

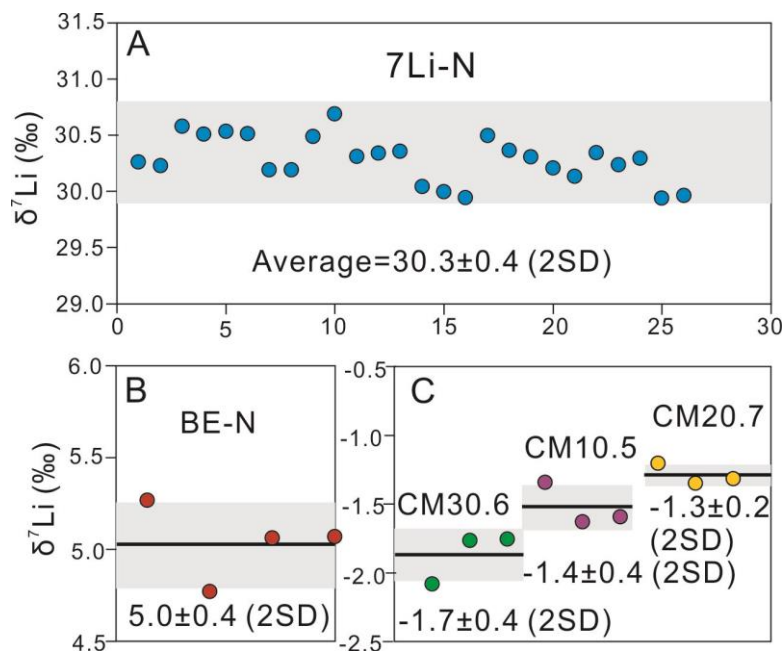


Figure 24 : Li isotope compositions ($\delta {}^7\text{Li}$) of 7Li-N, BE-N, CM30.6, CM10.5 and CM20.7. The 7Li-N solution were analyzed without column chemistry. These materials were used to verify the analytical accuracy.

Chapter 4: Progressive evolution of the Changjiang (Yangtze River) sediment weathering intensity since the Three Gorges Dam operation

Chemical weathering of silicate rocks plays a critical role in regulating the Earth's climate through the consumption of atmospheric carbon dioxide on geological timescales. Numerous studies have attempted to understand the interactive roles of climatic, tectonic, lithological and hydrological parameters on chemical weathering process (Garrels and Mackenzie, 1971; Bluth and Kump, 1994; Louvat and Allègre, 1997; Gaillardet et al., 1999a, 1999b; Kump et al., 2000; West et al., 2005; Gislason et al., 2009; Maher and Chamberlain, 2014; Torres et al., 2015; Winnick and Maher, 2018). To date, more than 60% of river worldwide longer than 1,000 km are strongly affected by human activities, especially by intense dam constructions (Dynesius and Nilsson, 1994; Syvitski et al., 2005; Grill et al., 2019). However, the impacts of these dams on downstream sediment chemistry remains poorly known, which hinders our understanding of continental weathering controls at large scale.

In this chapter, the temporal variations of elemental compositions of suspended particulate matter (SPM), river-bed sand (RBS), bank sediments and core samples collected downstream of the TGD were systematically investigated (Fig. 25), in aim to testify whether the Three Gorges Dam (TGD) construction has altered the chemistry of downstream sediment into the East China Sea. In order to achieve this goal, the evolution of sediment contribution from each end-members (i.e. upper reaches, Dongting Lakes, Poyang Lakes, Hanjiang River and resuspended river bed sediment in the mid-lower mainstream) and mobile element variability of downstream sediments were first estimated. Afterwards, based on the observation of K/Si changes since 2003, a possible mechanism responsible for downstream weathering signal variations was proposed. Overall, in this chapter, by comparing our results with literature data for sediments collected from the Changjiang basin over the last two decades, we confirm a significant downstream temporal variation of sediment-weathering intensity, and highlight the potential impact of the TGD on altering dissolved element fluxes to the East China Sea. This study has published on JGR: Earth Surface.

Abstract :

Chemical composition of river sediments and dissolved load are classically used to infer controls on continental weathering, and therefore exert an important role on the understanding of the global carbon and biogeochemical cycles. To date, most studied river basins are strongly impacted by dam constructions, however, the effects of dams on sediment chemical compositions are little known. The Three Gorges Dam (TGD) is one of the largest dams in the world and was constructed in 2003 in the Changjiang basin. In order to investigate the impact of this dam on downstream sediment chemistry, temporal variation of sediment weathering intensity is reported here based on analyzed and compiled data from between 1997 and 2018. Downstream sediments collected before 2003 are characterized by weak weathering intensity, in agreement with the overwhelming flux and fast transfer of sediments derived from the mountainous upper watershed. After the TGD construction, strong mid-lower riverbed erosion changed the roles of the mid-lower reaches from important sinks to major sources of sediments delivered to the East China Sea. This resulted in a progressive change of the sediment chemistry because the eroded mid-lower riverbed sediments were more deeply weathered, as confirmed by 150-year-old sediment cored in the lower mainstream, and by mass-balance calculations. This more intensive weathering may be explained by warmer climate and longer water-rock interaction time in the mid-lower basin. Thus, this study suggests the need to quantify potential bias in weathering intensity and controls caused by damming activity in large river systems.

Keywords: Continental weathering; Three Gorges Dam; Changjiang (Yangtze River); Geochemistry, Anthropogenic activities, River sediments

4.1 Introduction

Chemical weathering of silicate rocks plays a critical role in regulating the Earth's climate through the consumption of atmospheric carbon dioxide on geological timescales. Numerous studies have attempted to understand the interactive roles of climatic, tectonic, lithological and hydrological parameters on chemical weathering process (Garrels and Mackenzie, 1971; Bluth and Kump, 1994; Louvat and Allègre, 1997; Gaillardet et al., 1999a, 1999b; Kump et al., 2000; West et al., 2005; Gislason et al., 2009; Maher and Chamberlain, 2014; Torres et al., 2015; Winnick and Maher, 2018). These studies mainly focused on chemical composition of dissolved and particulate phases of rivers draining large portions of the upper continental crust, from the mountainous valley of headwaters to flat floodplain basins in the mid-lower reaches. To date, more than 60% of river worldwide longer than 1,000 km are strongly affected by human activities, especially by intense dam constructions (Dynesius and Nilsson, 1994; Syvitski et al., 2005; Grill et al., 2019). However, the impacts of these dams on downstream sediment chemistry remains poorly known, which hinders our understanding of continental weathering controls at large scale.

As the largest river in China, the Changjiang (Yangtze River) historically transported about 470 Mt/yr sediments into the marginal sea (Milliman and Farnsworth, 2013), which represents ca. 2.5% of the present-day estimate for the global sediment flux. The annual flux of total dissolved solids from the Changjiang is about 1.54×10^8 tons, placing it as the second highest in the world just after the Amazon River (Gaillardet et al., 1999b; Chen et al., 2002; Moon et al., 2014). The study of weathering and erosion processes in the Changjiang catchment is therefore of great significance for better understanding continental weathering and material cycling from a global perspective. However, the Changjiang basin is one of the most populated areas in the world, with 15–20% of total dissolved solids coming from anthropogenic inputs (Chetelat et al., 2008). In particular, more than 50,000 dams have been constructed within the catchment, among which the Three Gorges Dam (TGD) is the world's largest hydroelectric engineering project (Yang et al., 2014). These dams have largely disturbed the natural sediment “source-to-sink” systems, with more than 80% of sediments derived from the Himalaya mountains and the Tibetan Plateau (Fig. 25a), being retained efficiently in these reservoirs (Yang et al., 2006; Yang et al., 2014). Sediment-transport patterns in the downstream of the TGD also changed from transport-deposition balance to net riverbed erosion. This pattern changed because the sediment-carrying capacity of downstream water flow exceeded the supply of suspended material (Chen et al., 2010; Luo et al., 2012; Lai

et al., 2017). In addition, Wang et al. (2018) reported increased dissolved Si flux in the lower mainstream in recent years, and attributed it to increased flux of biogenic silica redissolution in response to the riverbed erosion downstream of the TGD.

Generally, silicate weathering in the Changjiang basin displays great spatial heterogeneity and is primarily driven by monsoonal climate, while provenance lithology plays a subordinate role (Yang et al., 2004). The upper reaches are overall featured by a weathering-limited regime with significant physical erosion in the eastern Tibet, while the mid-lower reaches are characterized by a transport-limited regime because of its stable tectonics and gentle relief as well as warmer and wetter climate (Bi et al., 2015). Recent studies suggested that the floodplain weathering in the Changjiang basin was likely not significant before the TGD construction. For instance, the averages of Chemical Index of Alteration (CIA) estimated from the sediments sampled in the upper reaches and at the river mouth were not significantly different (Yang et al., 2004, 2013), which implies a weak chemical alteration during the sediment source-to-sink transport. In addition, Chetelat et al. (2013) found that the suspended sediments sampled in 2006 from the mid-lower reaches likely experienced similar extent of chemical weathering compared with that from the upper reaches. These observations seemingly question the importance of floodplain weathering in the Changjiang basin. To our knowledge, the floodplain, colluvial and alluvial plains (mostly <500 m in altitude) are well developed in the mid-lower Changjiang valley, occupying about 44% of the total catchment area.

To date, the influence of TGD construction on weathering signal propagation in the Changjiang basin is less constrained. Most previous studies focused on studying the role of lithology and climate on weathering intensity registered in river sediments. Moreover, their sampling scopes were limited. In order to verify the role of floodplain weathering in the mid-lower Changjiang valley and if the TGD construction has altered the chemistry of downstream sediment, this study investigates the temporal variations of elemental compositions of suspended particulate matter (SPM), river-bed sand (RBS), bank sediments and core samples collected downstream of the TGD. By comparing our results with literature data for sediments collected from the whole river system over the last two decades, we confirm a significant downstream temporal variation of sediment-weathering intensity, and highlight the potential impact of the TGD on altering dissolved element fluxes to the East China Sea.

4.2 River setting

The Changjiang is the largest river in Asia and the third longest river in the world. It is more than 6,300 km long, and has a catchment area of 1.8×10^6 km². In terms of water discharge and sediment flux, the Changjiang River transports nearly 900 km³/yr and 470 Mt/yr to the East China Sea (Milliman and Farnsworth, 2013). According to hydrological and geographic settings, the Changjiang drainage basin is generally divided into three sections (Fig. 25a). The upper reaches indicate the portion from the headwater to Yichang city with 4,500 km in channel length. The middle reaches are 950 km long, running from Yichang to Hukou city. The lower reaches extend from Hukou to the river mouth with a length of about 850 km. The Changjiang catchment is dominated by the East Asia monsoon climate, with the rainfall belt occurring in the mid-lower basin between March and June, and then gradually migrating to the upper basin starting in July (Chen et al., 2010; Yang et al., 2013). The annual average precipitation over the whole basin is ~1100 mm, ranging from 150 mm to 1000 mm in the upper basin and averaging 1200 mm in the mid-lower basin (Chen et al., 2010). More than 60% of the annual precipitation falls during the wet season from May to October. Correspondingly, water discharge during the wet season accounts for 60-70% of its total water discharge. Geographically, the upper watershed features active tectonics and steep mountains, especially in the Jinshajiang valley, with an elevation above 3500 m. The elevations of middle and lower reaches are mostly below 500 m, and floodplains and lakes are widely distributed.

The TGD is located 40 km upstream of Yichang city, which is considered to be the boundary between the upper and middle reaches. The elevation of the TGD is 185 m above the sea level. Impoundment of water began in June 2003, and started its full operation since 2009. Currently, the Three Gorges Reservoir covers upstream river channel over a distance of 660 km (Fig. 25a). The storage capacity of the reservoir is designed to be 39.3 km³, and the water level within the reservoir fluctuates seasonally by 30 m between 145 m and 175 m for flood control (Yang et al., 2014). According to records at Datong (Fig. 25), which is the most seaward gauging station without tidal influence, the sediment flux has decreased from ~ 430 Mt/y between 1950s and 2002 to 152 Mt/y in 2016.

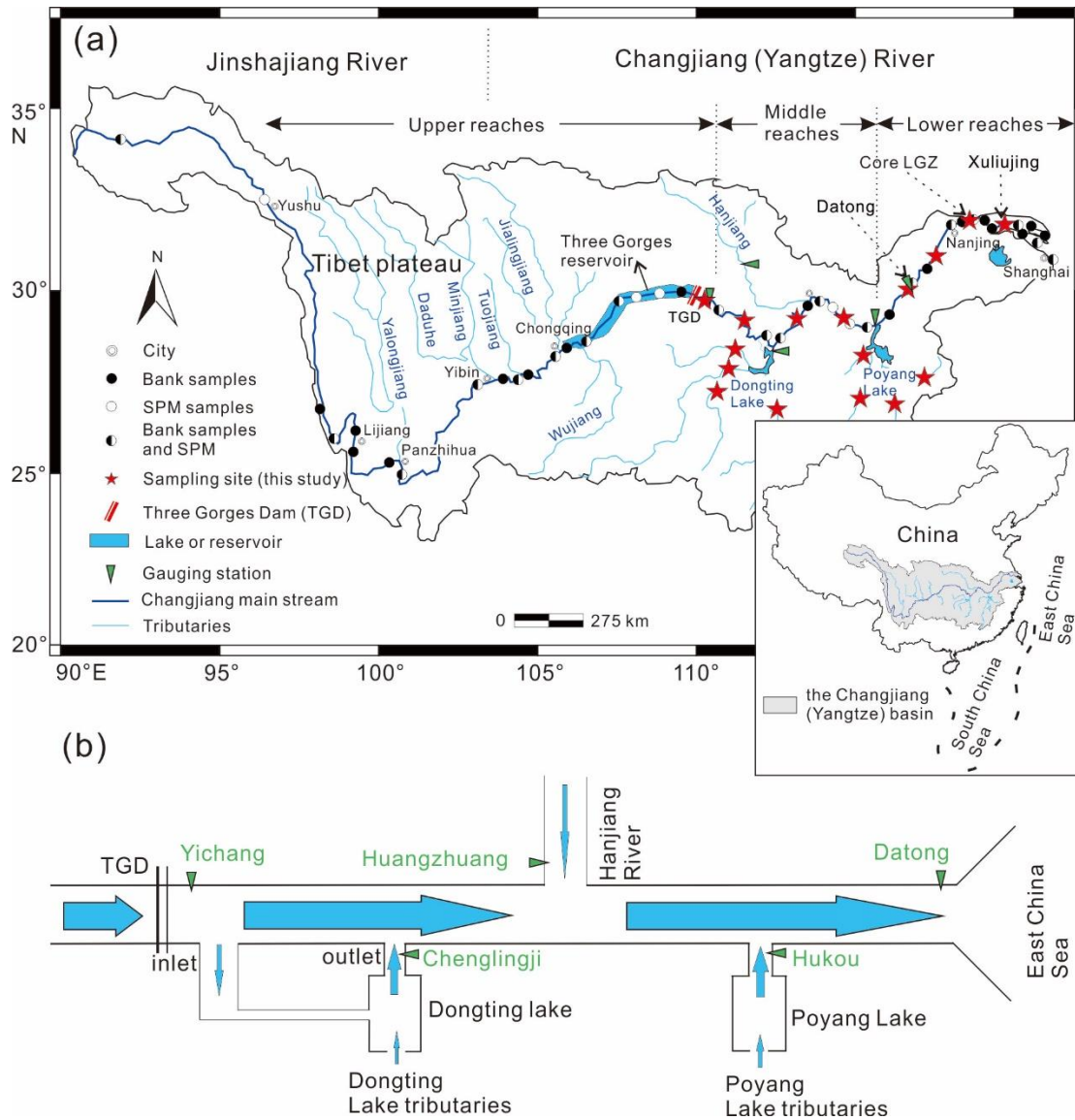


Figure 25 : (a) Schematic map showing the Changjiang drainage basin and (b) a cartoon showing the relative position of tributaries, lakes and gauging stations. Red stars display sampling sites of this study, and circles represent sampling sites for data collected from literatures (Yang et al., 2004, 2013; Ding et al., 2014; He et al., 2015).

4.3 Materials and Methods

4.3.1 Sample collection

A total of 18 suspended particulate matter (SPM) samples were collected in wet season (i.e. June, August, and October) of 2014 at Xuliujing gauging station, approximately 100 km landward from the river mouth (Fig. 1a). The average water depth at Xuliujing during the sampling period was 50 m. For each month, 6 SPM samples were collected along a vertical profile from 0 to 50 m in depth with a sampling interval of 10 m. Generally, about 50 L river water was drawn for each sampling and filtered on-site through a 0.45 μm membrane

of cellulose acetate later to collect particulate matter. The river bank sediment samples were collected within the mid-lower basin in May 2018, including 9 from the Changjiang mainstream, 5 from the Dongting Lake tributaries, 7 from the Poyang Lake tributaries and 2 from the Hanjiang river (Fig. 1a). A total of five river-bed sand (RBS) samples were collected by ship-based grab sampler in 2010 and 2011 at Datong gauging station, 600 km landward of the river mouth. Core LGZ, 2 m long, was collected in the central bar at the lower Changjiang mainstream in 2008 (33°18'39.3 N, 119°45'21.8 E), about 150 km upstream of the river mouth (Fig. 25a). The core was split and subsampled at 2-cm intervals, and stored in the State Key Laboratory of Marine Geology since 2008. The depositional age of bottom sediments can date back to about 150 years ago, based on the ²¹⁰Pb geochronology (Zhan et al., 2010). In this study, only 16 samples were taken throughout Core LGZ for major-element analyses, with average temporal resolution of ~10 years. All of these samples were dried to constant weight at 40°C temperature in the laboratory.

In this study, the published data are also compiled in order to thoroughly investigate weathering signal changes. These samples include bank sediments collected in 1997 (Yang et al., 2004) and 2003 (Yang et al., 2013), SPM collected between 2003 and 2007 (Ding et al., 2014) and fine-grained (<63 μm) sediments collected in 2009 (He et al., 2015).

4.3.2 Major element analyses

In this study, the SPM and RBS samples were analyzed for major elements by Inductively Coupled Plasma-Optical Emission Spectrometers (ICP-OES, model: IRIS Advantage), and the bank sediment and core samples were analyzed by X-ray fluorescence (XRF, model: AXIOSmAX). The instrument precisions are better than 1% for XRF and 0.5% for ICP-OES. These analyses were conducted in the State Key Laboratory of Marine Geology at Tongji University.

About 1 g of each sample was ground in an agate mortar, and then ignited in a muffle furnace at 600°C in order to weigh loss of ignition (LOI) and remove organic matter before acid digestion. In order to verify a potential bias related to the sample pre-treatment, we selected 6 SPM samples and treated them with 1M HCl following the method of Bi et al. (2015), while all other data come from untreated samples. The objective of the 1M HCl treatment was to remove the carbonate fraction. For the ICP-OES measurement, about 50 mg powder samples were dissolved with a mixture of 1:1 concentrated HNO₃ and HF in a tightly closed Teflon vessel for at least 48 h at 190°C. After drying, samples were re-dissolved in

HNO₃ to remove any fluorides. Finally, samples were re-digested in 2 ml 30% HNO₃ at 190°C. The Si concentration was obtained by assuming the total content of major oxide and trace elements in the residues is 100%, following the calculation method of Guo Y et al. (2018). The errors of calculated Si concentration are less than 8%. For the XRF method, the powder samples were directly fused with lithium tetraborate (Li₂B₄O₇) at 1050°C to make a glass disk for the XRF measurement. The analytic precision and accuracy were monitored by the simultaneously processed standards of BCR-2 for ICP-OES and GSR-3 for XRF. The results showed that the accuracy of major element is generally better than 5% and the precision (one standard deviation) is better than 1%.

4.3.3 Chemical weathering proxy

As suggested by Lupker et al. (2012), the diagram of ratios of major element (Me) to Si (Me/Si, Y axis) vs. Al/Si (X axis) can be used to discriminate hydrodynamic sorting and silicate weathering (i.e. leaching) intensity. Mineral and grain size sorting can be recognized by a mixing trend, showing higher Al/Si ratios in finer sediments enriched in clays, and lower Al/Si ratios in coarser sediments enriched in quartz. In contrast, change of weathering intensity is discerned by a vertical trend, showing a decrease of mobile element/Si ratio (caused by leaching) at constant Al/Si. In the following, the temporal variability of element/Si ratio means the comparison is done at a given Al/Si ratio.

4.3.4 Monte-Carlo simulation

In order to calculate the elemental ratio (i.e. K/Si and Al/Si ratio) variations of mid-lower riverbed sediments, and compare them with the data measured in the sediment core (see Discussion section), a Monte-Carlo simulation was developed. Briefly, the sources of Changjiang sediments into the East China Sea mainly come from five end-members: upper reaches, Dongting Lake, Poyang Lake, Hanjiang River and mid-lower riverbed (Yang et al., 2018). The ranges of elemental ratios for the first four end-members are published (*Ding et al., 2014*). Based on simple mass balance equations, the elemental ratios for mid-lower riverbed sediments can be simulated, with an assumption of conservative elemental behavior during transport and mixing. The Monte-Carlo simulation was performed with MATLAB 2018a software.

4.4 Results

The Al/Si ratios of Xuliujing SPM samples range from 0.2 to 0.4 (Fig. 26), within the reported range of SPM samples collected in the Changjiang mainstream (Ding et al., 2014). The Al/Si ratios of samples from Core LGZ range from 0.28 to 0.45, reflecting enrichment of fine-grained materials. The grain size of core samples reflected by Al/Si ratios is similar to that of SPM. Relative to the SPM and core samples, the Al/Si ratios of RBS samples show apparent lower values and narrow variation, ranging from 0.1 to 0.15. The mobile elements, i.e. K, Na, Ca and Mg, display different mobility, with lower K/Si, Ca/Si and Mg/Si ratios but higher Na/Si ratios in the RBS relative to the SPM. As a function of Al/Si ratios, SPM K/Si and Mg/Si ratios increase from 0.06 to 0.10 and from 0.04 to 0.06, respectively (Figs 26a and 26d). In contrast, SPM Na/Si and Ca/Si ratios decrease from 0.04 to 0.02 and from 0.10 to 0.07, respectively (Figs 26b and 26c). In Core LGZ, the K/Si ratios range from 0.05 to 0.10, similar to that measured in the SPM samples. The different variation trends among K, Na, Mg and Ca are possibly related to their respective behaviors during clay formation. K and Mg can be re-incorporated into illite and smectite, while Na and Ca are preferentially leached during chemical weathering (He et al., 2013).

A linear correlation exists between K/Si and Al/Si ratios for the coarse-grained RBS and the fine-grained SPM (Fig. 26a), and for the core samples as well. For other mobile elements, the relationship is non-linear or nonexistent. After 1 M acid pre-treatment, apart from K, other mobile elements show apparently lower Me/Si ratios for a given Al/Si ratio, especially for Ca and Mg. A significant part of Ca and Mg are concentrated in the carbonate and dolomite minerals. After the 1 M HCl pretreatment, Na/Si, Ca/Si and Mg/Si ratios decreased by 0.002, 0.07 and 0.03, respectively. Compared to Na/Si and Mg/Si, Ca/Si ratios of decarbonated sediments are homogeneous with an average below 0.02 (Figs. 26b and 26c). The slope of the linear relationship between K/Si vs. Al/Si (Fig. 26a) is not modified by the HCl pre-treatment

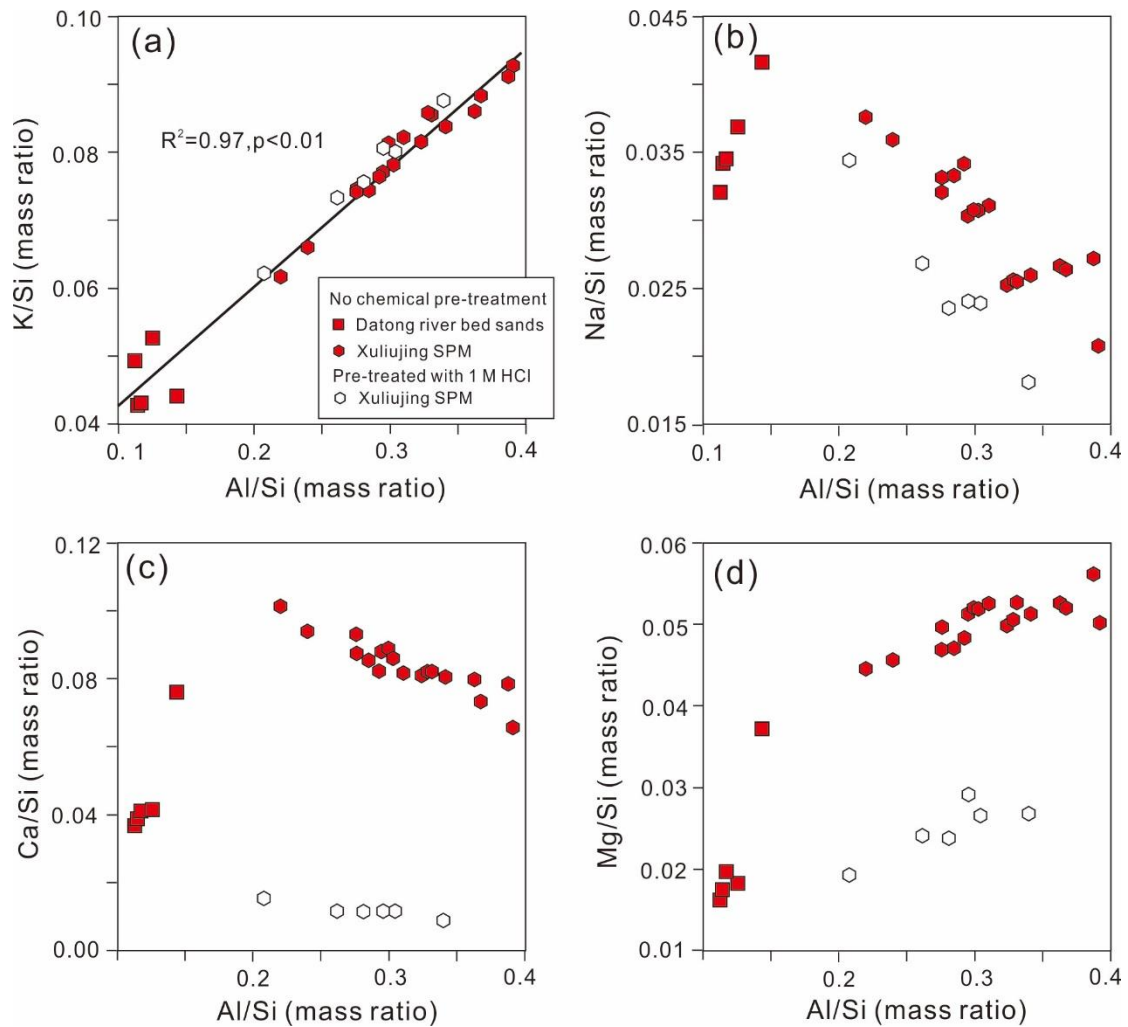


Figure 26 : The influence of 1M HCl pre-treatment on river suspended matter (SPM) and bed sands K/Si (a), Na/Si (b), Ca/Si (c) and Mg/Si (d), all reported as a function of Al/Si, considered as a proxy of grain size effects related to mineral sorting during transport (Lupker et al., 2012).

4.5 Discussion

Human activities, especially dam constructions, have long been a concern for their influence on riverine sediment routing system. Dams have been considered as the leading contributors to the disturbance of sediment transport and river connectivity (Dynesius and Nilsson, 1994; Syvitski et al., 2005; Grill et al., 2019), however, dams' impact on chemical composition of downstream sediment is poorly understood still. Herein, the impact of the TGD construction on river sediment weathering intensity is determined, which provides an important example for the studies of chemical weathering in large river systems during post-dam periods worldwide.

4.5.1 Large Na depletion in fine-grained sediments

In Fig. 27, Na/Si ratios correlate negatively with Al/Si ratios. The Na concentration in the fine fraction is lower and yields higher values in coarse grains. The downward Na/Si variation as a function of Al/Si for SPM reflects weathering of bedrock, as Na is hard to be incorporated into secondary phases, in contrast to K. The range of Al/Si ratios measured in the upstream-derived and the mid-lower mainstream SPM are similar. Nevertheless, Na/Si ratios are slightly lower for the mid-lower mainstream SPM (Fig. 27). In contrast to K/Si, no temporal trend can be clearly observed for Na/Si ratios of the mid-lower mainstream SPM between 2003 and 2014 (Figs. 27, 28 and 29). This is likely due to the strong Na leaching in the upper basin, resulting in very low Na/Si ratios in the highest Al/Si ratio of SPM. Thus, the large Na depletion of finest sediments due to its high mobility and incompatibility with secondary phases precludes any precise observation about SPM Na/Si temporal variation.

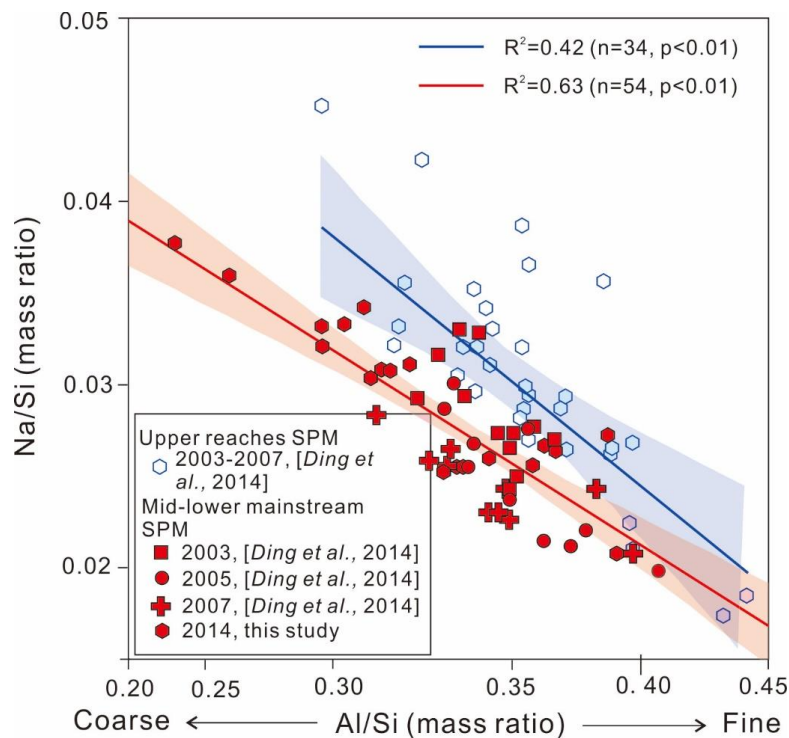


Figure 27 : Na/Si vs. Al/Si ratios measured for river bed sands and suspended particulate matter (SPM) of the Changjiang River (mainstream). Because there is a discrepancy for Na/Si ratios between different acid pre-treatment, only data of samples without acid pre-treatment are displayed here.

4.5.2 Stronger K leaching intensity after 2003

As illustrated in Figure 28, the compiled dataset (2003–2014) plotted in the K/Si vs Al/Si diagram follow two distinct regression lines, with statistically different slopes. Al/Si

ratios are regarded as a proxy for particulate size, and are particularly sensitive to mineral sorting during transport, while K/Si ratios can be used as an index of the leaching intensity of silicates. Sediments collected in rivers draining the upper reaches define a straight line with a strong slope (in blue dash line in Fig. 28). This is in agreement with a relatively weak leaching of potassium in fine-grained sediments (i.e. high Al/Si ratio), mostly concentrated in K-bearing silicates of the upper highland rocks and soils. This feature is consistent with weathering-limited conditions in mountainous regions with thin soils, where sediment residence times are short (West et al., 2005). In contrast, data points of river sediments collected downstream of the TGD (in red in Fig. 28) define a linear trend with a lower slope, showing a significant depletion in K compared to sediments collected from the upper reaches albeit with similar Al/Si ratios. This observation suggests a stronger weathering (leaching) intensity registered in the sediments collected downstream of the TGD.

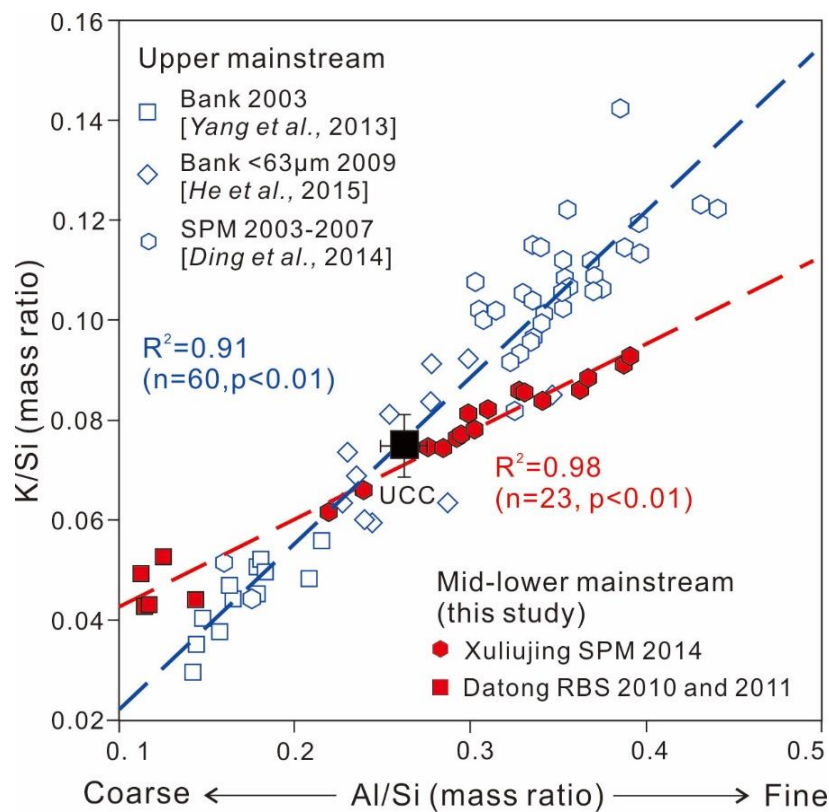


Figure 28 : K/Si vs. Al/Si ratios measured for bank sediments and suspended particulate matter of the Changjiang River (mainstream). Sediments collected from the upper reaches (in blue) display a distinct relationship from the mid-lower reaches (in red). The black square represents the average value of the source rock of the Upper Continental Crust (Rudnick and Gao, 2003). Major element data of bank sediments, fine-grained (< 63 µm) sediments and SPM are from Yang et al. (2004, 2013), He et al. (2015) and Ding et al. (2014), respectively.

Examining in details the data provided by sediments collected in the mid-lower mainstream show that a progressive depletion in K/Si can be observed since 2003, i.e. the beginning of the TGD construction (Fig. 29a). Before 2003, the K/Si ratios of SPM and bank sediments display a weathering intensity that is similar to the one of the upstream-derived sediments (for a given Al/Si value). Then, between 2003 and 2007, a progressive and significant depletion of K (relative to Si) is exhibited by the SPM samples from the same river section (see Fig. 29b). The Three Gorges Reservoir can be a potential reactor for further weathering by favoring long storage time for the upstream sediments. However, sediments collected from the Three Gorges Reservoir exhibit no change in K depletion (Fig. 28). This implies that the leaching process did not happen upstream of the TGD during the reservoir trapping. The acid rain deposition in the Changjiang basin is mainly constrained in the Chongqing-Guiyang region of the Jinshajiang valley (Chen et al., 2002). No severe atmospheric acid deposition events were reported recently in the mid-lower basin. We thus infer that the process resulting in SPM K leaching may be related to either continuous leaching in the mid-lower basin, or to a progressive change of the SPM provenance in response to the TGD construction, or the combined effect of both in the mid-lower basin.

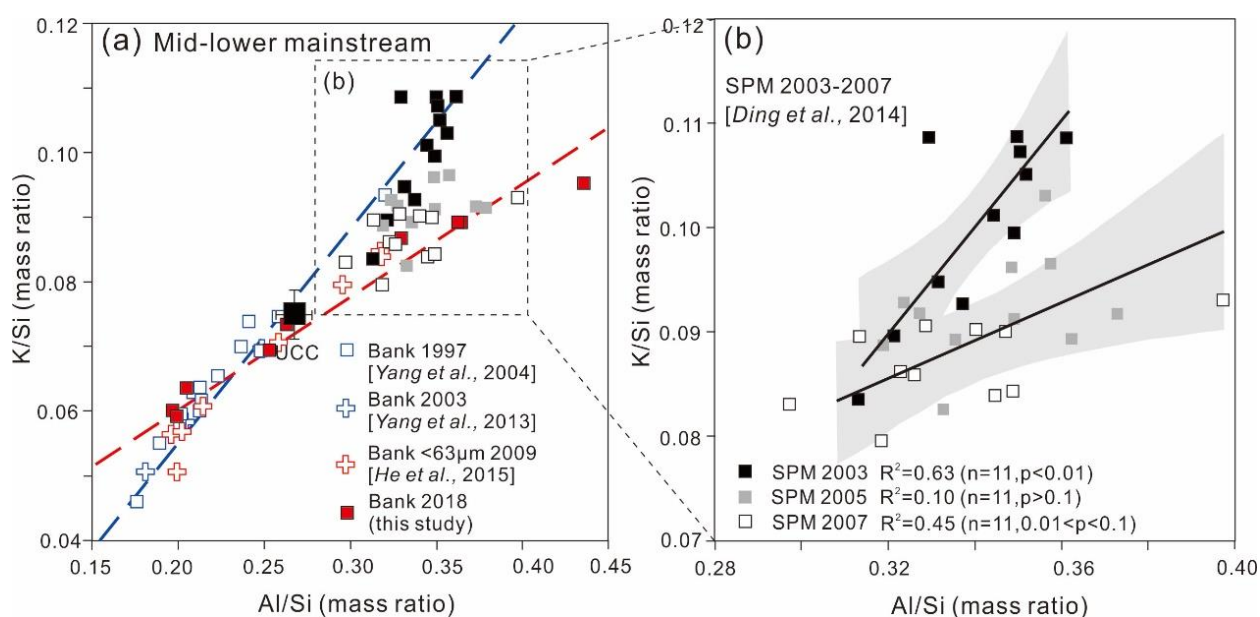


Figure 29 : K/Si vs. Al/Si ratios measured for bank sediments and SPM sampled from the mid-lower Changjiang River (mainstream). (a) Between the time of the TGD operation and 2014, SPM and bank sediments from the mid-lower reaches (downstream of the Dam) display a progressive depletion in K (compared to Si). (b) K/Si vs Al/Si for SPM collected in the mid-lower reaches mainstream of the Changjiang Basin (Ding et al., 2014). The statistical test for SPM collected in 2005 is insignificant, and the best-fits line is not shown.

It is interesting to note that the mean K/Si and Al/Si ratios of the Upper Continental Crust (UCC, black square) roughly fall between the bank sediments and SPMs or fine fractions ($<63\ \mu\text{m}$) for both trends (blue and red, see Fig. 28). This confirms that the average composition of rocks drained by waters in the large catchment of the Changjiang is representative of the UCC (Yang et al., 2004), thus justifying the use of sediments in large river systems to investigate general information regarding global weathering.

4.5.3 Significant impact of TGD on the sediment source-to-sink process

The mid-lower Changjiang basin is one of the most populated areas of the world. In this region, most parts of the river are constrained by artificial embankment. This means that the direct sediment contribution from nearby floodplain is limited. Bank sediments mainly come from the deposition of river suspended load, as shown by numerous studies and observations (Maharana et al., 2018). Previous studies (Yang et al., 2016; Chen et al., 2010; Guo et al., 2018) have shown that the major sources of Changjiang sediments into the East China Sea include the upper reaches, Dongting Lake, Hanjiang River, Poyang Lake and mid-lower riverbed (Fig. 24b). The Dongting and Poyang lakes are located downstream of the TGD, and have received a huge amount of sediment derived from the upper reaches before the TGD construction in 2003. Thus, the lakes as well as the mid-lower riverbed were important depositional sinks for upstream-derived Changjiang sediments (Chen et al., 2010; Guo L et al., 2018). However, with the TGD impoundment in 2003, these two lakes and the mid-lower riverbed have undergone serious erosion and thus shifted to important sources of sediments into the East China Sea (Yang et al., 2006; Luo et al., 2012; Yang et al., 2014; Guo L et al., 2018).

In order to investigate further these aspects, a more quantitative approach can be applied using monitored sediment flux (Fig. 30 and Table 7). As illustrated by the hydrological observations at Datong gauging station between 2002 and 2015 (Fig. 30a), the Changjiang water discharge was relatively constant during this period. The sediment flux decreased steadily since 2003, and became relatively constant after 2006, mainly because of the balance between significant trapping of upstream-derived sediments by the TGD and sediment supply from the mid-lower reaches. This change resulted in downstream sediment concentration lower than sediment carrying capacity, leading to a visible physical erosion within the Dongting Lake and within the mid-lower riverbed (Lai et al., 2017).

Table 7: Water discharge and sediment flux for each end-member. The data were collected from the Changjiang Water Resources Commission website: <http://www.cjw.com.cn/>.

Year	Total water discharge (km ³ /yr)	Sediment flux (Mt/yr)					
		Upper reaches (F _U)	Dongting (F _D)	Hanjiang (F _H)	Poyang (F _P)	Total (F _T)	Riverbed (F _E)
2002	992.6	228	-16	2.7	14	275	46.3
2003	924.8	97.6	17.5	14	17.6	206	59.3
2004	788.4	64	14.3	5	13.7	147	50
2005	901.5	110	15.9	17.1	15.5	216	57.5
2006	688.6	9.1	15.2	2.8	14.1	84.8	43.6
2007	770.8	52.7	11.2	8.3	12.3	138	53.5
2008	829.1	32	17.4	4.6	7.3	130	68.7
2009	781.9	35.1	16.7	4.9	5.7	111	48.6
2010	1022	32.8	26.2	12.4	15.9	185	97.7
2011	667.1	6.2	14.6	5.4	7.7	71.8	38
2012	1002	42.7	25.6	3.7	14	161	75
2013	787.8	30	29	1.5	11.2	117	45.3
2014	891.9	9.4	22.6	0.7	12.1	120	75.2
2015	913.9	3.7	24.5	1.7	12	116	74.1

Note: the sediment flux of mid-lower riverbed (E) was calculate based on a mass balance method (E=T-U-D-H-P)

Following previous studies (Yang et al., 2006; Yang et al., 2018), the monitored sediment flux at Datong, Yichang, Huangzhuang, Chenglingji and Hukou gauging stations (Fig. 25b) represents the total sediment flux into the East China Sea (F_T), sediment flux from the upper reaches (F_U), the Hanjiang River (F_H), the Dongting Lake (F_D) and the Poyang Lake (F_P), respectively (Changjiang Water Resources Commission, 2002–2015). Then, the mid-lower riverbed sediment flux (F_E) can be estimated using the equation (1) below, with assumption of a conservative mixing. Then, we can estimate the relative sediment contributions of these five sources to total sediment flux (F_X/F_T, X represents sediment source).

$$F_T = F_U + F_D + F_H + F_P + F_E \quad (1)$$

Results show that the upper reaches dominated the source of sediments into the East China Sea before the TGD construction, with a proportion up to 83% in 2002 (Fig. 30b). Since the TGD impoundment in 2003, the relative contribution of upstream-derived sediment decreased rapidly, especially by 2015 when almost all of the upstream-derived sediment was trapped upstream of the TGD. In contrast, the proportion of sediments eroded from the mid-lower riverbed rapidly increased from ~17% in 2002 to ~30% in 2003 and then to ~50% after the TGD in full operation (2008–2012), and finally increased to nearly 65% after cascade dams operated on the Jinshajiang River since 2013 (Fig. 25b). As described above, the mid-

lower riverbed erosion is mostly related to sediment carrying capacity of river flow exceeding suspended material concentration. We also estimate that the relative contributions of Dongting and Poyang Lakes increased by nearly ~20% and ~5%, respectively. The sediment contribution from the Hanjiang River did not show significant variation during this period (<6%) (Fig. 30c). Note that parts of upstream-derived sediment are transported into the Dongting Lake through three inlets downstream of the Yichang gauging station (Fig. 25b), the sediment flux monitored in Yichang gauging station therefore represent the maximum flux of upstream-derived sediment (F_U). Considering progressively decreased flux of upstream-derived sediment and of sediments into the Dongting Lake since 2003 (Guo L et al., 2018), we estimate this bias to the calculation above is minor.

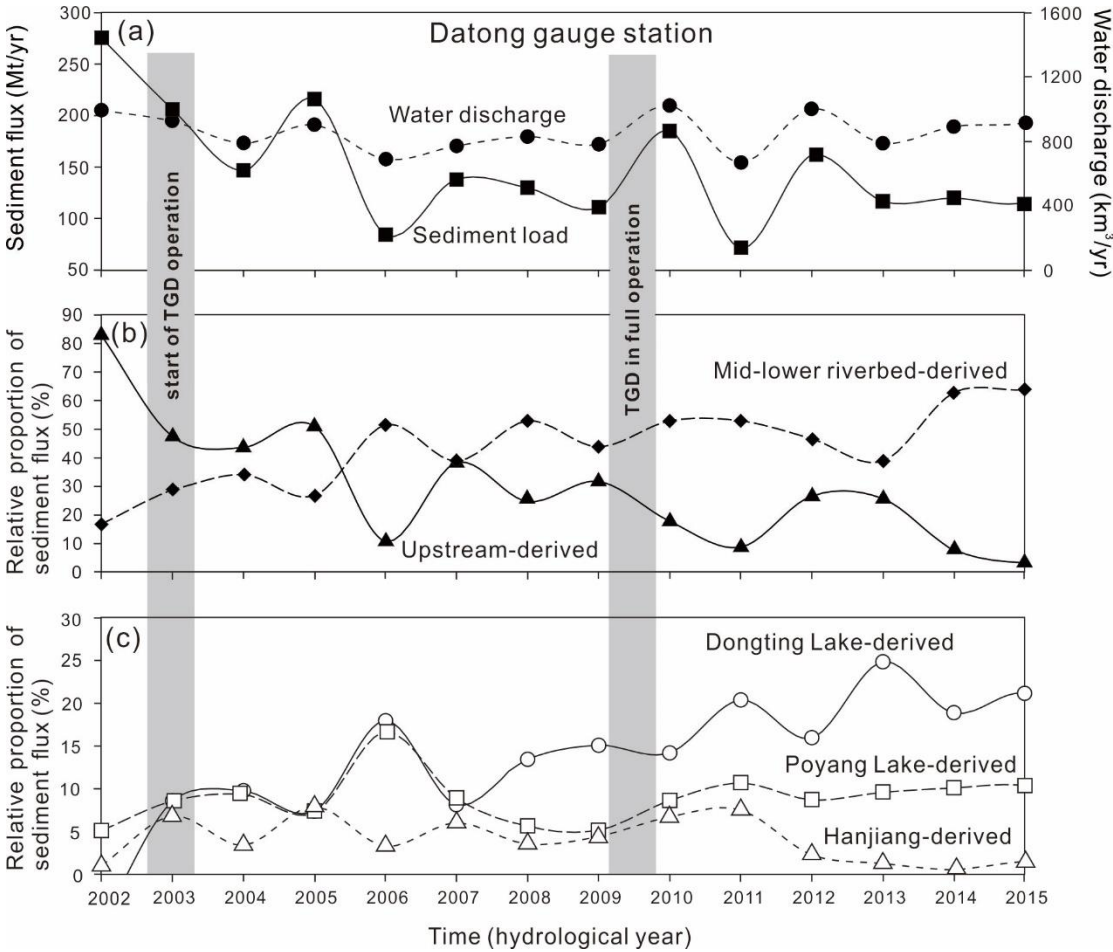


Figure 30 : (a) Water discharge and sediment flux as a function of time recorded at the Datong Gauging Station, located in the lower reaches (see Fig. 25). The sediment flux significantly decreased with time since the TGD operation, but the water discharge was little affected. (b) and (c) Relative contribution of the different sources of sediments to the total load. The data of water discharge and sediment flux were collected from the CWRC website: <http://www.cjw.com.cn/>.

4.5.4 Possible mechanism responsible for downstream weathering signal variations

As discussed above, the relative proportions of sediment contributions from the Poyang Lake, Dongting Lake and mid-lower riverbed increased by about 5%, 20% and 40% respectively during the observation period (2002–2015) (Figs. 30b and 30c). Sediment source changes may account for the change of the downstream K leaching signal. Previous studies indicated that the kaolinite content of the Poyang Lake-derived sediments increased, while the dissolved load was also enriched in Si after the TGD construction (Wang et al., 2018; Zhao et al., 2018). However, our results are in contrast to this hypothesis since the sediments collected in the Poyang Lake in 2018 are characterized by a similar weathering intensity as for samples collected during the previous periods (Fig. 31a). Compiled altogether, these data show that the weathering signal, at least for K/Si ratios, did not change significantly in sediments collected from the Poyang Lake basin during the last decades (Fig. 31a). Thus, a slightly increased proportion of sediments from Poyang Lake (Fig. 30c) cannot explain the significant K depletion of the Changjiang SPM in the lower basin.

The Dongting Lake was identified as a sediment sink before the TGD construction, receiving a large amount of sediments from its four tributaries and from the Changjiang upstream as well (Guo L et al., 2018). After the TGD construction, Dongting Lake gradually changed from a major sink of upstream-derived sediment to a source of sediments into the East China Sea (Guo L et al., 2018). As illustrated in Figure 30a, the sediments from the Dongting Lake tributaries show a lower K/Si ratio, in contrast to data of upstream-derived sediments. In that sense, the weathering signal of sediments from the Dongting Lake is primarily determined by two sources, i.e. strongly weathered sediments from its tributaries and weakly weathered sediments from the Changjiang upper reaches. Interestingly, the sediments collected in the Dongting Lake outlet (i.e. the one that contribute to the Changjiang River) show a weak weathering intensity, and have a chemical composition close to that of the sediment derived from the upper reaches (see Fig. 31a). This can be easily interpreted using hydrological data (Guo L et al., 2018), as the average annual sediment flux from its low-land tributaries (35.2 ± 23.5 Mt/yr in 1953–1984) is much smaller than the one from the Changjiang upper reaches (200.2 ± 59.4 Mt/yr in 1956–1968). Thus, the Dongting Lake is mostly fed by weakly-weathered sediments derived from the upper Changjiang. Furthermore, in comparison with pre-TGD period, the kaolinite concentration (~30%) in Dongting Lake remains constant (Zhao et al., 2018) and the dissolved Si flux even decreased from 0.76×10^6 t/yr in 1958–2002 to 0.67×10^6 t/yr in 2003–2014 (Wang et al., 2018). All of those

observations suggest that the outflowing Dongting Lake sediments are characterized by weak weathering intensity (i.e. high K/Si ratio). Therefore, we infer that sediments from Dongting Lake have no significant influence on the downstream weathering signal change, despite its 20 % increase of relative sediment contribution after 2003.

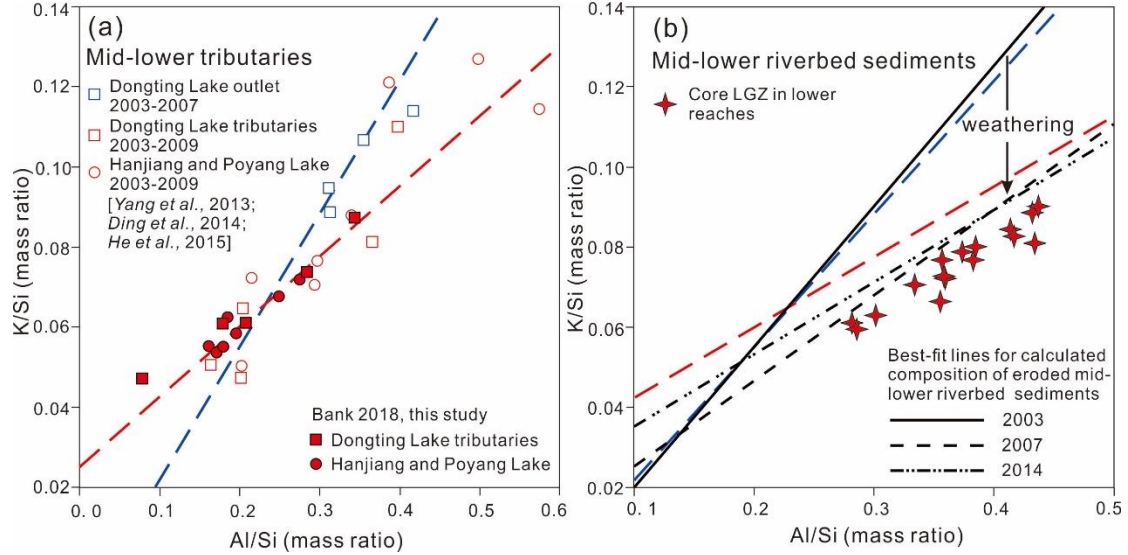


Figure 31 : The variation of K/Si vs. Al/Si of samples collected in the mid-lower reaches tributaries (a), of Core LGZ samples collected in lower mainstream and best-fit lines for simulated riverbed sediments (b). The blue and red dash lines are drawn based on Figure 27. The K/Si vs. Al/Si ratios of mid-lower riverbed sediments are simulated by Monte-Carlo method

Given these findings, the most possible explanation would be that mid-lower riverbed sediments, which deposited downstream before the TGD construction, have been subjected to significant physical and chemical erosion. Otherwise, the weathering signal would have remained constant, because the mid-lower riverbed sediments primarily originate from the upper reaches (Yang et al., 2006; Xu and Milliman, 2009; Yang et al., 2018). The correlations between K/Si and Al/Si for resuspended mid-lower riverbed sediments were analyzed using Monte-Carlo simulations in order to identify whether or not the data are compatible with strong potassium depletion of these phases (Table 8). We assume that particulate Si is conservative during sediment transport, and the K/Si and Al/Si mixing equations are expressed as follows:

$$\left(\frac{K}{Si}\right)_T = \sum_i^n \left(\frac{K}{Si}\right)_i \times f_i(Si)$$

$$\left(\frac{Al}{Si}\right)_T = \sum_i^n \left(\frac{Al}{Si}\right)_i \times f_i(Si)$$

$$\sum_i^n f_i(Si) = 1$$

Where i represents each sediment end-member, and $f_i(Si)$ is the fraction of Si carried by each component, with an assumption that it could reflect the percentage of each component contributing to the total flux of sediments (T). The simulation parameters and results are shown in Table 8.

Table 8: Parameters (Al/Si, K/Si and sediment flux proportion deduced from monitored fluxes and hydrological data) for each end-member used in the Monte-Carlo simulations

Year	Location	f (%)	Al/Si (ppm:ppm)	K/Si (ppm:ppm)
2003	Upper reaches (U)	47.4	0.3454±0.0114	K/Si=Al/Si*0.3515-0.0106 (R ² = 0.63)
	Dongting (D)	8.5	0.3493±0.0496	K/Si=Al/Si*0.2534+0.0071(R ² = 0.87)
	Hanjiang (H)	6.8	0.3169±0.0323	K/Si=Al/Si*0.1882+0.0231(R ² = 0.86)
	Poyang (P)	8.5	0.5365±0.0538	K/Si=Al/Si*0.1882+0.0231(R ² = 0.86)
	Total sediment (T)	100	0.3376±0.0179	K/Si=Al/Si*0.4694-0.0597 (R ² = 0.63)
	Riverbed (E)	28.8		K/Si=Al/Si*0.4349-0.0401 (R ² = 0.96)
2005	Upper reaches (U)	50.9	0.3761±0.0163	K/Si=Al/Si*0.3486-0.0163 (R ² = 0.53)
	Dongting (D)	7.4	0.3493±0.0496	K/Si=Al/Si*0.2534+0.0071(R ² = 0.87)
	Hanjiang (H)	7.9	0.3169±0.0323	K/Si=Al/Si*0.1882+0.0231(R ² = 0.86)
	Poyang (P)	7.2	0.5365±0.0538	K/Si=Al/Si*0.1882+0.0231(R ² = 0.86)
	Total sediement (T)	100	0.3557±0.0176	K/Si=Al/Si*0.0800+0.0643(R ² = 0.10)
	Riverbed (E)	26.6		K/Si=Al/Si*0.1401+0.0051(R ² = 0.64)
2007	Upper reaches (U)	38.2	0.3934±0.0476	K/Si=Al/Si*0.2830+0.0023(R ² = 0.70)
	Dongting (D)	8.1	0.3493±0.0496	K/Si=Al/Si*0.2534+0.0071(R ² = 0.87)
	Hanjiang (H)	6.0	0.3169±0.0323	K/Si=Al/Si*0.1882+0.0231(R ² = 0.86)
	Poyang (P)	8.9	0.5365±0.0538	K/Si=Al/Si*0.1882+0.0231(R ² = 0.86)
	Total sediment (T)	100	0.3462±0.0253	K/Si=Al/Si*0.1789+0.0282(R ² = 0.45)
	Riverbed (E)	38.8		K/Si=Al/Si*0.2126+0.0040(R ² = 0.95)
2014	Upper reaches (U)	7.8	0.3716±0.0344	K/Si=Al/Si*0.3313-0.0111(R ² = 0.91)
	Dongting (D)	18.8	0.3493±0.0496	K/Si=Al/Si*0.2534+0.0071(R ² = 0.87)
	Hanjiang (H)	0.6	0.3169±0.0323	K/Si=Al/Si*0.1882+0.0231(R ² = 0.86)
	Poyang (P)	10.1	0.5365±0.0538	K/Si=Al/Si*0.1882+0.0231(R ² = 0.86)
	Total sediment (T)	100	0.3485±0.0369	K/Si=Al/Si*0.1750+0.0252(R ² = 0.97)
	Riverbed (E)	62.7		K/Si=Al/Si*0.1809+0.0170(R ² = 0.98)

Note: the correlation between K/Si and Al/Si for mid-lower riverbed sediments (E) is simulated result

As illustrated in Figure 31b, K/Si vs. Al/Si values of mid-lower riverbed sediments show an intensified K-leaching. This is consistent with our data from SPM and bank sediments that the bank sediments sampled downstream of the TGD also show different chemical composition before and after 2003 (Fig. 29a). In detail, for samples collected in 1997 and 2003, they plot along the upper-reaches trend (in blue in Fig. 29a), while between

2009 and 2018 they display stronger weathering signals (in red). Therefore, the onset of the TGD impoundment in 2003 seems to be a threshold.

As illustrated in Figure 30b, the relative proportion of mid-lower riverbed sediments is estimated to be ~30% of the total sediment flux in 2003. However, the corresponding data from mid-lower mainstream bank sediments still plot along the upper-reaches trend in Figure 29a. Our simulated trend in Figure 31b also plot very close to the upper-reaches trend, with fine fractions displaying weak weathering degree. This implies that the K depletion process is significant in the deep sediment layers, and there was not enough time for more superficial recently deposited sediments to release K. The data from Core LGZ demonstrate that the sediments with longer depositional age do provide a higher weathering intensity because sediments exhibit lower K/Si ratios (Fig. 31b). Because the mid-lower riverbed sediments are primarily derived from the upper reaches, these data strongly support the interpretation that the weathering occurred in situ in the mid-lower riverbed. This reinforces our hypothesis of more significant contribution from mid-lower riverbed sediments for explaining the shift of the weathering signal observed after 2003. More intensive weathering of sediments deposited in the mid-lower reaches is consistent with recent work on the Ganga Basin, indicating that floodplains play a significant role in weathering of K-bearing silicates (Lupker et al., 2012).

We propose a conceptual model for how the TGD construction affects sediment source-to-sink processes and the related weathering signal propagation in the downstream Changjiang sediments (Fig. 32). Before the TGD construction, parts of upstream-derived sediments deposited continuously in the mid-lower reaches (lakes, floodplain and riverbed), in response to higher suspended material concentration than sediment carrying capacity of the water flow. These newly-deposited sediments overlay the older sediments, masking the floodplain weathering signal (Fig. 32a). In 2002, for the first time, the sediment flux at Datong exceeded that at Yichang, reflecting the beginning of net riverbed erosion in the mid-lower reaches (Xu and Milliman, 2009). However, the relative proportion of upstream-derived sediment was still dominant, with contribution reaching 83% (Fig. 30b). Additionally, sediments eroded from the mid-lower riverbed were newly deposited with weak weathering intensity at that time (Fig. 32b). Consequently, enhanced weathering signals in mid-lower reaches could not be observed, despite existence of downstream net riverbed erosion before the TGD construction. However, the scenario changed after the 2003, when the TGD effectively trapped a huge amount of sediment from the upper reaches. This change resulted in downstream sediment concentration lower than sediment carrying capacity, leading to

visible erosion in the mid-lower riverbed (Lai et al., 2017). Downstream of the TGD, the erosion depth in the mid-lower river channel is estimated to be ~3.7 m on average in Yichang, and less than 1 m in the middle reaches (Lai et al., 2017). Sediments having been retained for a long time in the mid-lower basin have reached an equilibrium with surrounding environment, thus producing the observed and calculated floodplain weathering signals (Fig. 32b). After the TGD construction, the samples collected in the mid-lower reaches were dominated by these older and more weathered sediments, as observed in the downstream bank sediments sampled in 2014 and 2018 (Fig. 29b).

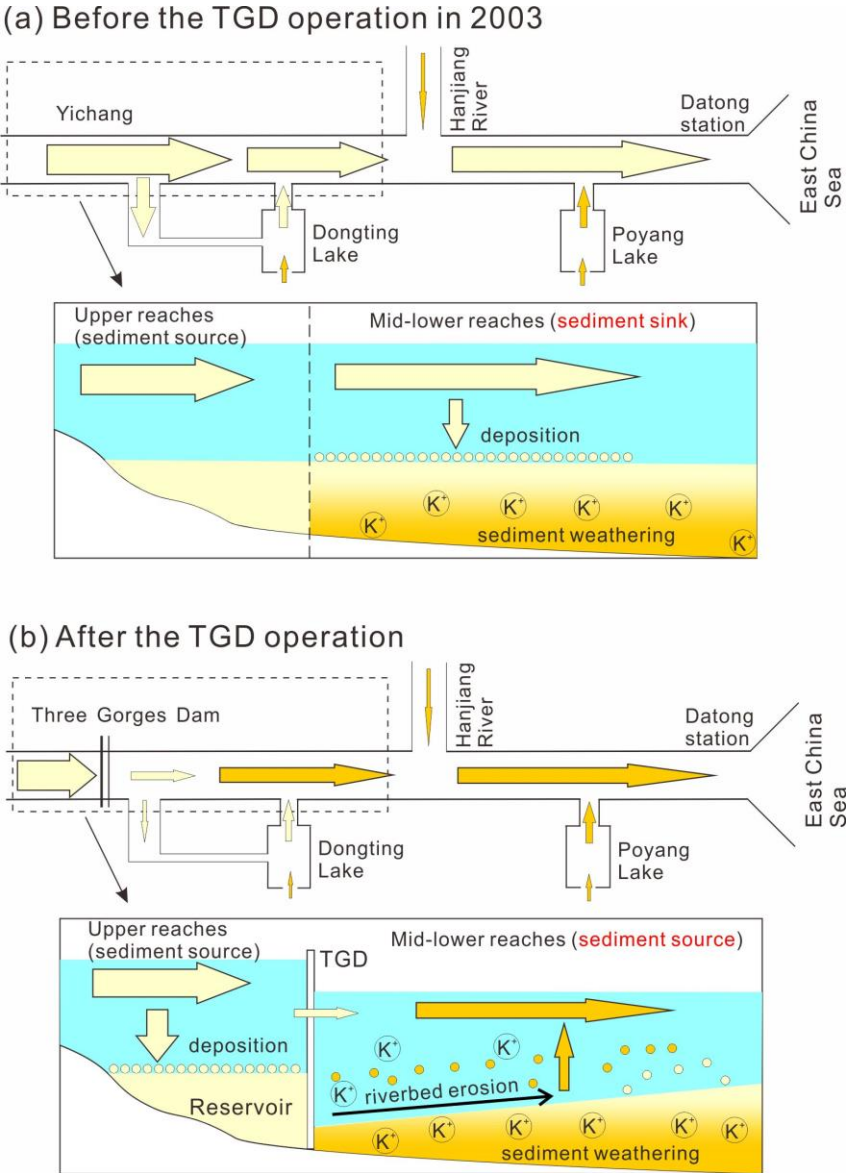


Figure 32 : Schematic drawing showing sediment-transport pattern changes before (a) and after (b) the TGD construction, and the possible mechanism for increased weathering signal after 2003. The width of arrow represents the amount of sediment flux, i.e. the wider arrow means larger sediment flux. The dark yellow represents the sediments experiencing stronger weathering during storage in floodplain and riverbed.

4.5.5 Implication for dissolved fluxes from the floodplain

Generally, river flow conditions are dominated by the mixing of rapid surface runoff and deep groundwater (Calmels et al., 2011). In this study, the warm climate and long water-rock reaction time in the mid-lower Changjiang basin may be responsible for the sediment weathering in situ, resulting in enrichment of K in the interstitial waters (Fig. 32). With time, these solutions reach a chemical equilibrium with the weathering products presented within the sediments (Ibarra et al., 2016; Winnick and Maher, 2018). The downstream riverbed erosion since 2003 exposed highly-weathered riverbed sediments, and thus perhaps released significant amounts of interstitial water which rich in ions. This is confirmed by the increase of the dissolved K flux observed between 2003 and 2013 for the samples collected at Datong gauging station (Table 8). Indeed, the annual flux of dissolved K increased from $\sim 52.3 \times 10^9$ mol/yr in 2003–2007 to $\sim 60.9 \times 10^9$ mol/yr in 2010–2013 (Table 9), suggesting an increase of 8.6×10^9 mol/yr.

It is possible to roughly estimate the K contribution from interstitial water to this increase. If we set the Al/Si ratio of sediments from the upper Changjiang to 0.35 ± 0.03 (the SPMs average), the corresponding K/Si values for upstream-derived and mid-lower riverbed sediments can be estimated using the corresponding regression equations (Table 8). Thus, we calculate that the percentage of K leached from the upstream-derived sediment during their storage within the mid-lower reaches is $23.2 \pm 2.5\%$, with the assumption of constant Si concentration as a function of time. If we set particulate K concentration to 0.64 ± 0.06 mol/kg (the SPMs average of the upper reaches), the K loss per unit sediment during their storage within the mid-lower reaches is 0.15 ± 0.02 mol/kg. The average mid-lower riverbed sediment flux in 2010–2013 increased by ~ 11 Mt/yr with respect to that in 2003–2007 (CRWC, 2003–2013). As a consequence, the increased K flux released by interstitial water to the mainstream is $1.7 \pm 0.2 \times 10^9$ mol/yr. In spite of the large uncertainty, such as the lack of correction for anthropogenic input, the release of interstitial water due to increased sediment flux from mid-lower riverbed accounts for $\sim 20\%$ of the increase of the riverine dissolved K flux measured between 2003 and 2013. Yang et al. (2014) speculated that the total volume of upstream-derived sediments deposited in the mid-lower Changjiang valley in 1950–2000 is approximately 3.2 km^3 (ca. 4000 Mt). The potential K release flux from the interstitial water within the Changjiang floodplain is thus estimated to be $6 \pm 0.8 \times 10^{11}$ mol, one order of magnitude higher than annual flux of dissolved K released to the marginal sea. Our simple calculation implies that the TGD is responsible for $\sim 15\%$ excess of dissolved K flux released

to the East China Sea, in response to the erosion of downstream riverbed sediments and corresponding interstitial water

Table 9: The total dissolved K flux into the sea of the Changjiang (Yangtze) River

	2003		2005		2007		2010		2013	
	wet	dry								
[K ⁺] (μM)	58.9 ^a	63.5 ^d	59.6 ^a	63.5 ^d	58.6 ^a	63.5 ^d	59.0 ^b	63.0 ^b	82.9 ^c	63.5 ^d
water discharge (×10 ⁹ m ³) ^e	647	278	627	274	550	221	730	292	531	257
[K] flux (×10 ⁹ mol/yr) ^f	55.7		54.8		46.3		61.5		60.3	

a. Ding et al. (2014); b. Wang et al., (2018); c. Zhang et al., (2016)

d. the average of K⁺ concentration of dry season in 2004 and 2006, data come from Ding et al. (2014);

e. data come from the CWRC website: <http://www.cjw.com.cn/>.

f. dissolved K flux = K⁺ concentration × water discharge

Human activities in large river systems and especially dam construction have significantly altered the sediment source-to-sink transport process and reduced sediment flux into the ocean, as is already evident in the Changjiang River (Chen et al., 2010; Yang et al., 2018). This work further reveals that not only the downstream sediment routing system is affected, but also the sediment chemistry. Before the TGD construction, the weathering signals of samples collected along the mainstream overall reflect the general weathering characteristic of the sediments coming from the upper reaches, rather than floodplain weathering, because of the dominance of sediment contribution from the upper Changjiang. Most previous studies on chemical weathering in the Changjiang basin were based on samples collected before or during initial period of the TGD construction. A large bias is therefore possibly introduced while using these samples to constrain continental weathering and its controls at large scale.

Dams retain almost all of the sediments derived from upper mountainous regions, which will limit the supply of fresh materials to the floodplain. For instance, at least 100 Mt/yr of upstream-derived sediments were trapped in the mid-lower lakes and valley due to overbank deposition before the TGD construction (Yang et al., 2006). As illustrated in Figure 31, the present-day mid-lower Changjiang basin is covered by cation-depleted older sediments, and there is a shortage of fresh materials or new sediments from the upper mountainous region. This change suggests the complex internal dynamic balance of sediment budget and chemistry in a large river system that is facing intense anthropogenic activities.

Similar cases have been observed in almost all the large rivers worldwide, such as the Mississippi, and Ebro Rivers (Batalla et al., 2004; Harmar et al., 2005). A total of 47,425 large dams (>15 m height) have been constructed all over the world (Milliman and Farnsworth, 2013). Although the dams indeed increased dissolved chemical flux by releasing interstitial water over short timescales, we argue that these dams artificially separate sediment connection between upper mountainous area and lower floodplain region, and thus indirectly weaken the role of floodplain on regulating continental weathering and terrestrial material cycling over long timescales. Moreover, the human activities in large catchments, in particular dam constructions, exert a potential influence on the output flux of dissolved load. The anthropogenic perturbation on natural surface processes in large river systems deserves more in-depth integrated studies to verify these effects at a larger scale in the future.

4.6 Conclusions of this chapter

This study investigated the impact of one of the largest dams in the world, the Three Gorges Dam, on the chemical composition of the downstream sediments, over a period of 10 years after its construction. The major conclusions can be summarized as follows:

(1) The TGD construction affected sediment chemical composition and inferred weathering intensity. Before the TGD construction, overwhelming flux and rapid transfer of upstream-derived sediments deposited in the mid-lower reaches, masking the floodplain weathering signal. The sediments collected along the mid-lower mainstream at that time mostly reflect the weak weathering signals of the upper mountainous region. Since 2003, the upstream-derived sediments were largely retained upstream of the TGD, and a floodplain weathering signal was gradually disclosed in the mid-lower Changjiang basin. A possible consequence of this effect is an apparently stronger weathering degree of mid-lower mainstream sediments than expected, which is not representative of modern conditions. Caution should therefore be taken in studies of the downstream parts of large basins for determining control laws of continental weathering.

(2) The release of interstitial water associated with erosion of deep layers of riverbed sediments in the mid-lower Changjiang mainstream likely resulted in the significant increase of dissolved K flux. Overall, the TGD not only affected the chemical composition of riverine sediments but has also introduced a small but not negligible bias to the chemical composition of the Changjiang dissolved load, resulting in potential artifacts in the quantification of continental weathering at large scale. Globally, the floodplains are well developed in large

river systems, and have a large potential ability for regulating silicate weathering and related CO₂ consumption. Intensive damming activities artificially decrease the supply of fresh materials from mountainous regions, which indirectly weaken the role of floodplain in regulating continental weathering over long timescales. More work would therefore be necessary to quantify more precisely these effects in the Changjiang basin and in other large river basins in the future.

Chapter 5: Behavior of Li isotopes along a 2D transect in the Changjiang (Yangtze) Estuary

The elements transported to the oceans by rivers in dissolved and particulate forms are a major process of the biogeochemical cycles (Gaillardet et al., 1999a, 1999b). For instance, basaltic particle dissolution or Ca-for-Na exchange with seawater were considered as particularly important for global climate stabilization, although these processes still need to be quantified at large scale (Sayles and Mangelsdorf, 1979; Gislason et al., 2006). Over the last 60 Ma, associated with the Cenozoic cooling, the seawater $\delta^7\text{Li}$ recorded by planktonic foraminifera increased by $\sim 9\text{‰}$ (Misra and Froelich, 2012). Several studies to date ascribed the cause of it to changes in continental weathering, since riverine Li flux and/or $\delta^7\text{Li}$ in response to changes of weathering rate, intensity or congruency (Misra and Froelich, 2012; Li and West, 2014; Vigier and Godderis, 2015). All these studies implicitly or explicitly assume that Li flux and isotope composition behave conservatively in the estuaries. However, thus far, this has not been demonstrated at large scale. By its characterization (described in chapter 2), the Changjiang Estuary represents an ideal site for this investigation.

In order to investigate Li behavior in the Changjiang Estuary, waters and suspended particulate matter (SPM) over depth profiles from salinity 0.1 to salinity 34.6 were collected. SPM samples collected along depth profiles performed at Xuliujing gauging station (XLJ, Fig. 33) were also sampled for comparison. In this chapter, the basic parameters (e.g. salinity, water temperature, pH), mineral compositions, Li concentrations and isotope compositions were first described. Then, the dissolved, suspended and exchangeable Li behavior was explored. Finally, conclusions and implications were demonstrated. This study is still in preparation.

5.1 Introduction

The elements transported to the oceans by rivers in dissolved and particulate forms are a major process of the biogeochemical cycles (Gaillardet et al., 1999a, 1999b). As the interface between the continents and the oceans, the estuaries typically feature the gradients of ionic strength and suspended load concentration, providing an ideal environment for the studies of water-sediment interactions. Over the last decades, numerous studies have suggested that riverine elemental flux and isotopic compositions (e.g. U, Sr, Nd and Ba) can be modified by physical, chemical and/or biological processes occurring during the transport through the estuaries (Lacan and Jeandel, 2005; Jones et al., 2012, 2014; Jeandel and Oelkers, 2015; Samanta and Dalai, 2016; Zhang et al., 2020). For instance, basaltic particle dissolution or Ca-for-Na exchange with seawater were considered as particularly important for global climate stabilization, although these processes still need to be quantified at large scale (Sayles and Mangelsdorf, 1979; Gislason et al., 2006).

River Li isotope composition ($\delta^7\text{Li}$) is thought to be a powerful proxy for chemical weathering degree (e.g. Huh et al., 1998; Kısakürek et al., 2005; Vigier et al., 2009; Dellinger et al., 2014; Wang et al., 2015; Pogge von Strandamann et al., 2017). During the weathering process, ^6Li is preferentially incorporated into the solid phase and leaves ^7Li in the dissolved phase (Pistiner and Henderson, 2003; Vigier et al., 2008; Wimpenny et al., 2010). As a result, the average Li isotope composition of global rivers (+23‰; Huh et al., 1998) is significantly higher than the average upper continental crust ($0 \pm 2\%$; Teng et al., 2004). Over the last 60 Ma, associated with the Cenozoic cooling, the seawater $\delta^7\text{Li}$ recorded by planktonic foraminifera increased by $\sim 9\%$ (Misra and Froelich, 2012). Several studies to date ascribed the cause of it to changes in continental weathering, since riverine Li flux and/or $\delta^7\text{Li}$ in response to changes of weathering rate, intensity or congruency (Misra and Froelich, 2012; Li and West, 2014; Vigier and Godderis, 2015). In several transition periods, variations of marine carbonate $\delta^7\text{Li}$ have also been attributed to changes of weathering conditions, leading to key interpretations for mass extinction or for short-term global warming (e.g. Pogge von Strandmann et al., 2003; Sun et al., 2018). Recently, the clay-size Li isotope composition of sediments deposited in delta areas were used to determine paleo-environments and past variation of continental weathering (Bastian et al., 2017). All these studies implicitly or explicitly assume that Li flux and isotope composition behave conservatively in the estuaries. This means that all estuarine processes related to the salinity increase, particle aggregation or alteration, ion and isotopic exchange, do not significantly bias the river Li concentration and

isotope composition. However, thus far, this has not been demonstrated at large scale. Indeed, there are only few published studies, mostly of small estuaries, with two of them highlighting a non-conservative behavior of Li isotopes (Pogge von Strandmann et al., 2008; Murphy et al., 2014). It becomes therefore critical to undertake the study of estuaries of large rivers, which carry significant amounts of particles and dissolved Li to the ocean.

During the KECES cruise organized in September, 2019, we performed a transect of ~400 km in the mixing zone of the Changjian Estuary (Fig. 33). Water and suspended particulate matter (SPM) over depth profiles from salinity 0.1 to salinity 34.6 were collected. We systematically measured Li concentrations and Li isotope compositions of the dissolved phase (an operational definition of the fraction in water that pass through 0.45 μm pore-size filter), SPM samples and its exchangeable phase (fraction extracted using NH_4Cl). Additionally, Li and its isotope compositions of SPM samples collected in depth profiles at Xuliujing gauging station (Fig. 33) are also reported. The primary goal was to determine the impact of the estuarine zone on Li isotope, which is classically used to estimate continental weathering conditions.

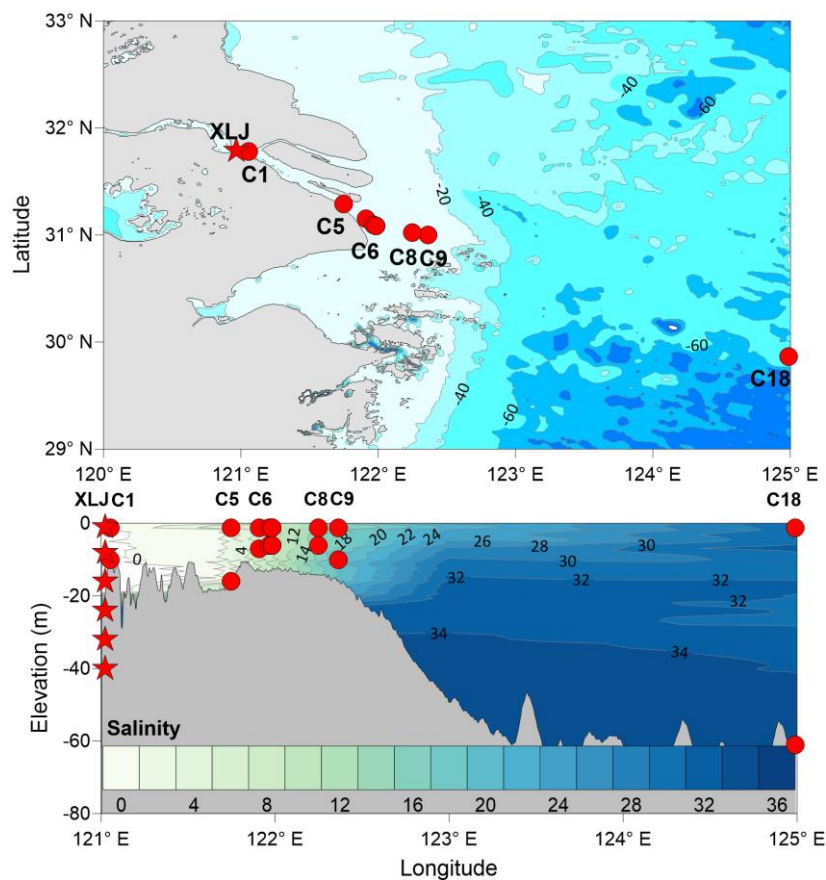


Figure 33 : Maps showing (A) the Changjiang estuary, sampling strategy, and (B) salinity variation during the sampling period. The blue color associated with isobath in (A) refer to water depth below the modern sea-level.

5.2 Distribution of salinity, pH, temperature and SPM concentration

In the studied location, the salinity generally increases from the Changjiang river to the adjacent shelf, and increases from surface to bottom (see Fig. 32C). From sampling station C1 to C9, the salinity showed variation in the range of 0.1 – 20.0‰. The surface sample at station C18 (i.e. C18S) has salinity of 32.0‰, while the salinity of C18B (bottom sample) is typical of deep China Sea, with salinity of 34.6‰ (Fig. 32C). The water pH of most samples is 7.8, without difference between surface and bottom layer. Water pH of samples C6S and C18S is slightly higher, with value of 8.0 and 8.2, respectively. On average, the water temperature decreases slightly from the river mouth (C1 and C5: 28.9 – 29.1°C) to shelf area (C9: 26.8 – 27.1°C). Generally, water temperature in surface layer is equal or higher than the bottom. Among all the water samples, the surface temperature at the outermost station (i.e. C18S) are the highest (29.4°C), while the bottom water (C18B) have the lowest temperature of 21.9°C. The SPM concentration ranges from 5.1 mg/l to 2363.7 mg/l, showing a heterogeneous distribution. The area with maximum SPM concentration (SSC) lies between station C5 to station C8, with salinity of 0.1 – 12.5‰. Overall, the SSC increases from the river end-member (C1: 41.7 – 58.4 mg/l) to the turbidity maximum zone (384.1 – 2363.7 mg/l), and then decreases to the outermost station (C18: 5.1 – 26.5 mg/l). Generally, the bottom water contains more particles than the surface water.

5.3 Mineralogy

The mineral contents of SPM samples are listed in Table 10. Overall, mineral compositions at station C1 is distinctly different, displaying lower primary mineral contents but higher clay minerals contents than SPM at other stations. From station C5 to C8, mineral contents show narrow variation range. Quartz is the most abundant mineral, with an average content of $41.0 \pm 2.9\%$. Albite and K-feldspar have average content of $11.2 \pm 1.9\%$ and $4.0 \pm 0.6\%$, respectively. Illite dominates the composition of clay minerals, with an average of $24.3 \pm 3.5\%$. Chlorite and kaolinite have average contents of $8.9 \pm 0.6\%$ and $2.8 \pm 0.7\%$, respectively. Calcite contents are estimated to be $5.2 \pm 0.6\%$, and dolomite has a content of $2.7 \pm 0.7\%$. No smectite and Fe-oxyhydroxide were detected, mostly due to their low content. Considering up to 5% of mineral content uncertainty, no remarkable trend can be observed from station C5 to station C8.

Table 10: Mineral compositions of SPM samples in the Changjiang Estuary

	Quartz %	Albite %	K-feldspar %	Illite %	Chlorite %	Kaolinite %	Calcite %	Dolomite %
C1S	25	6	3	39	6	16	4	2
C1B	27	8	5	34	6	13	4	3
C5S	43	15	3	20	9	3	5	3
C5B	44	13	3	21	9	2	5	4
C6S	41	11	4	24	9	3	5	4
C6B	42	12	4	23	9	2	5	3
C6-1S	40	11	4	25	10	3	5	2
C6-2S	35	8	4	32	10	4	5	2
C6-2B	39	9	4	27	9	3	6	3
C6-3S	41	11	4	24	10	3	6	2
C6-3B	45	14	5	21	8	2	5	2
C8S	40	11	4	25	9	3	6	2
C8B	40	10	5	26	8	4	6	2

5.4 Li concentration and isotope composition of dissolved, SPM and exchangeable phases

The dissolved Li concentrations ($[Li]_{diss.}$) range from 0.8 $\mu\text{mol/l}$ to 26.1 $\mu\text{mol/l}$, showing steadily increasing trend along the sampling transect (Fig. 33A). No significant variation of $[Li]_{diss.}$ can be observed in water column for low salinity site C1-C5 (Fig. 34A). However, consistently with higher salinity of bottom water from site C6, $[Li]_{diss.}$ in the bottom water are slightly higher than the surface water as well. We extracted the exchangeable Li from the SPM and express the corresponding Li concentrations ($[Li]_{exc.}$) as weight per milligram of SPM. Most $[Li]_{exc.}$ range from 0.4 ng/mg to 0.7 ng/mg. This is consistent with desorption experiments conducted by Zhang et al. (1998) who estimated a range of 0.5 – 0.6 ng/mg for Louisiana shelf sediments. The samples collected seaward of station C6-1 (salinity > 3) contain more exchangeable Li than those collected at low salinity (Fig. 34B). The $[Li]_{exc.}$ difference between surface and bottom samples is always insignificant, except at station C9 with difference of 0.4%. In the exchangeable phase, undetectable Al contents demonstrate negligible silicate dissolution during NH_4Cl saturation. The Li concentration of residual phase ($Li_{residue}$), i.e. SPM samples after NH_4Cl saturation, varies from 44.2 $\mu\text{g/g}$ to 83.7 $\mu\text{g/g}$. Along the transect, Li concentration of residual phase decreases from station C1 to C5, and then slightly increase towards outer stations (Fig. 34C). As shown in Figure 33C, no significant difference of $Li_{residue}$ concentrations between surface and bottom samples can be observed.

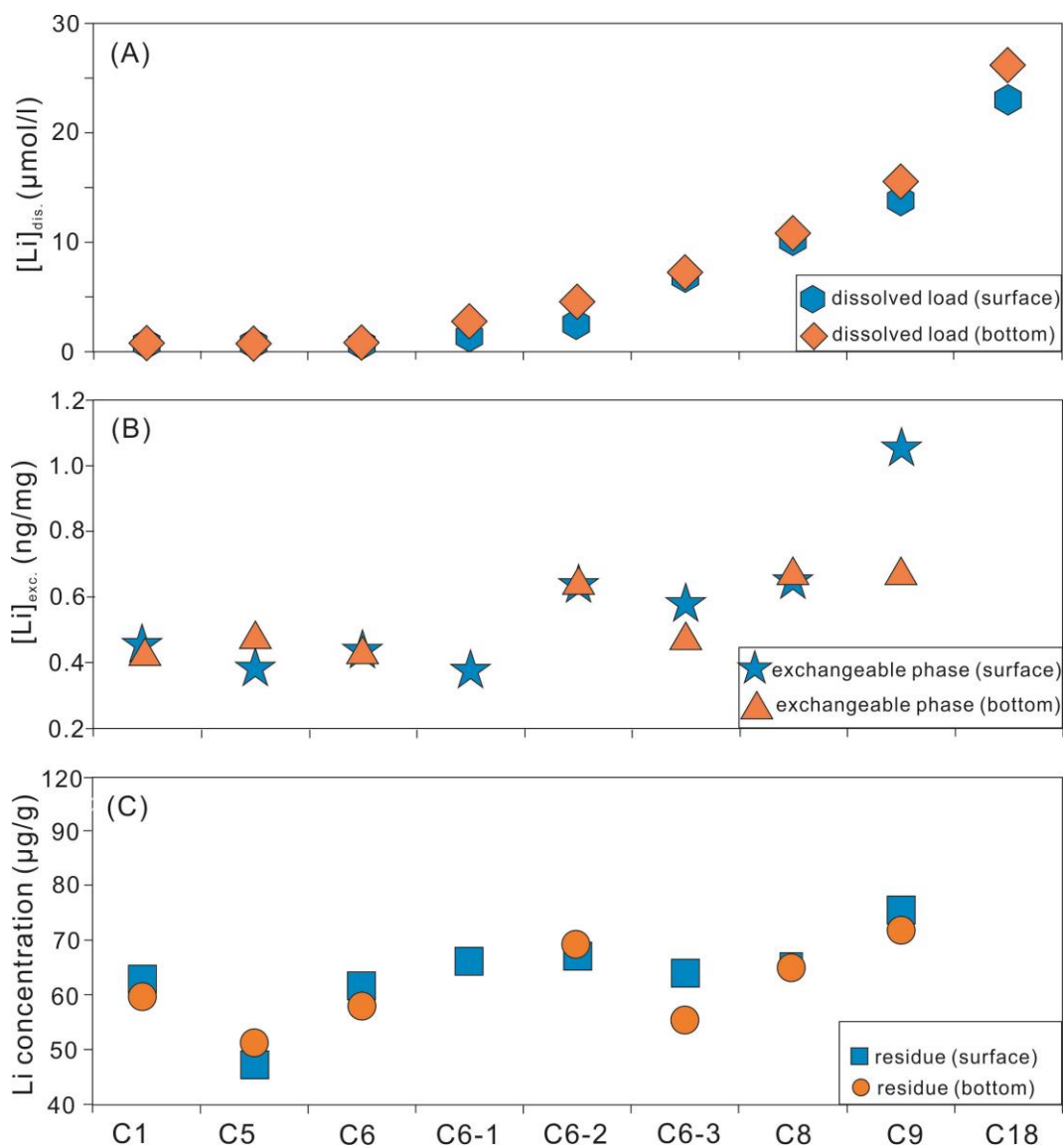


Figure 34 : Li concentrations of (A) the dissolved load, (B) exchangeable phase, (C)residual phase. The residue represents SPM samples after NH_4Cl saturation.

The dissolved Li isotope compositions ($\delta^7\text{Li}_{diss.}$) range from 17.1‰ to 31.6‰, showing increasing trend along the sampling transect. Except station C6-1 and C6-2, $\delta^7\text{Li}_{diss.}$ difference between surface and bottom water is insignificant (Fig. 35A). The Li isotope compositions of exchangeable phase ($\delta^7\text{Li}_{exc.}$) ranged from 2.2‰ to 18.6‰, showing an increasing trend along sampling transect as well (Fig. 35B). The difference of $\delta^7\text{Li}_{exc.}$ between surface and bottom samples at station C9 is up to $\sim 7\%$, while it is minor at other stations. The Li isotope compositions of SPM samples ($\delta^7\text{Li}_{residue}$) show the lowest value at station C1 of -1.3‰ at surface and -1.5‰ at bottom. From station C6 to C9, $\delta^7\text{Li}_{residue}$ show narrow variation, ranging from -0.5‰ to +0.5‰, and no observable trend can be determined along with sampling transect (Fig. 35C).

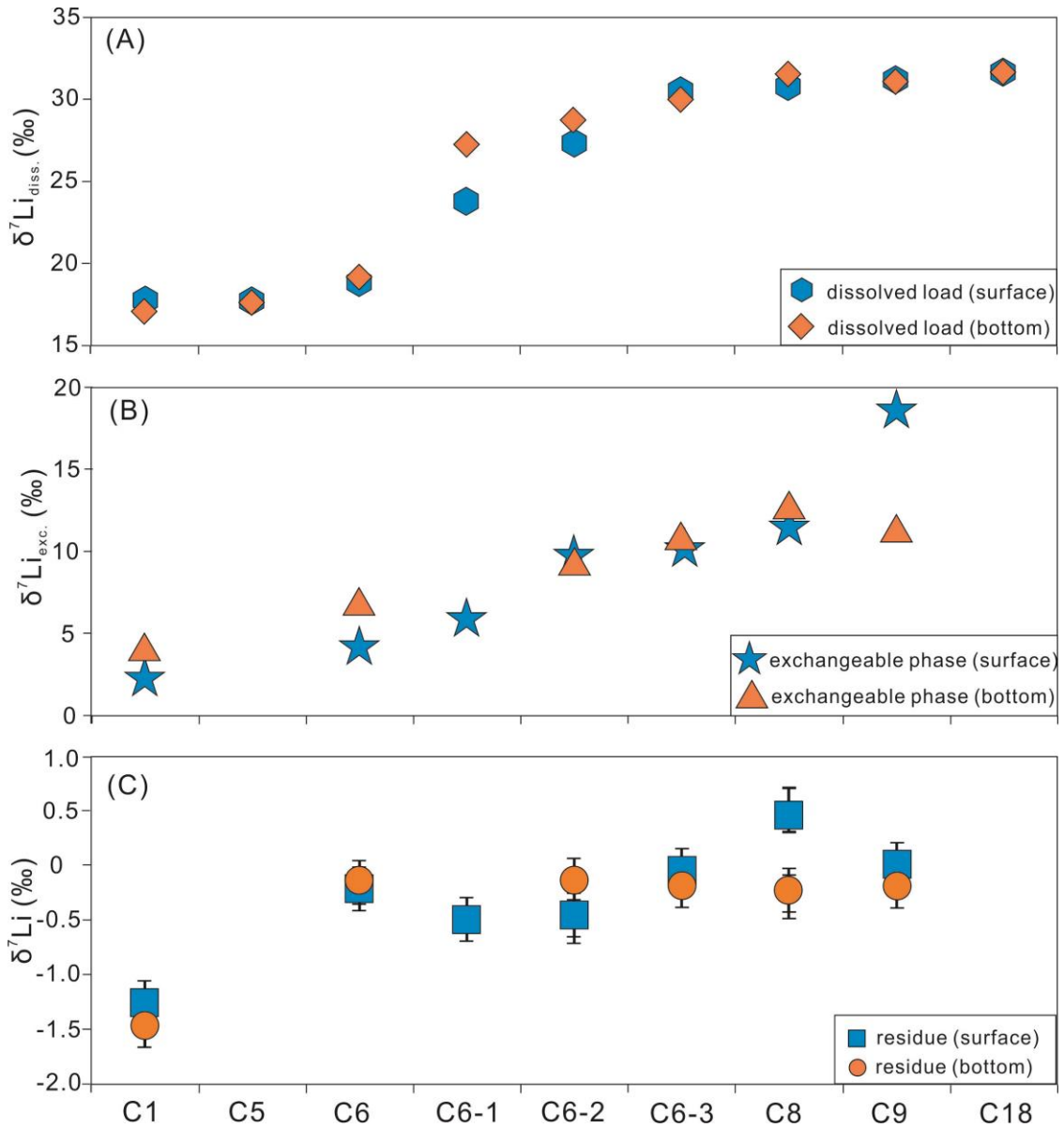


Figure 35 : Li isotope compositions of (A) the dissolved load, (B) exchangeable phase, (C) residual phase. The analytical uncertainty on $\delta^7\text{Li}$ ($2\text{SD}=0.4\text{‰}$) is smaller than the symbol size of the dissolved load and exchangeable phase.

5.5 Conservative mixing of dissolved Li and $\delta^7\text{Li}$ in the estuary

Beyond conservative mixing between river- and sea-water, geochemical and isotope compositions of the dissolved phase sampled within mixing zones of estuaries can be potentially affected by several processes, such as groundwater inputs, particle and sediment dissolution/precipitation, adsorption/desorption, cation exchange and pollution (Gislason et al., 2006; Pogge von Strandmann et al., 2008; Jones et al., 2014; Zhang et al., 2015; Zhu et al., 2018; Zhang et al., 2020). In the Changjiang Estuary, the submarine groundwater discharge ($0.2\text{-}1.0\times 10^9 \text{ m}^3\text{d}^{-1}$) was estimated to be 6-30% of the Changjiang water discharge during

flood season (Gu et al., 2012), which could be an important Li source if this groundwater is enriched in Li compared to the river or the sea-water. However, as shown in Figure 36, dissolved Li concentrations are linearly related to salinity variation, and all the data plot along a mixing line linking two end members: Li-poor Changjiang river water and Li-rich seawater. This implies that groundwater inputs have no significant influence on dissolved Li concentration. Based on a radium mass balance model, Gu et al. (2012) estimated that the residence time of water in the Changjiang Estuary is about 5-7 days. Thus, the influence of particle dissolution is likely negligible, because the dissolution rate of quartz, albite and that of clay minerals (i.e. major minerals of Changjiang SPM) determined from laboratory experiments are long-term processes in salty water. Finally, isotope exchanges between particles and dissolved load can re-distribute isotope compositions between both phases without affecting elemental concentrations significantly. For instance, this was shown for Sr isotopes in an Iceland estuary (Jones et al., 2012a, 2012b). However, in the diagram of $\delta^7\text{Li}_{\text{diss.}}$ vs. $[\text{Li}]_{\text{diss.}}$ (Fig. 37), we observe that, considering the analytical uncertainty, almost all the data are distributed on the mixing line between the Changjiang river water and seawater. Again, this strongly supports that Li is primarily explained by a simple binary mixing process and remains little affected by secondary processes such as isotope exchange, dissolution/precipitation or groundwater addition.

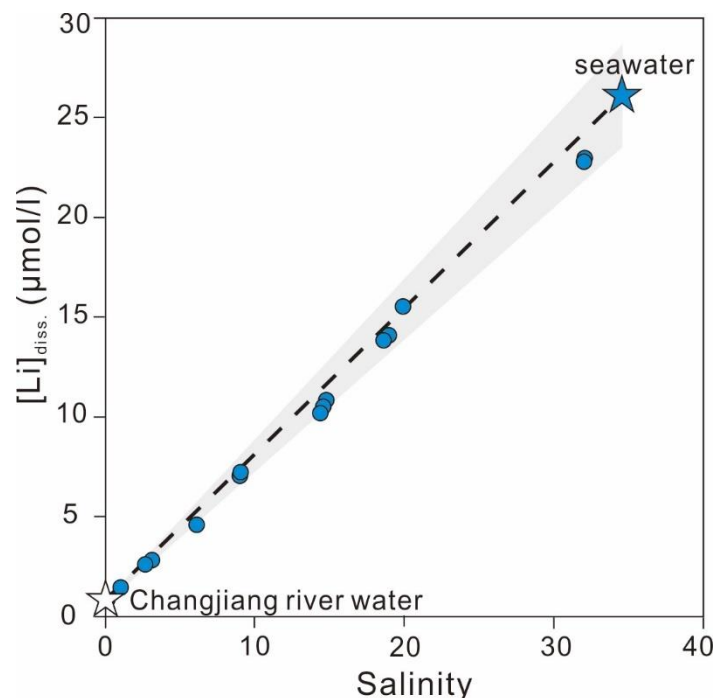


Figure 36 : The linear variation of dissolved Li concentrations as a function of salinity. The dash line represents the theoretical mixing line between seawater (26.1 $\mu\text{mol/l}$) and the Changjiang water (0.8 $\mu\text{mol/l}$). The light grey area displays related analytical uncertainties, with a 10% error for Li concentrations.

In this study, the water samples with salinity equal to 0.1 are used as the Changjiang River end-member. The $[\text{Li}]_{\text{diss.}}$ and $\delta^7\text{Li}_{\text{diss.}}$ are $0.8 \mu\text{mol/l}$ and 17.5‰ , respectively. For seawater endmember, $[\text{Li}]_{\text{diss.}}$ and $\delta^7\text{Li}_{\text{diss.}}$ are $26.1 \mu\text{mol/l}$ and 31.6‰ , respectively. Assuming a conservative mixing, we calculated the corresponding salinity and $\delta^7\text{Li}_{\text{diss.}}$ values with increasing seawater addition. As shown in Figure 37, at low salinity, small quantity of seawater contribution can result in large changes of $\delta^7\text{Li}_{\text{diss.}}$, due to the large concentration difference. In particular, 1% of seawater added to the river dissolved load causes $\delta^7\text{Li}_{\text{diss.}}$ increase of more than 3‰. Therefore, at salinity as low as 7, the $\delta^7\text{Li}_{\text{diss.}}$ value ($\sim 30\text{‰}$) is already close to seawater end-member. Nearly 90% of the $\delta^7\text{Li}_{\text{diss.}}$ variation is completed with only 20% of seawater contribution to the Changjiang Estuary (Fig. 37). At salinity higher than 7, $\delta^7\text{Li}_{\text{diss.}}$ becomes logically insensitive to further addition of seawater. As compiled by Huh et al. (1998), the average Li concentrations and isotope compositions of global rivers into the oceans are 215 nmol/l and 23‰ . If we use this as the river endmember (instead of the Changjiang), we can calculate that a contribution of only 5% of seawater can deviate the mean riverine $\delta^7\text{Li}$ by 30‰. Thus, the behavior of dissolved Li isotope highlighted above is likely universal.

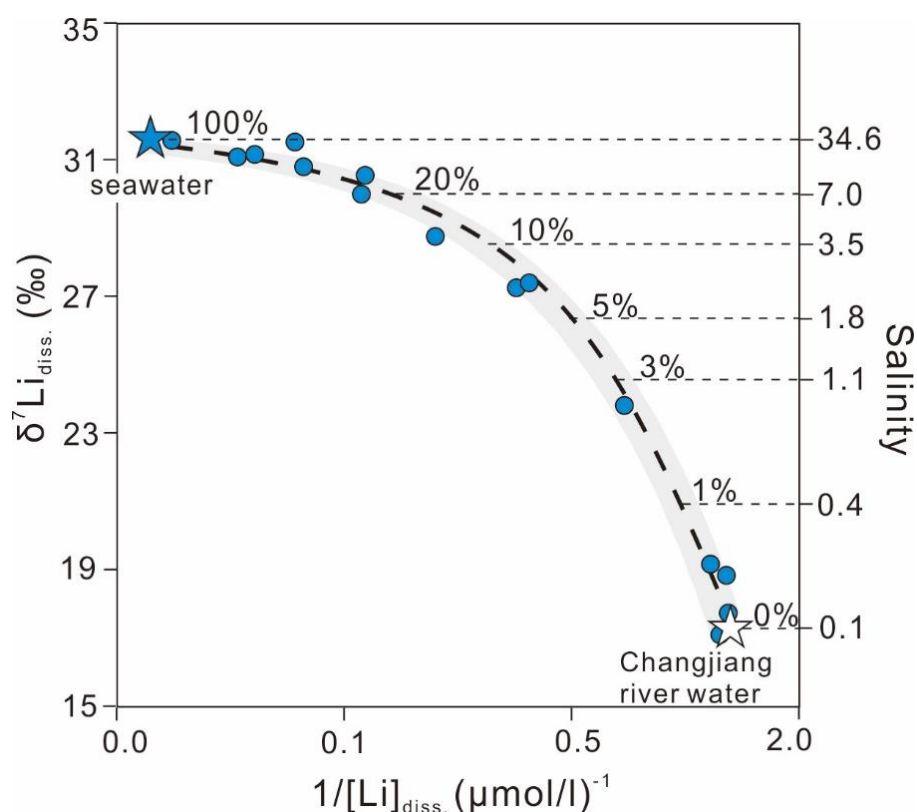


Figure 37 : The diagram for $\delta^7\text{Li}_{\text{diss.}}$ vs. $1/[\text{Li}]_{\text{diss.}}$. The x-axis is logarithmic. The dash lines represent conservative mixing lines, and the grey area represents analytical uncertainties of 0.4‰ (2SD) for Li isotope compositions.

5.5 Particulate Li and $\delta^7\text{Li}$ behavior in the Changjiang Estuary

As shown in Figure 38A, the correlations between Li/Si and Al/Si for riverine SPM (orange symbols) and estuarine SPM (blue symbols) are both positive but with different slope. This first evidences the dominant control of clay minerals (high Al/Si ratios) on Li concentration. Then, previous studies have suggested that the different slope can be caused either by weathering intensity difference or sediment source changes (Lupker et al., 2012; Yang et al., 2019). Thus, the increased slope (orange line to blue line in Fig. 38A) may imply the formation of clay minerals enriched in Li (e.g. reverse weathering) or physical alteration of clay mineral composition (e.g. flocculation and/or resuspension) during SPM transport through the estuary. These two processes can be further examined using Li isotopes. As shown in Figure 38B, $\delta^7\text{Li}$ values of riverine SPM collect at XLJ decrease with increasing Al/Si ratios. Due to the size, density and shape differences of detrital minerals carried in the SPM, hydrodynamic sorting likely control mineralogical variability, as well as geochemical differentiation in riverine SPM. The $\delta^7\text{Li}$ variation trend of XLJ SPM is consistent with the observation in Amazon River (Dellinger et al., 2014), supporting a mixing between coarse primary minerals and fine clay minerals. In contrast, $\delta^7\text{Li}$ variation of estuarine SPM cannot be explained by this mixing. $\delta^7\text{Li}$ value of SPM collected at station C1 (i.e. river end-member) are the lowest among all the estuarine SPM, with low Al/Si ratios (Fig. 38B).

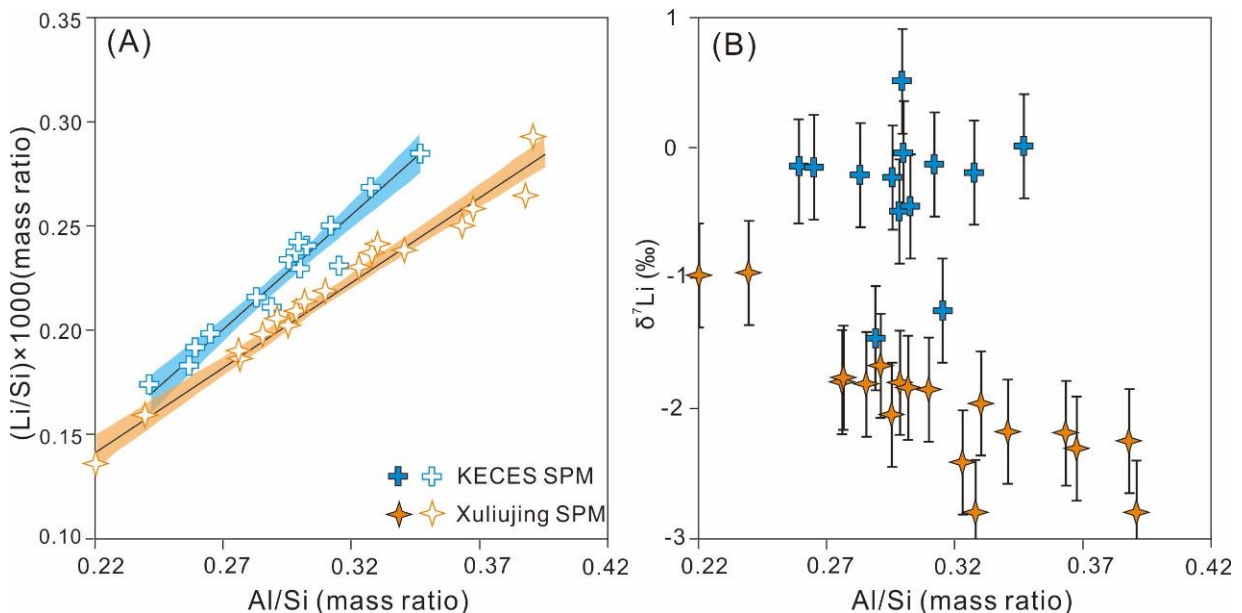


Figure 38 : (A) SPM Li/Si ratio and (B) $\delta^7\text{Li}$ variation as a function of corresponding Al/Si ratio. The linear correlation between Li/Si and Al/Si ratios are displayed with 95% confidence interval. The orange symbols represent data of Xuliujing SPM, and blue symbols represent data of estuarine SPM.

In the diagram of $\delta^7\text{Li}$ vs. Li/Al ratio (Fig. 39), it can be clearly observed that the riverine SPM (i.e. XLJ SPM) show a binary mixing of SPM derived from the upper Changjiang basin and middle sub-basin (i.e. Dongting and Poyang Lakes). This is consistent with the explanation of hydrodynamic sorting above. In the Changjiang basin, the upstream-derived SPM mainly consists of primary minerals, and is characterized by UCC-like $\delta^7\text{Li}$ values. In contrast, due to the abundant weathering product (i.e. kaolinite), SPM contributed by the Dongting and Poyang Lakes are characterized by lower $\delta^7\text{Li}$ values, with average of $-4.0 \pm 0.8\text{‰}$ (Wang et al., 2015). The clay formation could result in the decrease of Li/Al ratio and $\delta^7\text{Li}$ values. As shown in Figure 39, the estuarine SPM variations are distinctly different from the mixing/sorting and clay formation. Toward outer shelf, $\delta^7\text{Li}$ values of estuarine SPM progressively approach the zone of binary mixing defined globally between shale and igneous minerals (Fig. 39). All these evidences strongly suggest that the variability of $\delta^7\text{Li}$ values of estuarine SPM are mostly caused by another process.

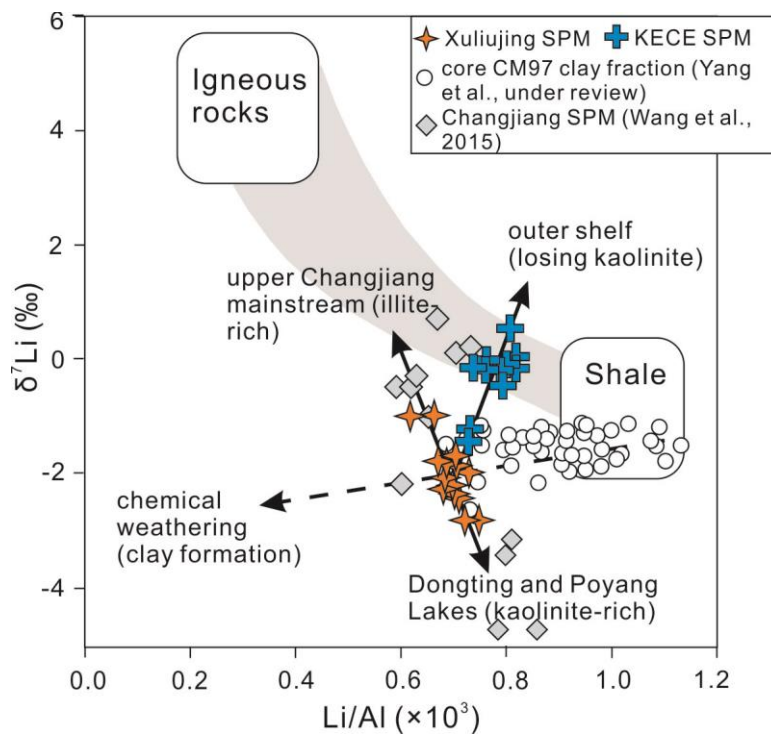


Figure 39 : $\delta^7\text{Li}$ variation as a function of Li/Al ratio. The igneous rocks and shale end-members are modified after Dellinger et al. (2014). KECES SPM define a positive trend between sampling site C1 (lowest $\delta^7\text{Li}$ data) and high salinity C9 site. This effect is best explained by a preferential removal by decantation of low $\delta^7\text{Li}$ clay minerals (probably kaolinite).

Generally, flocculation and resuspension are fundamental processes occurring in the estuaries. For instance, during sediment passing through the Changjiang Estuary, nearly 40%

of sediment load is aggregated and deposited rapidly on the seafloor (Milliman et al., 1985). Compared to other clay minerals, kaolinite was proposed to flocculate and settle particularly fast when encountering the alkaline seawater (Liu et al., 2016). The sediment resuspension in the Changjiang Estuary is supported by several orders of magnitude higher SPM concentration from station C6, compared to station C1 (i.e. river end-member). The XRD results demonstrate that the content of clay minerals decrease during sediment transported offshore. We thus propose that large amount of clay minerals, especially kaolinite and illite, deposited in the sea floor during from sampling site C1 to C5. Out of the river mouth (from C6 to C9), primary minerals are greatly resuspended due to tidal influence. The combined effect resulted in the UCC-like SPM $\delta^7\text{Li}$ values due to the lose of kaolinite.

5.6 Negligible influence of isotope exchange in the Changjiang Estuary

$[\text{Li}]_{\text{exc.}}$ range from 0.4 – 0.7 ng/mg, which is two orders of magnitude lower than the SPM Li concentrations (44 – 76 $\mu\text{g}/\text{mg}$). This range is consistent with desorption experiments conducted by Zhang et al. (1998) on Louisiana shelf sediments, where the exchangeable Li was 0.5 – 0.6 ng/mg. Considering exchangeable $\delta^7\text{Li}$ increase from 2.2‰ to 12.5‰, the influence of exchangeable phase on SPM $\delta^7\text{Li}$ remain no more than 0.1‰, within analytical uncertainty.

As shown in Figure 40A, $\delta^7\text{Li}$ values of the exchangeable fractions vary negatively with their $\text{Li}/(\text{Na}+\text{K})$ ratios. When compared with the binary mixing described by the dissolved phases, the exchangeable fractions are isotopically different, presenting a systematic enrichment in ^6Li . This isotope bias is neither compatible with a binary mixing, nor with a process of Li enrichment due to clay neoformation, such as data of the Changjiang basin shown in Figure 40A (Wang et al., 2015; Ma et al., 2020). In contrast, the variation of isotope fractionation between the dissolved load and exchangeable phase ($\Delta_{\text{diss.-exc.}}$) reaches a plateau when the salinity increases (Fig. 40B). Generally, exchangeable Li can come from desorption from clay interlayer regions, edges sites or and basal planes (e.g. Vigier et al., 2008; Hindshaw et al., 2019; Li and Liu, 2020). In this study, swelling clay mineral of smectite was not detected, and interlayer adsorption can thus be ignored. Previous studies suggested that the process of Li adsorbed on basal planes is physisorption, while Li adsorbed on edge surface correspond to chemisorption (Ockert et al., 2013; Li and Liu, 2020). The Li adsorbed on basal planes can be easily removed by alkali elements, such as Na and K in seawater (Hindshaw et al., 2019; Li and Liu, 2020). We thus propose that the increase of $\Delta_{\text{diss.-exc.}}$ mostly represents

the process of Na/K exchanging for Li on basal planes. As described in section 5.4, the dissolved phase exhibits a conservative behavior, both for Li concentrations and for $\delta^7\text{Li}$. This strongly suggests a negligible influence of Li adsorption process occurring in the mixing zones on the ocean Li content and Li isotope ratio.

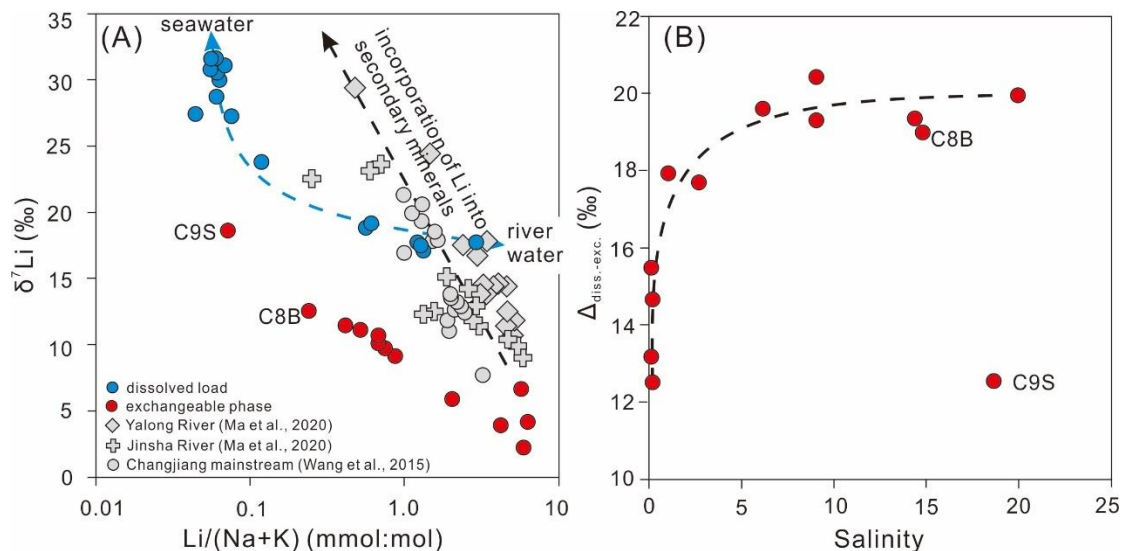


Figure 40 : (A) Li isotope variation as a function of $\text{Li}/(\text{Na}+\text{K})$ ratios, and (B) isotope difference between the dissolved load and exchangeable phase ($\Delta_{\text{diss.-exc.}}$) versus water salinity. The geochemical compositions of samples C8B and C9S are likely contaminated by seawater. These SPM samples were not rinsed with Milli-Q in the laboratory, and seawater might be left on the membrane during filtration.

5.7 Conclusion and Implications

I undertook the first extensive study of Li and its isotope in a large basin estuary (i.e. the Changjiang River). The dissolved Li concentrations and isotope compositions are highly and consistently variable and can be explained by a simple binary mixing between the river water and seawater. The SPM exchangeable fractions are isotopically fractionated compared to the dissolved loads, but this process concerns minimal amounts of Li, and therefore neither affect the dissolved loads nor the particulate matter. Finally, the SPM $\delta^7\text{Li}$ variations across the estuary, from the lowest salinity site to the highest one, are best explained by the preferential and early loss of clay minerals, likely kaolinite, by flocculation and decantation, while other Li-rich minerals reside in the water column for a longer time. More investigations are needed but this would be mostly a classical physical process related to aggregation of fine-grained particle with the increase of salinity and ionic strength.

For the first time, this study show that an estuary of a large river delivering lots of clay-rich particles to the ocean is associated to a very conservative behavior of Li and Li isotopes. This result strongly supports the studies aiming to reconstruct past weathering based

on Li isotopes. In terms of particulate materials, sedimentary particles seem resistant to chemical alteration in estuaries, and therefore can represent good archives for paleoclimate reconstructions. On the other hand, these materials are cation-depleted and less sensitive to chemical weathering as well, mainly due to the influence of recycled weathering products (i.e. mostly illite), abundant in the basin of Chinese rivers. The role of shales on affecting the ocean composition and weathering signature is a critical point that need to be further quantified. Indeed, it should be cautious when using Li isotopes in these catchments to infer information on modern weathering. For studies through time, it appears particularly important to associate Li isotopes to an independent source proxy, Nd isotopes in particular, as previously proposed (Bastian et al., 2017; Bayon et al., 2020).

Chapter 6: Clay Li and Nd isotopes response to hydroclimate changes in the Changjiang (Yangtze River) basin over the past 14,000 years

Chemical weathering of silicates plays a key role in shaping Earth's surface landscape, governing biogeochemical cycles (Gaillardet et al., 1999a), and exerting a critical feedback on global climate stabilization (Raymo and Ruddiman, 1992; Kump and Arthur, 1997; Frings, 2019). During this process, large amounts of sediments are transported by rivers into marginal seas or deep oceans, and potentially record continental weathering and hydroclimatic variations on various temporal scales. For instance, Lupker et al. (2013) interpreted the Bay of Bengal record as reflecting enhanced weathering intensity since ~21 ka, in response to more favorable Holocene climate than in the Last Glacial Maximum. Similar studies were also carried out worldwide, such as in the Changjiang (Yangtze) Delta and the Nile Delta (Wang and Yang, 2013; Bi et al., 2017; Bastian et al., 2017). However, the complex sediment source-to-sink processes and sedimentary recycling challenge the catchment weathering studies. The mechanism and feedbacks linking silicate weathering to the climate through time need to be further investigated.

In this chapter, I reported clay Li and Nd isotopes and element concentrations in core CM97 recovered from the Changjiang Delta and in modern river bank sediments (Fig. 41), in aim to investigate how chemical weathering response to hydroclimate variations in a large river basin. The influence of sediment source, grain size, early diagenesis and lithology on Li isotope were first investigated. Finally, I illustrate how riverine clay Li isotopes may indicate silicate weathering and the response of chemical weathering to climatic changes in large river systems. This study has been submitted to EPSL on 26, June, and now it is under review.

Abstract

In large river basins, the feedback between silicate weathering and climate change on various temporal scales is still highly debated. This study presents clay Li-Nd isotopes and elemental compositions of bank sediments from the Changjiang (Yangtze) River, and of sediments from core CM97 recovered from its delta. In the modern basin, the clay $\delta^7\text{Li}$ and ϵ_{Nd} values of bank sediments range from -4.1‰ to 0.9‰ and from -13.1 to -10.7. The clay Li-Nd isotopes are significantly lower in the middle basin (i.e. the Dongting and Poyang Lakes) compared to the upper reaches. Over the last 13 kyr, three periods can be distinguished in core CM97. During the Younger Dryas, clay Nd isotopes range from -12.2 to -12.0, while clay $\delta^7\text{Li}$ values display a positive excursion of +1.4‰. From 11 ka to 2 ka, the clay $\delta^7\text{Li}$ and ϵ_{Nd} show monotonous variations, and average at $-1.6 \pm 0.2\text{‰}$ and -11.9 ± 0.2 , respectively. Over the last 2 kyr, clay ϵ_{Nd} show lower values (-12.7 to -11.9), while clay $\delta^7\text{Li}$ exhibits larger fluctuations (-2.5‰ to -1.1‰). We infer that the variations of clay Li isotope at 13 – 2 ka are mostly indicative of weathering intensity changes, and less influenced by other factors, such as mineralogical sorting, sediment source, lithology and diagenesis. During the Younger Dryas, the noticeable positive excursion of clay $\delta^7\text{Li}$ is consistent with enhanced incongruent weathering of silicates and secondary mineral formation in the mid-lower Changjiang basin, in response to temperature cooling and increased rainfall. The minor variation of clay $\delta^7\text{Li}$ at 11 – 2 ka likely confirms that clay Li isotopes in basins characterized by large floodplain may be sensitive only to large variations of weathering intensity. Over the last 2 kyr, the fluctuation of clay $\delta^7\text{Li}$ is mostly caused by intensification of human activities in the mid-lower basin. This study supports the rapid response of silicate weathering to hydroclimate changes and to anthropogenic activities. It also provides new insights into the mechanism for Li isotope fractionations caused by continental weathering during the Quaternary period.

Keywords: Li and Nd isotopes; clay; the Changjiang River; Yangtze; continental weathering; paleoclimate

6.1 Introduction

Chemical weathering of silicates plays a key role in shaping Earth's surface landscape and modulating biogeochemical cycles (Gaillardet et al., 1999), and it is also one of the most important mechanisms for global climate stabilization (Raymo and Ruddiman, 1992; Frings, 2019). During this process, large amounts of sediments are transported by rivers into marginal seas or deep oceans, and potentially record continental weathering and hydroclimatic variations on various temporal scales. For instance, Lupker et al. (2013) interpreted the Bay of Bengal record as reflecting enhanced weathering intensity and weathering rate since ~21 ka, in response to more favorable Holocene climate than in the Last Glacial Maximum. Similar studies were also carried out worldwide, such as in the Changjiang (Yangtze) Delta and in the Nile Delta (Wang and Yang, 2013; Bi et al., 2017; Bastian et al., 2017).

The large river basins cover significant proportions of continental crust and various climatic regimes, and thus give advantages of studying weathering on a global scale (e.g. Gaillardet et al., 1999). However, the complex sediment source-to-sink processes and sedimentary recycling challenge our understanding on rapid response of weathering to climatic variation. For instance, the comminution age of fine siliciclastic sediments (<50 μm) in the Changjiang (Yangtze) basin can reach 300–400 kyrs, based on uranium-series disequilibrium (Li et al., 2016). Then, significant time lags may exist in sediment records for weathering responding to climate variation in large catchments. On the other hand, several lines of evidences have suggested that weathering-climate feedback in sediment records could be ascribed to sediment source changes caused by different erosional patterns within the basin or sedimentary dynamics during transport (Bi et al., 2017; Wan et al., 2017; Frings, 2019). In spite of these issues, there are clear examples indicating nearly synchronous co-variation between weathering and paleoclimate variation (Lupker et al., 2013; Bastian et al., 2017). Negligible source changes have been shown over short-term hydroclimate events (Bastian et al., 2017). Therefore, the mechanism and feedbacks linking silicate weathering to climate through time need to be further investigated.

Over the last decade, Li isotopes have been considered as one of the most powerful proxies for silicate weathering investigation. Li is predominantly derived from weathering of silicate rocks, even in carbonate dominated catchments (Huh et al., 1998; Kısakürek et al., 2005). Li cation is monovalent and not affected by redox reaction. During the weathering processes, primary mineral dissolution shows no significant Li isotope fractionation, which has been identified by laboratory experiments (Pistiner and Henderson, 2003; Wimpenny et

al., 2010; Verney-Carron et al., 2011) and by field studies (Ryu et al., 2015). In contrast, secondary minerals preferentially incorporate the light ${}^6\text{Li}$, leaving isotopically heavy ${}^7\text{Li}$ in river water (Huh et al., 1998; Dellinger et al., 2015; Wang et al., 2015). Hence, Li isotope compositions ($\delta^7\text{Li}$) are primarily controlled by the ratio of primary mineral dissolution to the secondary mineral formation. This ratio has been described as weathering congruency or intensity, with congruent weathering (i.e. high ratio) leading to low $\delta^7\text{Li}$ (e.g. Misra and Froelich, 2012; Dellinger et al., 2015, 2017; Bastian et al., 2017; Pogge von Strandmann et al., 2017). Recently, Li isotopes were used to decipher weathering-climate feedback over the geologic past, which suggest distinct response to climate variation. The increase of $\delta^7\text{Li}$ values in the middle-upper Datangpo Formation (Guizhou province, South China) reflects initiation of global cooling before the Marinoan glaciation (Wei et al., 2020). Bastian et al. (2017) observed higher clay $\delta^7\text{Li}$ values during several arid periods over the last 30 kyr in the Nile basin. In contrast, clay $\delta^7\text{Li}$ display much lower values during the glacial periods compared to modern times in the records of Himalayan terrace (Dosseto et al., 2015). To date, it is still unclear how $\delta^7\text{Li}$ from various sediment archives respond to silicate weathering over the geologic past.

As the largest and longest river in Asia, the Changjiang River originates from the Tibetan Plateau, and flows eastward into the East China Sea. The high-resolution sediment archives in the Changjiang Delta since the last deglaciation are now available. In this study, we report clay Li and Nd isotopes and element concentrations in core CM97 recovered from the Changjiang Delta and in modern river bank sediments (Fig. 41). In combination with published paleoclimatic records, we investigate how riverine clay Li isotopes may indicate silicate weathering and the response of chemical weathering to climatic variation in large river systems.

6.2 Regional background

The Changjiang, as one of the largest rivers in the world, originates from the Tibetan Plateau at an elevation above 5,000 m, and drains central China with a length of ca. 6,300 km and a catchment area of $1.8 \times 10^6 \text{ km}^2$ (Fig. 41A). The annual average sediment flux was 470 Mt, which represents ca. 2.5% of present-day estimate for the global sediment flux (Milliman and Farnsworth, 2013). Its drainage basin spans three-grade physiographic terraces in China, with average elevations of 3,000 – 5,000 m, 500 – 2,000 m and less than 500 m respectively (Fig. 41C). According to hydrological and geographic settings, the Changjiang drainage basin

is generally divided into three sections. The upper reaches are the section from river source to City Yichang (Fig. 41B), which are mostly located at the first and second-grade physiographic terraces. Before dam constructions, the upper reaches contributed at least 70% of the annually sediment flux to the East China Sea (Yang Z et al., 2006). The mid-lower reaches are from City Yichang to the river mouth, mostly <500 m in altitude (Fig. 41B). The floodplain and alluvial plains are well developed, occupying about 44% of the total basin area. The Dongting and Poyang Lakes are two major contributors of sediments into the Changjiang mainstream in the middle basin (Fig. 41B).

Geologically, the Changjiang drainage basin is primarily located in the South China Block, which is composed of the Yangtze Craton and the Cathaysia Block (Fig. 41A). It is bounded by the Qinling-Dabie orogenic belt to the north and by the Songpan-Garze terrain to its northwest. The intermediate, basic (e.g. Emeishan basalt province) and ultra-basic rocks are mainly distributed in the upper basin (Fig. 41B). The Changjiang catchment is strongly affected by the humid sub-tropical Asian monsoon climate, that is warm and humid in summer and cold but arid in winter. Generally, the upper basin is subject to the Indian Summer Monsoon (ISM), while the East Asian Summer Monsoon (EASM) dominates climatic changes in the mid-lower basin. At present, the period from May to October accounts for more than 70% of annual water discharge, with a peak mostly in July. Spatially, the annual precipitation increases eastward, from < 400 mm/yr in east Tibet, to about 1000 mm/yr at Chongqing and > 2,000 mm/yr in lower reaches. The mean annual precipitation over the whole basin is ~1,100 mm, and the water discharge into the sea is about 900 km³/yr. Except for the cold climate (below 4°C) in the river source area, the mean annual temperature in the mid-lower basin is about 16 – 18°C.

At the last deglaciation, the sea-level in the East China Sea was about 120 m below the present-day position (Fig. 41D), and the modern river mouth was occupied by a huge incised valley at that time, with the width and depth up to 70 km and 80 m, respectively (Li et al., 2002). With the postglacial sea-level rise, the incised valley was gradually filled by the Changjiang-derived sediments. At this period, the annual sediment mass deposited in the Changjiang estuarine and coastal areas was estimated to be 137 – 224 Mt/yr (Wang et al., 2018). With the sea-level reaching its highstand at 7 – 6 ka, the annual sediment influx was about 99 – 113 Mt/yr (Fig. 41D) and the modern delta initiated, while the strong human activities caused the annual sediment flux increasing to 162 Mt/yr on average during the last 2 kyr.

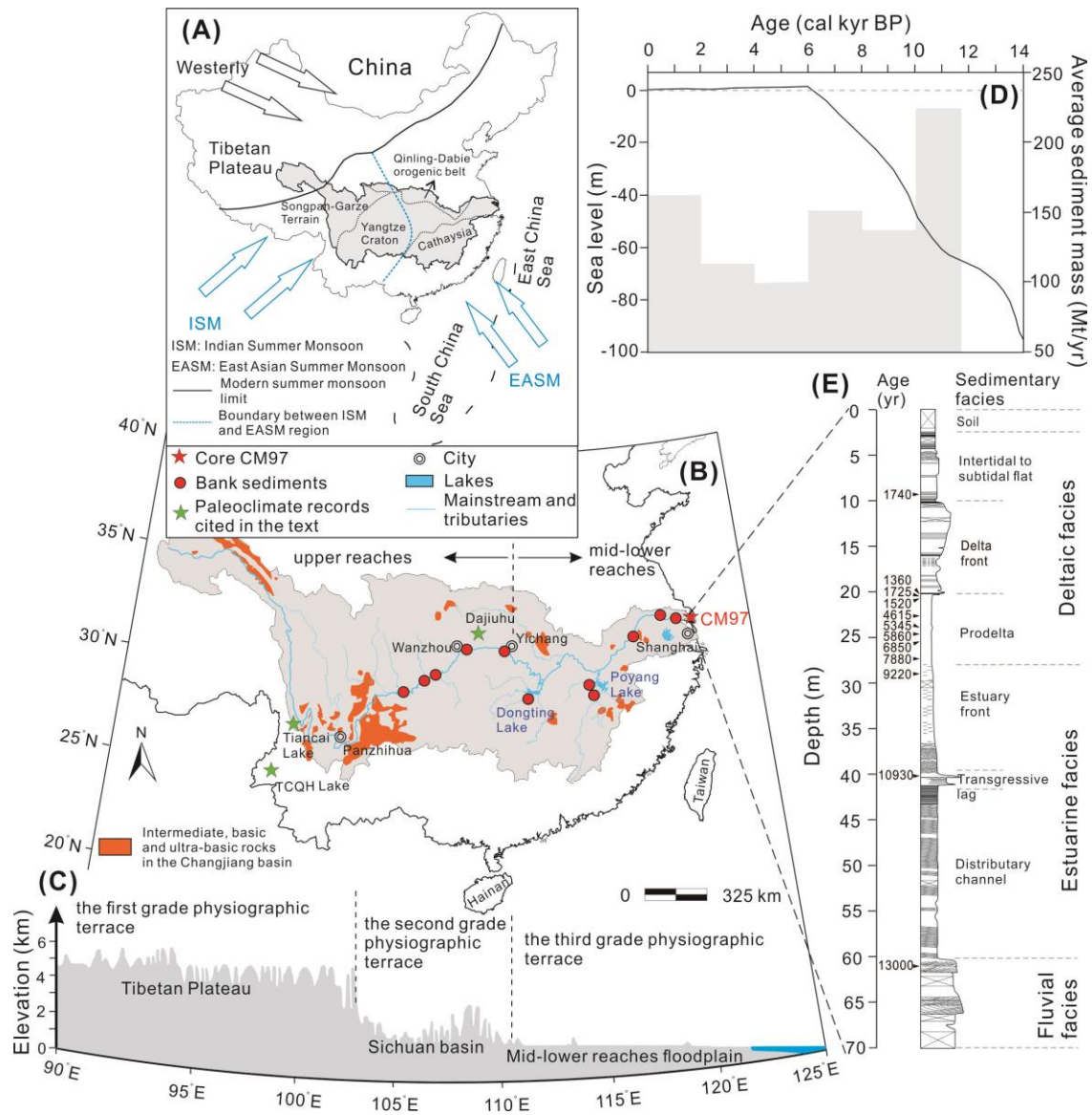


Figure 41 : Schematic map showing (A) Asian monsoon regimes, and major tectonic blocks, (B) sampling sites, drainage basin and (C) topography in the Changjiang basin. (D) The sea level changes since 14 ka in the East China sea (Hori et al., 2001) and annual sediment mass deposited in the Changjiang estuarine and coastal areas (Wang et al., 2018). (E) Downcore variation of sedimentary facies and depositional age of CM97. The detailed description about sedimentary facies can refer to Hori et al. (2001).

6.3 Materials and Methods

6.3.1 Samples

Core CM97 (~70 m in depth) was drilled at the modern Changjiang River mouth (31°37' N, 121°23' E) in 1997. The AMS ^{14}C dating on molluscan and/or snail shells was reported by Hori et al. (2001), and then the age model was gained using linear interpolation. Core CM97 thus recorded the depositional history over the past ~14,000 years, and the

sedimentary sequence primarily consist of fluvial and floodplain facies at the bottom (70 – 60.3 m in depth), estuarine to shallow marine facies in the middle part (60.3 – 20.1 m), and deltaic facies at the top (20.1 – 0 m). The detailed information about sedimentary facies was described in Horii et al. (2001). In this study, a total of 61 samples were selected from core CM97 for geochemical measurements. In order to constrain the provenance of core sediment, 11 riverine bank samples, including 5 from the upper reaches, 3 from the Dongting and Poyang Lake in the middle reaches, and 3 from the lower reaches, were taken in May and July, 2018 (Fig. 41B).

6.3.2 Clay fraction (<2 μm) separation and Li isotope analyses

About 1 g bulk sediment was first separated into two groups (i.e. > 63 μm sand fraction and < 63 μm fine-grained fraction) using wet sieving method. Then, the fine-grained fraction (<63 μm) was immersed into 20 ml 1N HCl for twenty minutes to remove carbonates at room temperature. This method is effective enough for carbonate removal, and only ~6% Li lost on average during the leaching for sediments in the Changjiang basin. The residue was washed three or four times with Milli-Q water until the supernatant pH closed to neutral. Afterwards, the clay fraction was separated from the fine-grained fraction by the pipette method following the Stoke's Law at room temperature. In order to remove exchangeable Li, the clay fraction was mixed with 20 ml 1 N Ammonia Chloride (NH_4Cl) solution (Vigier et al., 2008). Finally, the clay fraction was freeze-dried after washing with Milli-Q water two times.

About 10 mg samples were ground to <200 mesh in an agate mortar and then were digested first using 3:1 HF/ HNO_3 solution at 70°C for several hours. Afterwards, the solution was evaporated and re-dissolved with concentrated HNO_3 several times. The sample was then re-digested with 3:1 HCl/ HNO_3 solution. Finally, the solution was evaporated and re-dissolved in 4 ml 1 N HCl. At this stage, the solution is systematically centrifuged to ensure the lack of any solid residue. The Li purification was performed on a cationic resin column, following the method described in Vigier et al. (2008). All of these experiments described above were conducted at Laboratory of Oceanography of Villefranche-sur-Mer (LOV), Sorbonne University. Li isotopes measurement were performed using a MC-ICP-MS Neptune plus (ThermoFisher) at the Ecole Normale Supérieure de Lyon (National Facilities). The accuracy of the isotopic measurements was monitored by analyzing Li7-N pure Li solutions and BE-N basaltic rocks. Repeated measurements yielded mean $\delta^7\text{Li}$ value of $+30.3 \pm 0.6\text{‰}$

(2SD, n=26) and $+5.2 \pm 0.5\%$ (2SD, n=4), respectively. In addition, three samples were processed repeatedly using the same but independent chemical procedure, yielding values of $-1.9 \pm 0.4\%$ (2SD, n=3), $-1.5 \pm 0.3\%$ (2SD, n=3) and $-1.3 \pm 0.2\%$ (2SD, n=3), respectively.

6.3.3 Al, Na and Li concentrations and Nd isotope analyses

About 50 mg powder samples were ignited in muffle furnace at 600°C in order to remove organic matter before acid digestion. Afterwards, these powder samples were dissolved with a mixture of 1:1 concentrated HNO₃ and HF in a tightly closed Teflon vessel for at least 48 h with a temperature of 190°C. After drying, samples were re-dissolved in HNO₃ to break down any fluorides. Finally, samples were re-digested in 2 ml 30% HNO₃ with a temperature of 190°C. The Al, Na and Li concentrations were measured respectively by Inductively Coupled Plasma-Optical Emission Spectrometers (ICP-OES, IRIS Advantage) and Inductively Coupled Plasma Mass Spectrometry (ICP-MS, Agilent 7900) at the State Key Laboratory of Marine Geology, Tongji University. The analytic precision and accuracy were monitored by rock standards of BCR-2. The results showed that the precision and accuracy of elements is generally less than 5%, while Li concentration has an accuracy of 10%.

The Nd purification was conducted with a two-step method. The Rare Earth Elements (REE) were first separated using 2.5 N HCl elution on an ion-exchange column filled with Bio-Rad AG50W-X12, 200-400 mesh resin. Then, the Nd was separated from the REE solution using 0.25 N HCl. Finally, the Nd isotope ratios were determined using a MC-ICP-MS Neptune plus at the State Key Laboratory of Marine Geology, Tongji University. In this study, Nd isotope values are reported as ϵ_{Nd} , which is equal to $[(^{143}Nd/^{144}Nd)_{\text{samples}} / (^{143}Nd/^{144}Nd)_{\text{CHUR-1}}] \times 10^4$. The CHUR represents Chondritic Uniform Reservoir, with a value of 0.512638. The mean measured ϵ_{Nd} of BCR-2 is 0.0 ± 0.3 (2SD, n=10), well within the recommended values.

6.4 Results

The Li concentrations of clay fraction from CM97 sediments range from 78.6 µg/g to 99.1 µg/g, with an average of 88.0 ± 5.4 µg/g. Their δ^7Li values vary from -2.6‰ to -1.1‰, lower than the average value of $+0.6 \pm 0.6\%$ estimated for the upper continental crust (Sauzéat et al., 2015). As for the modern bank sediments, the clay δ^7Li of upstream-derived sediments vary from -0.3‰ to 0.9‰. These values are comparable with those reported for sedimentary rocks in the Tibetan Plateau (Weynell et al., 2017), well within the range of

upper continental crust (Fig. 42A). In comparison, the Li isotope compositions of clay-size sediments collected in the Dongting and Poyang basins are more negative, ranging from -4.1‰ to -2.3‰ (Fig. 42A). As demonstrated by Wang et al. (2015), the $\delta^7\text{Li}$ values of SPM samples collected in the upper Changjiang reaches are also higher than those in Dongting and Poyang Lakes (Fig. 42A), similar with the observation in clay fraction. The ϵ_{Nd} values of core CM97 clay fractions show a narrow variation, ranging from -12.8 to -11.6 (Fig. 42B). This is within the range measured for modern river sediments (Yang et al., 2007; He et al., 2015). The clay ϵ_{Nd} values vary from -11.5 to -10.7 in the upper reaches, and from -15.2 to -12.4 in the Dongting and Poyang Lakes. The clay ϵ_{Nd} values in the lower reaches range from -12.2 to -11.7. The difference of clay ϵ_{Nd} between the upper reaches and the middle basin is larger than analytical uncertainty, thus, it is still possible to use this proxy to determine the sediment provenance.

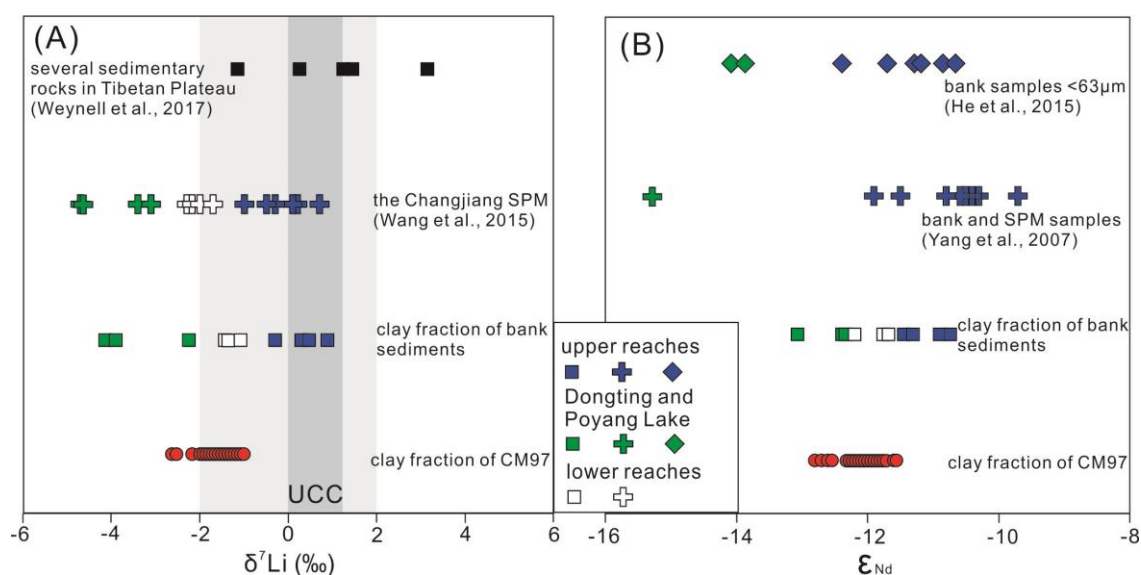


Figure 42 : (A) Li and (B) Nd isotope compositions in the sediments from the modern Changjiang River and core CM97. $\delta^7\text{Li}$ values of suspended particulate matter (SPM) are from Wang et al. (2015). The $\delta^7\text{Li}$ values of sedimentary rocks (i.e. mudstone, sandstone and shale) collected from northeastern Tibetan Plateau are from Weynell et al. (2017). The light and dark grey bars reflect the average $\delta^7\text{Li}$ values for the upper continental crust (UCC) published by Teng et al. (2004) and Sauzéat et al. (2015), respectively. The Nd isotope compositions of SPM and bank samples are from Yang et al. (2007) and He et al. (2015).

6.5 Discussion

6.5.1 Clay source discrimination and depositional environment changes

The provenance of core CM97 sediments has already been estimated using clay mineral assemblages and bulk sediment Sr-Nd isotope compositions (Wang and Yang, 2013;

Bi et al., 2017). These results indicate that sediments accumulated in the Changjiang Estuary typically represented an average composition of particulates sourced from the whole Changjiang basin (mainly from the mountainous upper reaches, as well as from the the middle basin). Nd isotopes are thought to be independent of Earth surface processes (e.g. chemical weathering and hydrodynamic sorting), and are widely used to discriminate river sediment sources (Bayon et al., 2015). Given that the Changjiang basin is tectonically stable since the late Pleistocene (Yang S et al., 2006), the provenance of core CM97 clay fraction can be further determined by comparing their Nd isotope compositions with those of modern river sediments. The Permian basalts widely distributed in the upper Changjiang basin are characterized by relatively higher ϵ_{Nd} values compared to those of granites and Quaternary fluvial-lacustrine sediments in the mid-lower basin (Yang et al., 2007; He et al., 2015). Therefore, the ϵ_{Nd} values of the Changjiang sediments decrease downstream with increasing sediment contribution from the mid-lower basin. In this study, we simply use Nd isotopes to constrain the source of clay fraction (Fig. 43A). As shown in Figure 3B, the content ratios of kaolinite to illite (i.e. kaolinite/illite) from Wang and Yang (2013) are also shown for comparison. Based on the investigation of modern Changjiang River, illite accounts for 60 – 80% of clay mineral assemblages in the upper basin, while sediments from the Dongting and Poyang Lakes are featured by relative higher kaolinite contents, because of stronger weathering there (He et al., 2013). Thus, higher kaolinite/illite ratio may reflect greater clay contribution from the middle Changjiang basin. It should be noted that clay mineral contents are also subject to the influence of chemical weathering, not only of sediment source, within the basin.

As illustrated in Figure 43A, clay ϵ_{Nd} values show an overall narrow variation at 13 – 2 ka and a negative shift during the last 2 kyr. It is worth noting that the negative excursions of clay ϵ_{Nd} at 4.3 – 4.1 ka are small but larger than analytical uncertainty, suggesting more clay contributions from the middle basin at this period. This result is overall consistent with the observation from kaolinite/illite ratio which shows stable values at 11 – 2 ka but higher values at 2 – 0 ka (Fig. 43B). The consistent results of clay ϵ_{Nd} and kaolinite/illite ratios confirm sediment source changes during the last 2kyr that more clay-size sediments in core CM97 were contributed by the middle Changjiang basin. In contrast, at 13 – 11 ka, kaolinite/illite ratios display higher values compared to relative stable clay ϵ_{Nd} variation. Kaolinite content can vary with soil formation process in the middle Changjiang basin, but Nd isotopes are not affected by this process. Therefore, the changes of kaolinite/illite ratios at 13

– 11 ka may imply the influence of chemical weathering, and we will further identify that using Li isotopes in section 6.5.3.

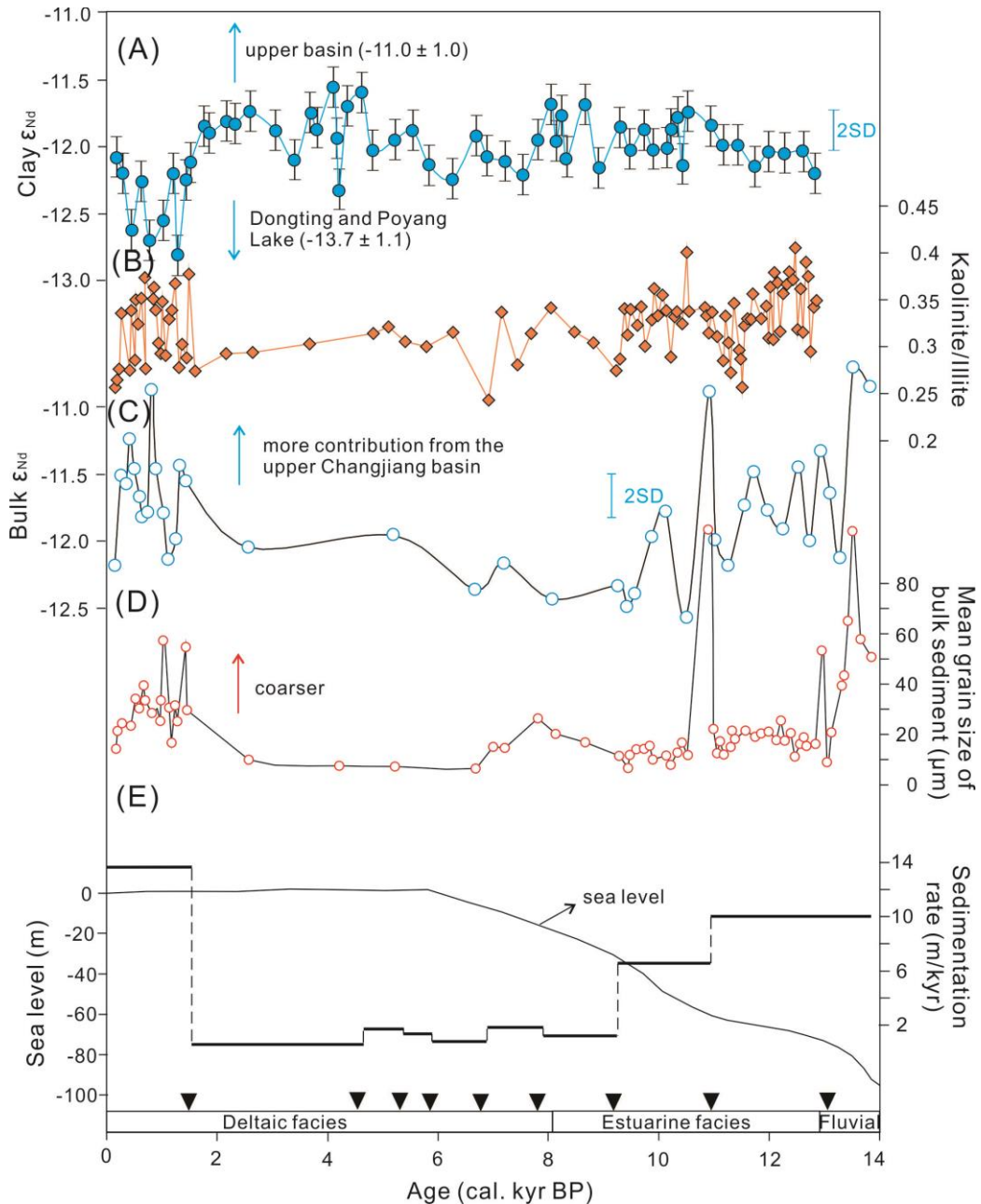


Figure 43 : (A) Clay ϵ_{Nd} , (B) content ratios of kaolinite to illite, (C) ϵ_{Nd} values in bulk sediments, (D) mean grain size of bulk sediment, and (E) mean sedimentation rate for the core CM97. The postglacial sea-level changes in the East China Sea are also shown. Sea-level changes and mean grain size are from Hori et al. (2001) and Bi et al. (2017). Kaolinite and illite contents are from Wang and Yang (2013). The inverted triangles represent sampling positions of molluscan shells which were used for ^{14}C dating (Hori et al., 2001). The end-member ϵ_{Nd} values of the upper Changjiang basin, the Dongting and Poyang Lakes are estimated by averaging data analyzed in this study and those published by Yang et al. (2007) and He et al. (2015).

With the sea-level rise during the last deglaciation, the local depositional environment has greatly changed. The sedimentary system in the East China Sea shifted from the transgressive system tract in the last deglaciation (15.4 – 7 ka) to the highstand system tract since 7 ka (Hori et al., 2001; Li et al., 2002). Correspondingly, the fluvial facies, estuarine to shallow marine facies, deltaic facies and their respective sub-facies can be observed in the core CM97 (Fig. 41E). The change in depositional environment may significantly affect provenance discrimination and weathering information recorded in core sediments. After comparison of sediment source proxies with local sedimentation parameters (Figs. 43C, 43D and 43E), we find that bulk ϵ_{Nd} values are higher in coarser sediments at periods with higher sedimentation rate (i.e. at 13 – 11 ka and 2 – 0 ka), but this is not observed for clay fractions in Figure 43A. There is an apparent inconsistency for sediment source between clay fraction and bulk sediments in core CM97. This strongly suggests that geochemical compositions of bulk sediments were largely affected by depositional environment and sea-level changes, while the fine clays are less sensitive to these aspects. The clay fraction may be more reliable to trace past chemical weathering, as argued in Bastian et al. (2017).

6.5.2 Grain size, lithological and diagenetic effects on clay Li isotopes

To our knowledge, Li is more concentrated in clay minerals, and coarse-grained quartz and feldspar are Li-poor host (Dellinger et al., 2014; Sauzéat et al., 2015). δ^7Li values of clay fraction are also generally lower than coarse-grained fraction, as more primary minerals exist in the latter. In this study, in order to minimize grain size effect, we focused on clay fractions. Particulate matters can be considered as mixture of different rocks and their weathering products (e.g. Dellinger et al., 2014, 2017). The bedrock in the Changjiang basin is characterized by igneous and sedimentary rocks, while high-grade metasedimentary rocks are distributed sporadically (Yang et al., 2007). Thus, we only tested the influence of igneous and sedimentary rocks in the following. As illustrated in Figure 44A, the geochemical compositions of SPM samples and bulk sediments of core CM97 both show a binary mixing between igneous end-member and weathering products. In contrast, clay δ^7Li values and Li concentrations show trends which are distinct from the bulk sediment mixing pattern (Fig. 44). This observation therefore supports the use of clay-size fraction in this study. Then, the elemental and isotopic variations in clay samples are not derived from the mixing with igneous rocks. Apart from chemical weathering, the trend defined for clay fraction also implies some influence of sedimentary recycling, i.e. recycled clay from sedimentary rocks

(Fig. 44). In the Changjiang basin, illite is mostly eroded from sedimentary rocks (He et al., 2013, Weynell et al., 2017), which can be identified by similar $\delta^7\text{Li}$ values between upstream-derived clay and sedimentary rocks (i.e. shale, sandstone and mudstone) in the Tibetan Plateau (Fig. 42A). Kaolinite is weathering product mainly produced in the Dongting and Poyang Lakes (He et al., 2013). To some extent, the influence of sedimentary rocks recycling can be roughly estimated by sediment source changes (i.e. kaolinite/illite ratios), and we will discuss that in section 6.5.3.

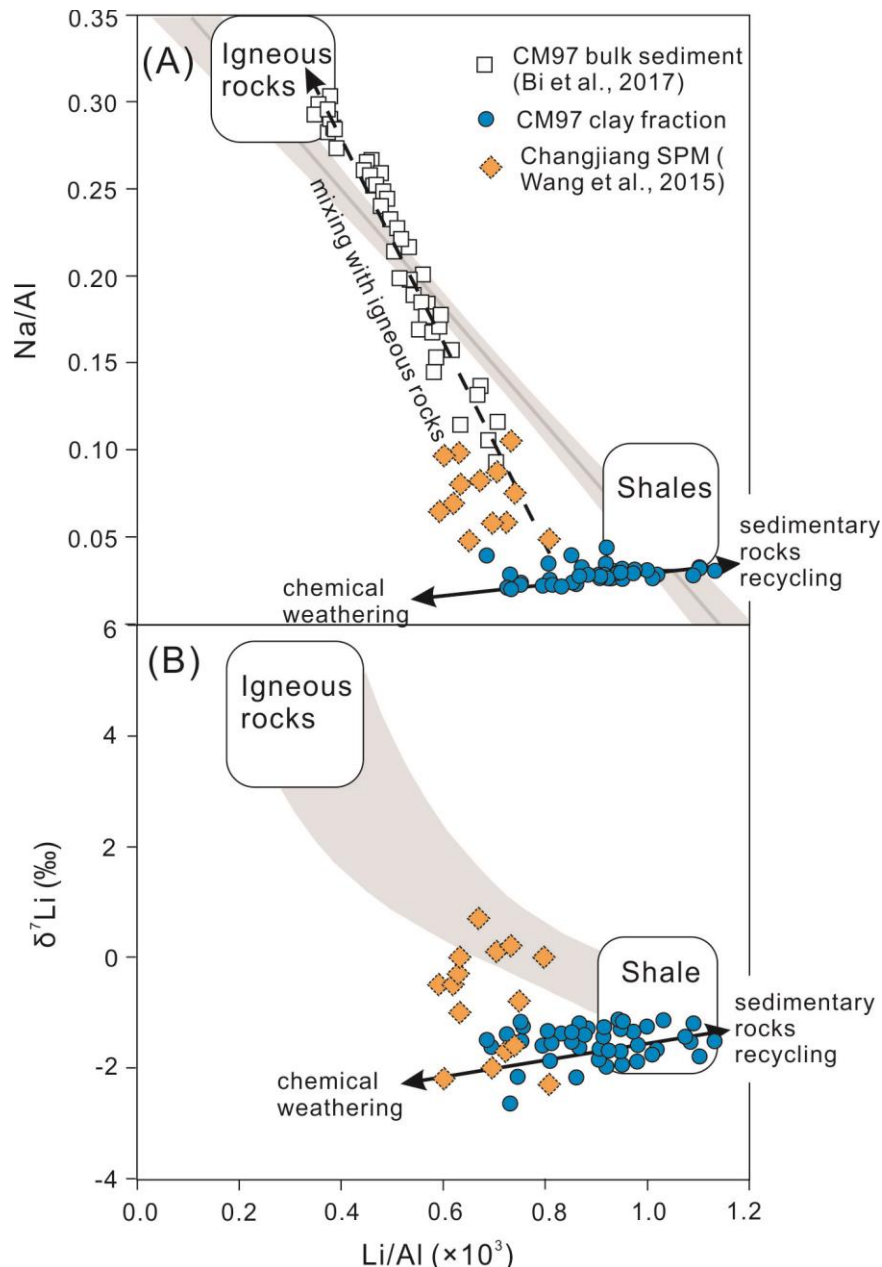


Figure 44 : (A) Na/Al ratios and (B) $\delta^7\text{Li}$ values as a function of Li/Al ($\times 1000$). The element concentrations of CM97 bulk sediments and suspended particulate matter (SPM) in the Changjiang basin are cited from Bi et al. (2017) and Wang et al. (2015). The end-members of igneous rocks and shales, and the mixing line with 95% confidence interval (grey) are cited from Dellinger et al. (2014).

Estuarine and early diagenetic reactions may also affect the geochemical compositions of deposited sediments. Due to the difference in ionic strength, pH and temperature between river and seawater, chemical compositions of river sediment can be modified in the estuary by adsorption-desorption, particle dissolution and/or ongoing weathering processes (Jeandel and Oelkers, 2015). For Li isotopes, Pogge von Strandmann et al. (2008) observed an increase of $\delta^7\text{Li}$ values ($\sim 5\%$) for particulate matter in the Borgarfjörður estuary in Iceland. Based on the investigation of sedimentary facies, the study area was suggested to be inundated since $\sim 9 - 10$ ka due to sea-level rise (Hori et al., 2001; Li et al., 2002). However, clay $\delta^7\text{Li}$ values of core CM97 fluctuate around -1.5% during the middle Holocene under the maximum marine transgression (Fig. 45A), and show no positive or negative excursion in response to ongoing reaction with seawater or particle dissolution. The possible adsorption of Li onto clay or Fe-Mn oxyhydroxides surface has been removed by NH_4Cl in clay fraction pretreatment. Combining all of these observations, we thus infer that estuarine processes do not significantly alter clay $\delta^7\text{Li}$ values in core CM97. Early diagenesis leads to an uptake of Li from seawater ($\delta^7\text{Li} = 32.3\%$), and then clay $\delta^7\text{Li}$ values should become heavier with authigenic clays formation. However, the ratios of Li/Al and clay $\delta^7\text{Li}$ values are close to shale end-member (Fig. 44), and no systematic downcore increase in clay $\delta^7\text{Li}$ is observed (Fig. 45A). All these observations suggest that early diagenesis cannot account for clay $\delta^7\text{Li}$ variation in core CM97.

6.5.3 Possible links between chemical weathering and climatic change

As illustrated in Figure 45A, core CM97 clay $\delta^7\text{Li}$ values exhibit a small but statistically significant increase of $\sim 1.4\%$ during the Younger Dryas (YD) from 13 ka to 11 ka. Then, relative stable $\delta^7\text{Li}$ values are punctuated by excursions at three short-term periods between 11 ka and 2 ka. These excursions occurred at 4.2 – 4.1 ka, 8.6 – 8.1 ka, 10.5 – 10.1 ka, possibly corresponding to the 4.2 ka, the 8.2 ka, the 10.3 ka climate events (Wanner et al., 2011). However, the ^{14}C ages used in this study may bear large uncertainties, and the temporal resolution is not sufficient to confirm the observed fluctuations of clay $\delta^7\text{Li}$ responding to these events. Thus, the mechanism for clay $\delta^7\text{Li}$ variations on centennial timescales will not be discussed in the following. It should be noted that the overall variation of clay $\delta^7\text{Li}$ at 11 – 2 ka is small compared to external reproducibility for the Li isotope analyses. In contrast, during the last 2 kyr, larger fluctuations of clay $\delta^7\text{Li}$ can be observed, mostly between -1.1% and -1.9% .

As a first approximation, the noticeable excursion of clay $\delta^7\text{Li}$ during the YD period can be caused by a change of Li isotope fractionation factor, as it is temperature-dependent (Vigier et al., 2008). The YD event corresponds to millennium-scale climate cooling, and punctuated the termination of the last glacial period at 12.9 – 11.7 ka. During this period, the temperature in central China was estimated to be $\sim 2 - 4^\circ\text{C}$ lower, based on branched fatty alcohol ratio (BNA15) in Dajiuhu peatland (Fig. 45E; Huang et al., 2013). However, a temperature decrease would lead to a decrease in clay $\delta^7\text{Li}$ values (Vigier et al., 2008), opposite from that observed during the Younger Dryas. Then, the influence of sediment source changes, i.e. ratio of upstream-derived sedimentary rocks to weathering products contributed by the middle basin, needs to be discussed, despite the minor changes of clay ϵ_{Nd} values. Assuming that higher kaolinite/illite ratios during the YD period was caused by more sediment contribution from the middle Changjiang basin (i.e. sediment source changes), which might be supported by decreased precipitation in the upper basin (Fig. 45F) but humid climate in the central China (Fig. 45G). As shown in Figure 42, clay-size sediments in the middle basin are mainly derived from soil formation, which are characterized by lower $\delta^7\text{Li}$ values than sediments produced by sedimentary rock erosion in the upper reaches. Thus, if weathering condition at 13 – 2 ka was consistent, more clay contribution from the middle basin should result in a decrease of clay $\delta^7\text{Li}$ values in core CM97. This is the opposite of the positive excursion of clay $\delta^7\text{Li}$ at 13 – 11 ka as well (Fig. 45A). Therefore, the remarkable higher kaolinite/illite ratio during the YD, associated with minor clay ϵ_{Nd} variation, is best explained by changed soil formation condition in the middle Changjiang basin, rather than sediment source changes. We then further propose that the variation in clay $\delta^7\text{Li}$ of core CM97 at the YD period is most likely indicative of changes in silicate weathering intensity in response to climatic evolution. As Li is quantitatively incorporated into the secondary minerals, clay $\delta^7\text{Li}$ values increased along with decreasing ratios of primary mineral dissolution to secondary minerals formation. At present, the middle Changjiang basin are characterized by high weathering intensity (i.e. more congruent weathering), which results in low clay $\delta^7\text{Li}$ values in the modern sediments (Fig. 42A). During the YD period, climate cooling in the middle Changjiang basin likely caused a more incongruent weathering condition (i.e. weakened weathering intensity), and then higher $\delta^7\text{Li}$ values. Consequently, more clay characterized by higher $\delta^7\text{Li}$ value was transported to the Changjiang Estuary during the YD period.

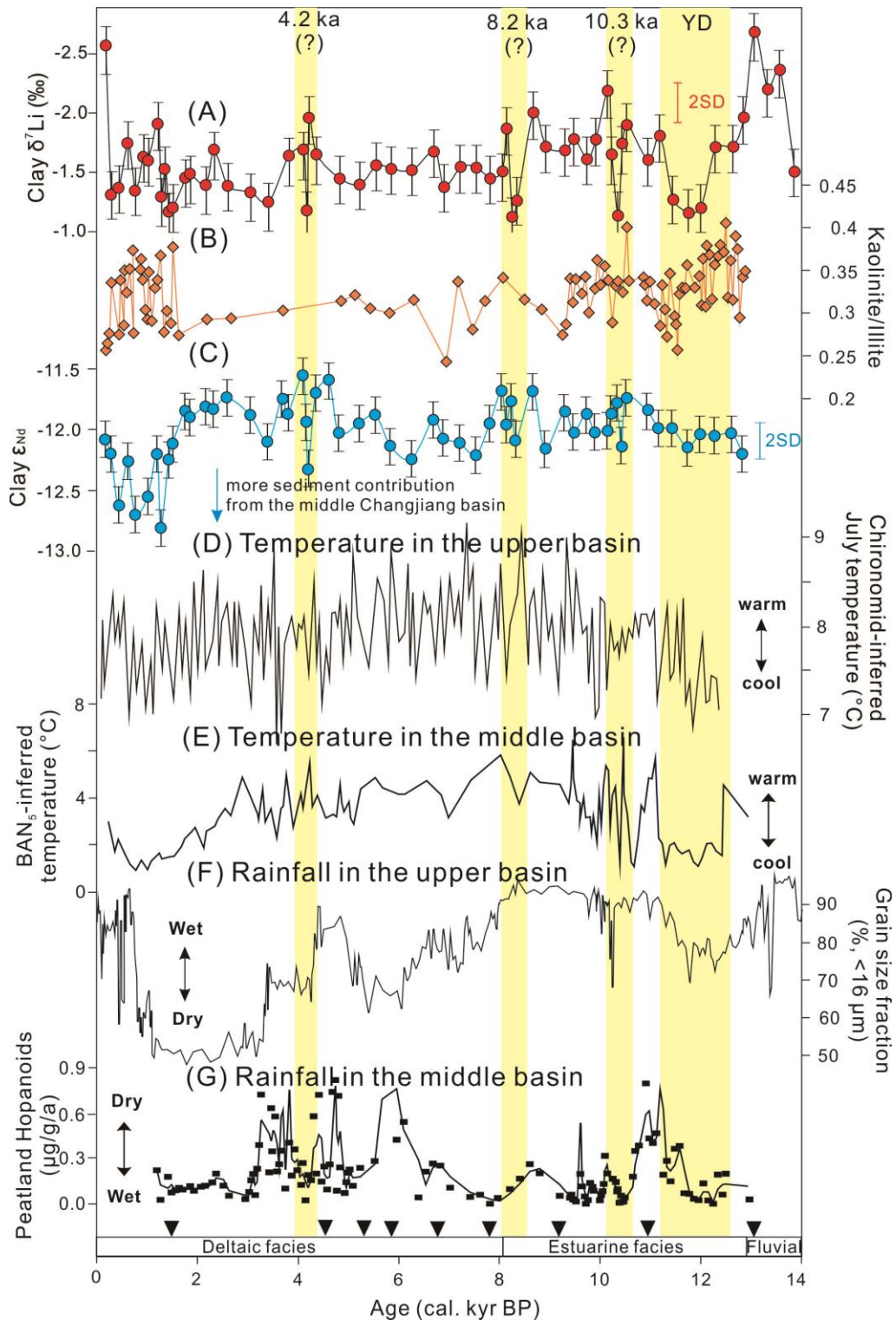


Figure 45 : Comparison of (A and C) clay Li-Nd isotopes and (B) kaolinite/illite ratios of CM97 with the temperature and rainfall records in the Changjiang basin. (D) Chironomid-inferred mean July temperature in Tiancai Lake, southeastern margin of the Tibetan Plateau (Zhang et al., 2017a). (E) Temperature reconstructed by branched fatty alcohol ratio (BNA₁₅) in Dajiuhu peatland (Huang et al., 2013). (F) Grain size (<16μm) fraction of lacustrine sediments in TCQH (Zhang et al., 2017b), indicating rainfall variation in the upper basin. (G) Mass accumulation of aerobic hopanoids in Dajiuhu peatland, reflecting rainfall variation in the middle Changjiang basin (Xie et al., 2013).

At 11 – 2 ka, the kaolinite/illite ratios, clay ϵ_{Nd} and clay $\delta^7\text{Li}$ variations remain minor and monotonous (Figs. 45A, 45B and 45C). This likely suggests that the response of weathering intensity to climatic variation was dampened in this large river catchment. Due to the long residence time of sediment, large river basins can buffer any trace of changes caused by climatic variations (Li et al., 2016; Romans et al., 2016). However, this view is not consistent with the significant Li isotope variations observed during the YD period (Fig. 45A). Clay being the finest fraction in river sediments may be transported rapidly and then be less affected by long residence time in the flood/alluvial plains such as in the Nile Basin (Bastian et al., 2017). As mentioned above, sediment source changes were minor at 11 – 2 ka (Figs. 45B and 45C), which means relatively stable mixing between soil erosion in the upper reaches and soil formation in the mid-lower basin. As discussed above, clay sediments characterized mostly by illite in the upper Changjiang basin are predominantly eroded from sedimentary rocks. Clay $\delta^7\text{Li}$ variation here is insignificant and is not associated with weathering intensity. In contrast, soil formation in the mid-lower basin can modulate $\delta^7\text{Li}$ values of sediment there. Thus, in the context of negligible sediment source changes, the minor changes of clay $\delta^7\text{Li}$ in core CM97 indirectly demonstrate insignificant variation of weathering intensity in the mid-lower basin at 11 – 2 ka. As illustrated in Figures 45E, climate variations in the mid-lower Changjiang basin were mild, which might support the minor variation of weathering intensity as well.

During the last 2 kyr, clay ϵ_{Nd} and kaolinite/illite ratios both indicate additional clay contribution from the middle Changjiang basin as discussed in section 6.5.1. Thus, sediment source changes should be considered, as it possibly accounts for clay $\delta^7\text{Li}$ variations (Fig. 45A). Over the last 2 kyr, human activities not only considerably migrated to the upper Changjiang basin (Wang and Yang, 2013; Bi et al., 2017), but also greatly enhanced in the mid-lower basin with the fast development of society and civilization. Several studies reported that the reduction in trees and shrubs pollen, in parallel with a rise of herbaceous pollen, in the lower Changjiang basin since 3,000 ka (Yao et al., 2017), which suggest the enhanced agricultural activities in this area. The lower Changjiang basin became a center of intensive rice production in the past 1,000 years (Zong et al., 2012). Therefore, soil erosion can be strongly affected by human activities, especially by cultivation and deforestation (Wang et al., 2011). Accordingly, more clay sediments were eroded from the middle basin and transported to the Changjiang Estuary. The clay $\delta^7\text{Li}$ fluctuation over the last 2 kyr likely reflects the interactive human-induced soil erosion and natural processes in the Changjiang basin. Nevertheless, due to analytical uncertainty of ^{14}C dating in this study, clay $\delta^7\text{Li}$

fluctuation on centennial or much shorter timescales cannot be exactly explained using materials of core CM97. More direct evidences and high-resolution observations are further required for better understanding the anthropogenic perturbation on natural weathering and erosion processes in large catchments.

6.5.4 Implications for the weathering-climate feedback

The glacial-interglacial cycles are of particular importance for understanding the weathering-climate feedback (Frings, 2019). In this study, the Changjiang Delta provides high-resolution sediment archives for investigating weathering and climatic changes over the past 14, 000 years. During this period, climate is the major external force for chemical weathering. However, hydrodynamic sorting, sediment recycling and long sediment residence time in the flood/alluvial plains make the interpretation of weathering proxies ambiguous. Guo et al. (2018) suggested that the suspended sediments or clay fraction in rivers can better reflect the modern weathering information. Herein, we further indicate that clay fraction more suitable, as bulk SPM are likely to be more influenced by the contribution of un-weathered bedrocks, especially coarse-grained igneous rocks (as shown in Fig. 44 and Dellinger et al., 2014). Clay Li isotopes faithfully record the YD event, suggesting fast response of chemical weathering to this climate event. The weathering signals registered in clay fraction are not altered during sediment “source-to-sink” processes because of their relatively rapid transport by waters and small grain size effects. Possibly, the comminution age calculated by Li et al. (2016) for fine-grained sediments (<50 μm) in the Changjiang basin is not suitable for evaluating the behavior of clay fraction. Moreover, our results confirm that silicate weathering, even in a large river system with complex climate and sediment routing processes, can respond rapidly to hydroclimate variability.

6.6 Conclusions of this chapter

This study presents clay Li-Nd isotope compositions and element concentrations in the core CM97 recovered from the Changjiang Delta and in the modern bank sediments. Several conclusions are drawn as follows:

(1) The core CM97 received more clay-size sediments from the middle Changjiang basin at 2 – 0 ka, while the clay source remained almost the same at 13 – 2 ka. The postglacial sea-level rise could significantly influence the source and compositions of bulk sediments in core CM97, but the clay fraction was less influenced.

(2) The clay Li concentration and isotope compositions in core CM97 were not significantly affected by contributions from igneous rocks, grain size sorting, estuarine and diagenetic effects. The variations of clay Li isotope compositions are mostly indicative of the changes of chemical weathering intensity and clay formation in the Changjiang catchment.

(3) Clay $\delta^7\text{Li}$ and ϵ_{Nd} values fluctuate strongly during the last 2 kyr, possibly suggesting the interactive human induced soil erosion and natural sediment transport processes. The minor $\delta^7\text{Li}$ and ϵ_{Nd} variations at 11 – 2 ka imply that clay Li isotopes only respond to significant weathering intensity variability in the mid-lower Changjiang basin. During the Younger Dryas, with temperature decrease in the middle Changjiang basin, the enhanced incongruent weathering of silicates (i.e. weakened weathering intensity) caused a noticeable positive excursion of clay $\delta^7\text{Li}$. Overall, the clay $\delta^7\text{Li}$ records suggest the complex response of silicate weathering and clay formation in the large catchments on various temporal scales.

Chapter 7: Conclusion and perspectives

7.1 Conclusions

The Changjiang (Yangtze) River is one of the largest rivers in the world. The large river basin cover significant proportions of upper continental crust and climatic regimes, and thus give advantages of studying weathering on a global scale. During my PhD, I participated to collect modern bank sediments, SPM and water samples, as well as got drilled core samples from Prof. Yang, with the objective to better understand the influences of various processes on sediment geochemical compositions, at different timescales (0 – 14 ka). The results shed new light on the interpretation of weathering signals recorded in sediments, and on the response of chemical weathering to hydroclimate variations in a large river basin. Major conclusions can be summarized as follows:

(1) Lots of care should be undertaken when studying the impact of climate on modern weathering conditions, since I show that dam constructions, such as the impressive Three Gorges Dam (TGD) construction, significantly and progressively changed not only sediment transport pattern, but also their geochemical compositions. Before the operation in 2003, large amounts of upstream-derived sediments were deposited in the mid-lower reaches. These sediments experienced further weathering in the floodplain. Since 2003, the upstream-derived sediments were largely retained upstream of the TGD, and sediments previously deposited in the mid-lower basin were resuspended and became the main source of sediment to the East China Sea. A possible consequence of this effect is an ‘artificially induced’ stronger weathering degree since 2003. Another potential implication of these findings is that, on a long-term basis, intensive damming activities decreasing the supply of fresh materials from mountainous regions, may weaken the role of floodplain in regulating continental weathering and CO₂ levels.

(2) Li and its isotopes exhibit conservative behavior in waters of the mixing zone of the Changjiang Estuary. The Li concentrations of SPM samples are dominated by clay minerals, and their variations are primarily controlled by binary mixing between primary minerals (i.e. quartz and feldspar) and clays (i.e. illite and kaolinite). During transport through the estuary, kaolinite are preferentially and physically flocculated and settled down, resulting in a slight increase of SPM $\delta^7\text{Li}$ values. I also find that the Li isotope compositions of particles are significantly affected by recycled materials derived from sedimentary rocks

(mostly illite in the Changjiang basin). As a consequence, SPM $\delta^7\text{Li}$ values may not directly reflect modern weathering conditions, as was highlighted by Dellinger et al. (2017). However, I also indicate that the combination of Li isotopes with a source proxy seems can help to better distinguish the role of sedimentary formation in the weathering signal. The exchangeable phase associated to the suspended particles represents only a small amount of Li in natural environment, and has no influence on dissolved and particulate Li. To conclude, our results highlight the role of large continental river estuaries in conservatively delivering dissolved and particulate Li to the oceans, which strongly supports all studies aiming at reconstructing paleo-weathering based on $\delta^7\text{Li}$ variation over geologic past.

(3) During the last 14 kyrs, the clay-size Nd isotope compositions in the core CM97 recovered from the Changjiang Delta show relatively constant sediment source at 13 – 2 ka. In contrast, since 2 ka, more sediments are derived from the Dongting and Poyang Lakes, located in the lower basins, likely in response to intensification of anthropogenic activities. During the Younger Dryas (13 – 11 ka), with temperature decrease but rainfall increase in the middle Changjiang basin, the enhanced incongruent weathering of silicates (with likely more secondary clay formation) is consistent with a significantly positive excursion of clay $\delta^7\text{Li}$. At 11 – 2 ka, clay $\delta^7\text{Li}$ variations are minor, and likely reflects insignificant changes of chemical weathering, which is supported by mild climate variability during the Holocene in the mid-lower Changjiang basin. Finally, during the last 2 kyr, clay $\delta^7\text{Li}$ values fluctuate strongly, likely due to the human induced soil erosion and change of sediment source. Overall, the clay $\delta^7\text{Li}$ variations of core CM97 is indicative of the changes of chemical weathering intensity and clay formation in the Changjiang catchment, and illustrates the complex response of these processes to climate variations and anthropogenic activities in large catchments.

7.2 Perspectives

During my PhD, the influence of dam construction on downstream sediment geochemical composition, the behavior of Li isotopes in the mixing zone of the Changjiang Estuary and how chemical weathering response to past climate changes in a large river basin were investigated. Although our studies shed new lights on the processes affecting chemical weathering or its interpretation, several questions related to the carbon cycle and to the application of Li isotopes are still need to be explored in more details :

(1) Several studies have suggested that floodplain weathering play an important role in regulating global climate and biogeochemical cycle (Lupker et al., 2012; Bouchez et al.,

2013). In the modern Changjiang basin, I also ascribed the intensified weathering intensity since 2003 to the combination effect of the TGD construction and further weathering of sediment in the downstream floodplain. However, the result of further weathering is indirectly inferred based on mass balance calculation. I think that it would be important to establish: 1) whether sediment deposited in the mid-lower basin can experience intensive weathering, and if yes, what is the related timescale and control law, and 2) to what extent floodplain weathering could regulate CO₂ consumption? Because it is hard to exclude the influence of the TGD on geochemical compositions of modern bank or SPM samples, I plan to sample two short core located upstream and downstream of the TGD, respectively (Fig. 46). A downstream short core could be sampled between the TGD and the Dongting Lake, where the influence of downstream sediment contribution can be ignored. The element ratios (i.e. K/Si and Al/Si) would then be used to distinguish weathering and grain size effect. The relative difference of Ca and Mg content and other isotope proxies (e.g. Li and Mg) could then be used to estimate CO₂ drawdown by further weathering in the floodplain.

(2) Li isotopes have long been considered as one of the most powerful proxies for chemical weathering indication. Most of field studies focused on the dissolved load and particulates. In the study of the Changjiang Estuary, I observed conservative behavior of dissolved Li and negligible Li isotopic changes of SPM samples. However, there is Li isotope fractionation between the dissolved load and exchangeable phase. This indicates that the Li isotope can respond rapidly to surrounding environment changes. Similarly, the reducible fraction (Fe/Mn (hydr)-oxides) of Hawaiian regoliths have higher $\delta^7\text{Li}$ values than the detrital phase, which likely reflects isotopic variation of pore water (Li et al., 2020). Recently, it has been shown that the difference in Nd isotope composition between Fe oxide fraction and corresponding detrital fraction was considered as a potential proxy for distinguishing the weathering of sedimentary vs. crystalline silicate (Bayon et al., 2020). In terms of Li isotope composition of the Fe oxide fraction, it would be interested to determine how it varies in the weathering profiles and river sediments, as well as in the mixing zone of estuaries. It is still unclear whether Li isotope in the reducible fraction can be a proxy of environmental changes, such as during an hypoxic event, and if this signature can be preserved after the sediment deposit. A standardized sequential extraction procedure could be developed for the sediments collected in the Changjiang Estuary to start with (Fig. 46). The influence of particle residence time, SPM concentration and estuary mixing on Li isotope composition of reducible fraction can also be determined using adsorption/desorption experiments. These are the main axes that

I could propose in the near future in order to further solve Earth Science issues using Li isotope.

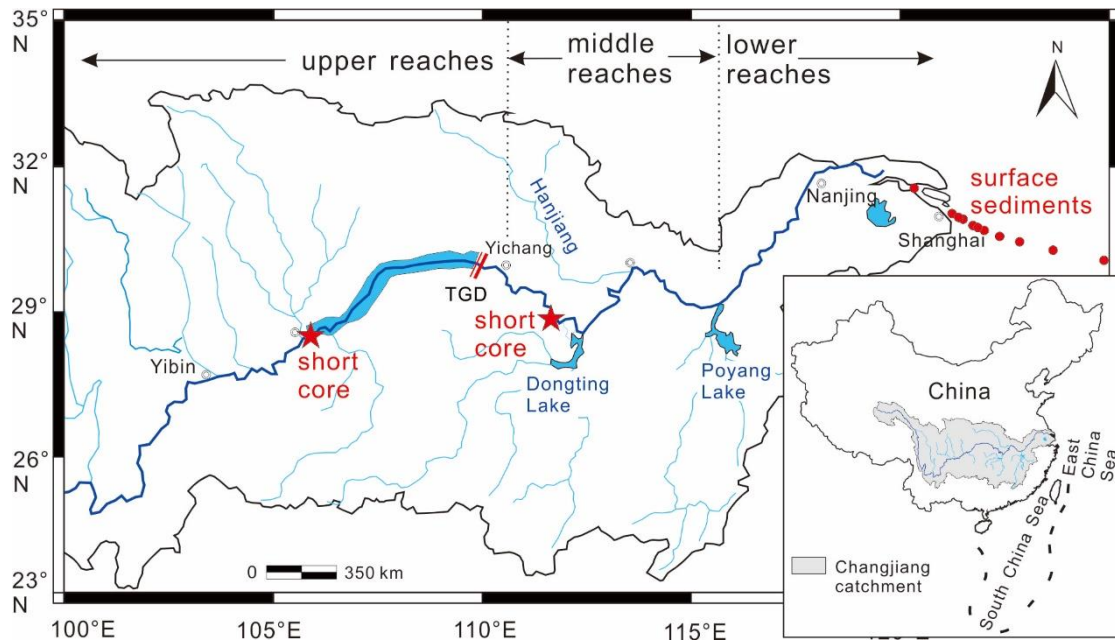


Figure 46 : Schematic map showing sampling sites that could be of interest in the near future.

Bibliographie

Bagard, M. L., West, A. J., Newman, K., Basu, A. R. Lithium isotope fractionation in the Ganges–Brahmaputra floodplain and implications for groundwater impact on seawater isotopic composition. *Earth and Planetary Science Letters*, 2015, 432: 404–414.

Barbour, G. B. Physiographic history of the Changjiang, *The Geographical Journal*, 1936, 87: 285-312.

Bastian, L., Revel, M., Bayon, G., Dufour, A., Vigier, N. Abrupt response of chemical weathering to Late Quaternary hydroclimate changes in northeast Africa. *Scientific reports*, 2017, 7: 44231.

Batalla, R. J., Gomez, C. M., Kondolf, G. M. Reservoir-induced hydrological changes in the Ebro River basin (NE Spain). *Journal of Hydrology*, 2004, 290(1-2), 117-136.

Bayon, G., Lambert, T., Vigier, N., Deckker, P., Freslon, N., Jang, K., Larkin, C., Piotrowski, A., Tachikawa, K., Thollon, M., Tipper, E. Rare earth element and neodymium isotope tracing of sedimentary rock weathering. *Chemical Geology*, 553, 119794.

Berner, R. A. and Caldeira, K. The need for mass balance and feedback in the geochemical carbon cycle. *Geology*, 1997, 955-956.

Berner, R. A., Lasaga, A. C., Garrels, R. M. The carbonate-silicate geochemical cycle and its effect on atmospheric carbon dioxide over the past 100 million years. *American Journal of Science*, 1983, 283(7): 641-683.

Bensimon M., Bourquin J. and Parriaux A. Determination of ultra-trace elements in snow samples by inductively coupled plasma source sector mass spectrometry using ultrasonic nebulization. *J. Anal. Atom. Spectrom.* 2000, 15: 731–734.

Bi, L., Yang, S., Li, C., Guo, Y., Wang, Q., Liu, J. T., Yin, P. Geochemistry of river-borne clays entering the East China Sea indicates two contrasting types of weathering and sediment transport processes. *Geochemistry, Geophysics, Geosystems*, 2015, 16(9): 3034-3052.

Bi, L., Yang, S., Zhao, Y., Wang, Z., Dou, Y., Li, C., Zheng, H., Provenance study of the Holocene sediments in the Changjiang (Yangtze River) estuary and inner shelf of the East China sea. *Quaternary International*, 2017, 441: 147-161,

Bluth, G. J., Kump, L. R. Lithologic and climatologic controls of river chemistry. *Geochimica et Cosmochimica Acta*, 1994, 58(10): 2341–2359.

- Bouchez, J., Gaillardet, J., Lupker, M., Louvat, P., France-Lanord, C., Maurice, L., Armijos, L., Moquet, J. S. Floodplains of large rivers: Weathering reactors or simple silos? *Chemical Geology*, 2012, 332: 166–184.
- Bouchez, J., von Blanckenburg, F., Schuessler, J. Modeling novel stable isotope ratios in the weathering zone. *American Journal of Science*, 2013, 313: 267-308.
- Bouchez, J., Gaillardet, J. How accurate are rivers as gauges of chemical denudation of the Earth surface? *Geology*, 2014, 42(2): 171–174.
- Brunskill, G. J., Zagorskis, I., Pfitzner, J. Geochemical mass balance for lithium, boron, and strontium in the Gulf of Papua, Papua New Guinea (project TROPICS), *Geochimica et Cosmochimica Acta*, 2003, 67(18): 3365-3383.
- Burton, K. W., Vigier, N. Lithium isotopes as tracers in marine and terrestrial environments. In *Handbook of Environmental Isotope Geochemistry* (pp. 41–59). Springer, Berlin, Heidelberg. 2012.
- Carter, A., Clift, P. D. Was the Indosinian orogeny a Triassic mountain building or thermotectonic reactivation event? *Comptes Rendues de l'Academie Scientifique, Geoscience*, 2008, 340: 83-93.
- Chan, L.H., Edmond, J.M., Thompson, G., A lithium isotope study of hot springs and metabasalts from mid-ocean ridge hydrothermal systems. *Journal of Geophysical Research* 1993, 98 (B6): 9653-9659.
- Chan, L. H., Hein, J. R. Lithium contents and isotopic compositions of ferromanganese deposits from the global ocean. *Deep Sea Research Part II: Topical Studies in Oceanography*, 2007, 54(11–13): 1147-1162.
- Chen, J., Wang, F., Xia, X., Zhang, L. Major element chemistry of the Changjiang (Yangtze River). *Chemical Geology*, 2002, 187(3-4): 231-255.
- Chen, L., Edmond, J. M. Variation of lithium isotope composition in the marine environment: A preliminary report. *Geochimica et Cosmochimica Acta*, 1988, 52(6), 1711-1717.
- Chen, X., Yan, Y., Fu, R., Dou, X., Zhang, E. Sediment transport from the Yangtze River, China, into the sea over the Post-Three Gorge Dam Period: A discussion. *Quaternary International*, 2008, 186(1): 55-64.
- Chen, Z., Wang, Z., Finlayson, B., Chen, J., Yin, D. Implications of flow control by the Three Gorges Dam on sediment and channel dynamics of the middle Yangtze (Changjiang) River, China. *Geology*, 2010, 38(11), 1043-1046.

- Chetelat, B., Liu, C.-Q., Zhao, Z. Q., Wang, Q. L., Li, S. L., Li, J., Wang, B. L. Geochemistry of the dissolved load of the Changjiang Basin rivers: Anthropogenic impacts and chemical weathering, *Geochimica et Cosmochimica Acta*, 2008, 72(17): 4254-4277,
- Chetelat, B., Liu, C. Q., Wang, Q., Zhang, G. Assessing the influence of lithology on weathering indices of Changjiang river sediments. *Chemical Geology*, 2013, 359: 108–115.
- Clift, P.D., Giosan, L. Sediment fluxes and buffering in the post-glacial Indus Basin. *Basin Research*, 2013, 25: 1-18.
- Colten, V. C., Hanor, J. S. Variations in dissolved lithium in the Mississippi River and Mississippi River estuary, Louisiana, U.S.A., during low river stage, *Chemical Geology*, 1984, 47(1-2): 85-96.
- Dai, Z., Liu, J. T. Impacts of large dams on downstream fluvial sedimentation: an example of the Three Gorges Dam (TGD) on the Changjiang (Yangtze River). *Journal of Hydrology*, 2013, 480: 10-18.
- Dai, Z., Fagherazzi, S., Mei, X., Gao, J. Decline in suspended sediment concentration delivered by the Changjiang (Yangtze) River into the East China Sea between 1956 and 2013. *Geomorphology*, 2016, 123-132.
- Dellinger, M., Gaillardet, J., Bouchez, J., Calmels, D., Galy, V., Hilton, R. G., Louvat, P., France-Lanord, C. Lithium isotopes in large rivers reveal the cannibalistic nature of modern continental weathering and erosion. *Earth and Planetary Science Letters*, 2014, 401: 359–372.
- Dellinger, M., Gaillardet, J., Bouchez, J., Calmels, D., Louvat, P., Dosseto, A., Gorge, C., Alanoca, L., Maurice, L. Riverine Li isotope fractionation in the Amazon River basin controlled by the weathering regimes. *Geochimica et Cosmochimica Acta*, 2015, 164: 71-93.
- Dellinger, M., Bouchez, J., Gaillardet, J., Faure, L., Moureau, J. Tracing weathering regimes using the lithium isotope composition of detrital sediments. *Geology*, 2017, 45(5): 411-414.
- Ding, T., Gao, J., Tian, S., Shi, G., Chen, F., Wang, C., Luo, X., Han, D. Chemical and isotopic characteristics of the water and suspended particulate materials in the Yangtze river and their geological and environmental implications. *Acta Geologica Sinica-English Edition*, 2014, 88(1): 276-360.
- Dynesius, M., Nilsson, C. Fragmentation and flow regulation of river systems in the northern third of the world. *Science*, 1994, 266(5186): 753-762.

- Fan, D., Li, C., Yokoyama, K., Zhou, B., Li, B., Wang, Q., Yang, S., Deng, B., Wu, G. Monazite age spectra in the late Cenozoic strata of the Changjiang delta and its implication on the Changjiang run-through time. *Science in China (Series D)*. 2004, 48: 1718-1727.
- Fan, D., Wang, Y., Wu, Y. Advances in provenance studies of Changjiang Riverine sediments. *Advances in Earth Science*, 2012, 27 (5): 515-528. (in Chinese with English abstract)
- France-Lanord, C., Derry, L. A. Organic carbon burial forcing of the carbon cycle from Himalayan erosion. *Nature*, 1997, 390(6655): 65-67.
- Frings, P. J. Palaeoweathering: How Do Weathering Rates Vary with Climate? *Elements*, 2019, 15(4): 259-265.
- Froelich, F., Misra, S. Was the late Paleocene-early Eocene hot because Earth was flat? An ocean lithium isotope view of mountain building, continental weathering, carbon dioxide, and Earth's Cenozoic climate. *Oceanography*, 2014, 27(1): 36-49
- Gaillardet, J., Dupré, B., Louvat, P., Allegre, C. J. Global silicate weathering and CO₂ consumption rates deduced from the chemistry of large rivers. *Chemical Geology*, 1999a, 159(1-4): 3-30.
- Gaillardet, J., Dupré, B., Allègre, C. J. Geochemistry of large river suspended sediments: silicate weathering or recycling tracer? *Geochimica et Cosmochimica Acta*, 1999b, 63(23-24): 4037-4051.
- Garrels, R. M., Mackenzie, F. T. Gregor's denudation of the continents. *Nature*, 1971, 231(5302): 382.
- Garzanti, E., Limonta, M., Resentini, A., Bandopadhyay, P., Najman, Y., Ando, S., Vezzoli, G. Sediment recycling at convergent plate margins (Indo-Burman Ranges and Andaman-Nicobar Ridge). *Earth-Science Reviews*, 2013, 123: 113-132.
- Gislason, S. R., Oelkers, E. H., Snorrason, A. Role of river-suspended material in the global carbon cycle. *Geology*, 2006, 34(1), 49-52.
- Gislason, S. R., Oelkers, E. H., Eiriksdottir, E. S., Kardjilov, M. I., Gisladottir, G., Sigfusson, B., Snorrason, A., Elefsen, S., Hardardottir, J., Torssander, P., Oskarsson, N. Direct evidence of the feedback between climate and weathering. *Earth and Planetary Science Letters*, 2009, 277(1-2): 213-222.
- Goddéris, Y., François, L. M. (1995). The Cenozoic evolution of the strontium and carbon cycles: relative importance of continental erosion and mantle exchanges. *Chemical Geology*, 126(2), 169-190.

- Gou, L., Jin, Z., Deng, L., Sun, H., Yu, H., Zhang, F. Efficient purification for Li and high-precision and accuracy determination of Li isotopic compositions by MC-ICP-MS. *Geochimica et Cosmochimica Acta*, 2017, 46(6): 528-537 (in Chinese with English abstract).
- Grill, G., Lehner, B., Thieme, M., Geenen, B., Tickner, D., Antonelli, F., Babu, S., Borrelli, P., Cheng, L., Crochetiere, H., Ehalt Macedo, H., Filgueiras, R., Goichot, M., Higgins, J., Hogan, Z., Lip, B., McClain, M. E., Meng, J., Mulligan, M., Nilsson, C., Olden, J. D., Opperman, J. J., Petry, P., Reidy Liermann, C., Sáenz, L., Salinas-Rodríguez, S., Schelle, P., Schmitt, R. J. P., Snider, J., Tan, F., Tockner, K., Valdujo, P. H., van Soesbergen, A., Zarfl, C. Mapping the world's free-flowing rivers. *Nature*, 2019, 569(7755): 215.
- Guo, L., Su, N., Zhu, C., He, Q. How have the river discharges and sediment loads changed in the Changjiang River basin downstream of the Three Gorges Dam? *Journal of Hydrology*, 2018, 560: 259-274.
- Guo, L., Su, N., Townend, I., Wang, Z. B., Zhu, C., Wang, X., Zhang, Y., He, Q. From the headwater to the delta: A synthesis of the basin-scale sediment load regime in the Changjiang River. *Earth-Science Reviews*, 2019, 197.
- Gou, L.-F., Jin, Z., Pogge von Strandmann, P. A. E., Li, G., Qu, Y.-X., Xiao, J., Deng, L., Galy, A. Li isotopes in the middle Yellow River: Seasonal variability, sources and fractionation. *Geochimica et Cosmochimica Acta*, 2019, 248: 88-108.
- Guo, Y., Yang, S. Y., Su, N., Li, C., Yin, P., Wang Z. Revisiting the effects of hydrodynamic sorting and sedimentary recycling on chemical weathering indices. *Geochimica et Cosmochimica Acta*, 2018, 227: 48-63.
- Harmar, O. P., Clifford, N. J., Thorne, C. R., Biedenharn, D. S. Morphological changes of the Lower Mississippi River: geomorphological response to engineering intervention. *River Research and Applications*, 2005, 21(10), 1107-1131.
- Hindshaw, R. S., Tosca, R., Goût, T. L., Farnan, I., Tosca, N. J., Tipper, E. T. Experimental constraints on Li isotope fractionation during clay formation. *Geochimica et Cosmochimica Acta*, 2019, 250: 219-237.
- He, M., Zheng, H., Huang, X., Jia, J., Li, L. Yangtze River sediments from source to sink traced with clay mineralogy. *Journal of Asian Earth Sciences*, 2013, 69: 60-69.
- He, M., Zheng, H., Bookhagen, B., Clift, P. D. Controls on erosion intensity in the Yangtze River basin tracked by U–Pb detrital zircon dating. *Earth-Science Reviews*, 2014, 136: 121-140.

He, M., Zheng, H., Clift, P. D., Tada, R., Wu, W., Luo, C. Geochemistry of fine-grained sediments in the Yangtze River and the implications for provenance and chemical weathering in East Asia. *Progress in Earth and Planetary Science*, 2015, 2(1): 32.

Henchiri, S., Clergue, C., Dellinger, M., Bouchez, J., Spencer, R. G. M. The influence of hydrothermal activity on the Li isotopic signature of rivers draining volcanic areas. *Procedia Earth and Planetary Science*, 2014, 10: 223 – 230.

Hoefs, J., Sywall, M. Lithium isotope composition of quaternary and tertiary biogenic carbonates and a global lithium isotope balance. *Geochimica et Cosmochimica Acta*, 1997, 61(13): 2679–2690.

Hori, K., Saito, Y., Zhao, Q., Cheng, X., Wang, P., Sato, Y., Li, C. Sedimentary facies and Holocene progradation rates of the Changjiang (Yangtze) delta, China. *Geomorphology*, 41(2-3), 2001, 233-248.

Hu, M., Stallard, R., Edmond, J. Major ion chemistry of some large Chinese rivers. *Nature*, 1982, 298: 550-553

Huang, X., Meyers, P. A., Jia, C., Zheng, M., Xue, J., Wang, X., Xie, S. Paleotemperature variability in central China during the last 13 ka recorded by a novel microbial lipid proxy in the Dajiuhu peat deposit. *The Holocene*, 2013, 23(8), 1123-1129.

Huh, Y., Chan, L. H., Zhang, L., Edmond, J. M. Lithium and its isotopes in major world rivers: implications for weathering and the oceanic budget. *Geochimica et Cosmochimica Acta*, 1998, 62(12): 2039–2051.

Huh, Y., Chan, L. H., Edmond, J. M. Lithium isotopes as a probe of weathering processes: Orinoco River. *Earth and Planetary Science Letters*, 2001, 194(1–2), 189–199.

Huh, Y., Chan, L. H., Chadwick, O. A. Behavior of lithium and its isotopes during weathering of Hawaiian basalt. *Geochemistry, Geophysics, Geosystems*, 2004, 5(9).

Jeandel, C., Oelkers, E. H. The influence of terrigenous particulate material dissolution on ocean chemistry and global element cycles. *Chemical Geology*, 2015, 50-66.

Jones, M. T., Pearce, C. R., Jeandel, C., Gislason, S. R., Eiriksdottir, E. S., Mavromatis, V., Oelkers, E. H. Riverine particulate material dissolution as a significant flux of strontium to the oceans. *Earth and Planetary Science Letters*, 2012, 51-59.

Jones, M. T., Gislason, S. R., Burton, K. W., Pearce, C. R., Mavromatis, V., Von Strandmann, P. A., Oelkers, E. H. Quantifying the impact of riverine particulate dissolution in seawater on ocean chemistry. *Earth and Planetary Science Letters*, 2014, 91-100.

- Krissansen-Totton, J., Catling, D. Constraining climate sensitivity and continental versus seafloor weathering using an inverse geological carbon cycle model. *Nature Communication*, 2017, 8: 15423.
- Kasting, J. F. The Goldilocks Planet? How Silicate Weathering Maintains Earth “Just Right”. *Elements*, 2019, 15(4): 235-240.
- Kısakürek, B., Widdowson, M., James, R. H. Behaviour of Li isotopes during continental weathering: the Bidar laterite profile, India. *Chemical Geology*, 2004, 212(1-2): 27-44.
- Kuehl, S. A., Yang, S., Yu, F., Copard, Y. Liu, J., Nittrouer, C. A., Xu, J. Asia’s mega rivers: Common source, diverse fates, *Eos*, 2020, 101
- Kump, L. R., Brantley, S. L., Arthur, M. A. Chemical Weathering, Atmospheric CO₂, and Climate. *Annual Review of Earth and Planetary Sciences*, 2000, 28(1): 611-667.
- Kump, L. and Arthur, M. A. Global chemical erosion during the Cenozoic: weatherability balances the budgets. In *Tectonic Uplift and Climate Change* (ed. W. F. Ruddiman). Plenum, New York, pp. 1997, 400-424.
- Lai, X., Yin, D., Finlayson, B. L., Wei, T., Li, M., Yuan, W., Yang, S., Dai, Z., Gao, S., Chen Z. Will river erosion below the Three Gorges Dam stop in the middle Yangtze? *Journal of Hydrology*, 2017, 554: 24–31.
- Lacan, F., Jeandel, C. Neodymium isotopes as a new tool for quantifying exchange fluxes at the continent-ocean interface. *Earth and Planetary Science Letters*, 2005, 232(3), 245-257.
- Lan, Z., Chen, Y., Su, B., Liu, F., Zhang, H. The origin of sandstones from the Songpan-Ganze Basin, Sichuan, China: evidence from SHRIMP U-Pb dating of clastic zircon. *Acta Sedimentologica Sinica*, 2006, 24(3): 321-332. (in Chinese with English abstract)
- Laskar, J., Robutel, P., Joutel, F., Gastineau, M., Correia, A. C. M., Levrard, B. A long-term numerical solution for the insolation quantities of the Earth. *Astronomy & Astrophysics*, 2004, 428(1), 261-285.
- Lemarchand, E., Chabaux, F., Vigier, N., Millot, R., Pierret, M. C. Lithium isotope systematics in a forested granitic catchment (Strengbach, Vosges Mountains, France). *Geochimica et Cosmochimica Acta*, 2010, 74(16): 4612–4628.
- Li, C., Yang, S., Zhao, J. X., Dosseto, A., Bi, L., Clark, T. R. The time scale of river sediment source-to-sink processes in East Asia. *Chemical Geology*, 2016, 446, 138-146.
- Li, G. and Elderfield, H. Evolution of carbon cycle over the past 100 million years, *Geochimica et Cosmochimica Acta*, 2013, 103: 11-25.

- Li, G., West, A. J. Evolution of Cenozoic seawater lithium isotopes: Coupling of global denudation regime and shifting seawater sinks. *Earth and Planetary Science Letters*, 2014, 401: 284-293.
- Li, W., Liu, X. Experimental investigation of lithium isotope fractionation during kaolinite adsorption: Implications for chemical weathering. *Geochimica et Cosmochimica Acta*, 2020, 284, 156-172.
- Liu, X. M., Rudnick, R. L., McDonough, W. F., Cummings, M. L. Influence of chemical weathering on the composition of the continental crust: Insights from Li and Nd isotopes in bauxite profiles developed on Columbia River Basalts. *Geochimica et Cosmochimica Acta*, 2013, 115: 73-91.
- Liu, X. M., Wanner, C., Rudnick, R. L., McDonough, W. F. Processes controlling $\delta^7\text{Li}$ in rivers illuminated by study of streams and groundwaters draining basalts. *Earth and planetary science letters*, 2015, 409: 212-224.
- Liu, Z., Wen, X., Brady, E. C., Otto-Bliesner, B., Yu, G., Lu, H., Cheng, H., Wang, Y., Zheng, W., Ding, Y., Edwards, R. L., Cheng, J., Liu, W., Yang, H. Chinese cave records and the East Asia summer monsoon. *Quaternary Science Reviews*, 2014, 83, 115-128.
- Lu, C., Zheng, H., Wu, W., Wang, P., Chen, Y., Wei, X. Sr-Nd isotope stratification along water depth: An example from Datong hydrological station of Yangtze River. 2012, 57 (21): 2022-2030.
- Lupker, M., France-Lanord, C., Galy, V., Lave, J., Gaillardet, J., Gajurel, A. P., Guilmette, C., Rahman, M., Singh, S., Sinha, R. Predominant floodplain over mountain weathering of Himalayan sediments (Ganga basin). *Geochimica et Cosmochimica Acta*, 2012, 84: 410-432.
- Lupker, M., France-Lanord, C., Galy, V., Lavé, J., Kudrass, H. Increasing chemical weathering in the Himalayan system since the Last Glacial Maximum. *Earth and Planetary Science Letters*, 2013, 365: 243–252.
- Macdonald, F. A., Swanson-Hysell, N. L., Park, Y., Lisiecki, L., Jagoutz, O. Arc-continent collisions in the tropics set Earth's climate state. *Science*, 2019, 364: 181-184.
- Maffre, P., Godd ris, y., Vigier, N., Moquet, J., Carretier, S. Modelling the riverine $\delta^7\text{Li}$ variability throughout the Amazon Basin. *Chemical Geology*, 2020, 532: 119336.
- Manaka, T., Otani, S., Inamura, A., Suzuki, A., Aung, T., Roachanakanan, R., Ishiwa, T., Kawahata, H. Chemical weathering and long-term CO₂ consumption in the Ayeyarwady and

Mekong river basins in the Himalayas, *Journal of Geophysical Research: Biogeosciences*, 2015, 120: 1165-1175.

Manaka, T., Araoka, D., Yoshimura, T., Zakir Hossain, H. M., Nishio, Y., Suzuki, A., Kawahata, H. Downstream and seasonal changes of lithium isotope ratios in the Ganges-Brahmaputra river system. *Geochemistry, Geophysics, Geosystems*, 2017, 18: 3003-3015.

Mao, C., Chen, J., Yuan, X., Yang, Z., Balsam, W., Ji, J., Seasonal variation in the mineralogy of the suspended particulate matter of the lower Changjiang River at Nanjing, China. *Clays and Clay Minerals*, 2010, 58: 691-706.

Mao, C., Chen, J., Yuan, X., Yang, Z., Ji, J. Seasonal variations in the Sr-Nd isotopic compositions of suspended particulate matter in the lower Changjiang River: Provenance and erosion constraints. *Chinese Science Bulletin*, 2011, 56: 2371-2378.

Maher, K., Chamberlain, C. P. Hydrologic regulation of chemical weathering and the geologic carbon cycle. *Science*, 2014, 343(6178): 1502-1504.

Meunier A. *Clays*. Springer-Verlag, Berlin. 2005.

Miller, K. G., Fairbanks, R. G., Mountain, G. S. Tertiary oxygen isotope synthesis, sea level history, and continental margin erosion. *Paleoceanography*, 1987, 2: 1-19.

Millot, R., Vigier, N., Gaillardet, J. Behaviour of lithium and its isotopes during weathering in the Mackenzie Basin, Canada. *Geochimica et Cosmochimica Acta*, 2010, 74(14): 3897–3912.

Milliman, J. D., Farnsworth, K. L. *River discharge to the coastal ocean: a global synthesis*. Cambridge University Press. 2013.

Misra, S., Froelich, P. N. Lithium isotope history of Cenozoic seawater: changes in silicate weathering and reverse weathering. *Science*, 2012, 335(6070): 818-823.

Moon, S., Chamberlain, C. P., Hilley, G. E. New estimates of silicate weathering rates and their uncertainties in global rivers. *Geochimica et Cosmochimica Acta*, 2014, 134: 257-274.

Nesbitt, H. W., Young, G. M. Early Proterozoic climates and plate motions inferred from major element chemistry of lutites. *Nature*, 1982, 299(5885): 715-717.

Pagani, M., Zachos, J. C., Freeman, K. H., Tipple, B. J., Bohaty, S. Marked decline in atmospheric carbon dioxide concentrations during the Paleogene. *Science*, 2005, 309(5734): 600-603.

Pagani, M., Caldeira, K., Berner, R., Beerling, D. The role of terrestrial plants in limiting atmospheric CO₂ decline over the past 24 million years. *Nature*, 2009, 460: 85-88.

- Penniston-Dorland, S., Liu, X. M., Rudnick, R. L. Lithium isotope geochemistry. *Reviews in Mineralogy and Geochemistry*, 2017, 82(1): 165–217.
- Pistiner, J. S., Henderson, G. M. Lithium-isotope fractionation during continental weathering processes. *Earth and Planetary Science Letters*, 2003, 214(1-2), 327-339.
- Pogge von Strandmann, P. A., Burton, K. W., James, R. H., van Calsteren, P., Gíslason, S. R., Mokadem, F. Riverine behaviour of uranium and lithium isotopes in an actively glaciated basaltic terrain. *Earth and Planetary Science Letters*, 2006, 251(1–2): 134–147.
- Pogge von Strandmann, P. A. P., James, R. H., van Calsteren, P., Gíslason, S. R., Burton, K. W. Lithium, magnesium and uranium isotope behaviour in the estuarine environment of basaltic islands. *Earth and Planetary Science Letters*, 2008, 274(3-4): 462-471.
- Pogge von Strandmann, P. A. P., Burton, K. W., James, R. H., van Calsteren, P., Gíslason, S. R. Assessing the role of climate on uranium and lithium isotope behaviour in rivers draining a basaltic terrain. *Chemical Geology*, 2010, 270(1–4): 227–239.
- Pogge von Strandmann, P. A., Henderson, G. M. The Li isotope response to mountain uplift. *Geology*, 2015, 43(1): 67–70.
- Pogge von Strandmann, P. A. P., Frings, P. J., Murphy, M. J. Lithium isotope behaviour during weathering in the Ganges Alluvial Plain. *Geochimica et Cosmochimica Acta*, 2017, 198: 17–31.
- Pogge von Strandmann, P. A. P., Fraser, W., Hannond, S., Tarbuck, G., Wood, I., Oelkers, E., Murphy, M. Experimental determination of Li isotope behaviour during basalt weathering. *Chemical Geology*, 2019, 517: 34-43.
- Raymo, M. E. and Ruddiman, W. F. Tectonic forcing of late Cenozoic climate. *Nature*, 1992, 359: 117-122.
- Richardson, N. J., Densmore, A. L., Seward, D., Wipf, M., Yong, L. Did incision of the Three Gorges begin in the Eocene? *Geology*, 2010, 38(6): 551–554
- Pistiner, J. S., Henderson, G. M. Lithium-isotope fractionation during continental weathering processes. *Earth and Planetary Science Letters*, 2003, 214(1–2): 327–339.
- Rothacker, L., Dosseto, A., Francke, A., Chivas, A. R., Vigier, N., Kotarba-Morley, A. M., Menozzi, D. Impact of climate change and human activity on soil landscapes over the past 12,300 years. *Scientific reports*, 2018, 8(1): 247.
- Rowley, D. B. Rate of plate creation and destruction: 180 Ma to present. *Geological Society of America Bulletin*, 2002, 114(8): 927-933.

- Rudnick, R. L., Gao, S. Composition of the Continental Crust. *Treatise on Geochemistry*, 2003, 2, 659.
- Rudolph W., Brooker M. H. and Pye C. C. Hydration of lithium ion in aqueous solution. *The Journal of Physical Chemistry*, 1995, 99: 3793–3797.
- Rugenstein, J. K., Ibarra, D. E., Von Blanckenburg, F. Neogene cooling driven by land surface reactivity rather than increased weathering fluxes. *Nature*, 2019, 571(7763): 99-102.
- Ryu, J. S., Vigier, N., Lee, S. W., Lee, K. S., Chadwick, O. A. Variation of lithium isotope geochemistry during basalt weathering and secondary mineral transformations in Hawaii. *Geochimica et Cosmochimica Acta*, 2014, 145: 103–115.
- Samanta, S., Dalai, T. K. Dissolved and particulate Barium in the Ganga (Hooghly) River estuary, India: Solute-particle interactions and the enhanced dissolved flux to the oceans. *Geochimica et Cosmochimica Acta*, 2016, 1-28.
- Sarmiento, J. L. and Gruber, N. *Ocean Biogeochemical Dynamics*. Princeton University Press, Princeton, NJ, 2006, 503 pp.
- Sayles, F. L., Mangelsdorf, P. C. The equilibration of clay minerals with seawater: exchange reactions. *Geochimica et Cosmochimica Acta*, 1977, 41, 951-960.
- Sauzéat, L., Rudnick, R. L., Chauvel, C., Garçon, M., & Tang, M. New perspectives on the Li isotopic composition of the upper continental crust and its weathering signature. *Earth and Planetary Science Letters*, 2015, 428: 181–192.
- Shao, J., Yang, S. Does chemical index of alteration (CIA) reflect silicate weathering and monsoonal climate in the Changjiang River basin? *Chinese Science Bulletin*, 2012, 57: 1178-1187.
- Stoffynegli, P. Conservative behaviour of dissolved lithium in estuarine waters. *Estuarine Coastal and Shelf Science*, 1982, 14(5): 577-587.
- Sun, X., Li, C., Kuiper, K. F., Zhang, Z., Gao, J., Wijbrans, J. R. Human impact on erosion patterns and sediment transport in the Yangtze River. *Global and Planetary Change*, 2016, 143: 88-99.
- Syvitski, J. P., Vörösmarty, C. J., Kettner, A. J., Green, P. Impact of humans on the flux of terrestrial sediment to the global coastal ocean. *Science*, 2005, 308(5720): 376-380.
- Tang, Y. J., Zhang, H. F., Ying, J. F. Review of the lithium isotope system as a geochemical tracer. *International Geology Review*, 2007, 49(4): 374–388.

- Tang, Y. J., Zhang, H. F., Ying, J. F. Discussion on fractionation mechanism of lithium isotopes. *Earth Science-Journal of China University of Geosciences*, 2009, 34(1): 43-55 (in Chinese with English abstract).
- Taylor, T. I., Urey, H. C. Fractionation of the lithium and potassium isotopes by chemical exchange with zeolites. *The Journal of Chemical Physics*, 1938, 6(8): 429–438.
- Teng, F. Z., McDonough, W. F., Rudnick, R. L., Dalpé, C., Tomascak, P. B., Chappell, B. W., Gao, S. Lithium isotopic composition and concentration of the upper continental crust. *Geochimica et Cosmochimica Acta*, 2004, 68(20): 4167–4178.
- Tomascak, P. B. Developments in the understanding and application of lithium isotopes in the earth and planetary sciences. *Reviews in Mineralogy and Geochemistry*, 2004, 55(1): 153–195.
- Verney-Carron, A., Vigier, N., Millot, R. Experimental determination of the role of diffusion on Li isotope fractionation during basaltic glass weathering. *Geochimica et Cosmochimica Acta*, 2011, 75(12), 3452-3468.
- Vezzoli, G., Garzanti, E., Limonta, M., Ando, S., Yang, S. Erosion patterns in the Changjiang (Yangtze River) catchment revealed by bulk-sample versus single-mineral provenance budgets. *Geomorphology*, 2016, 177-192.
- Vigier, N., Decarreau, A., Millot, R., Carignan, J., Petit, S., France-Lanord, C. Quantifying Li isotope fractionation during smectite formation and implications for the Li cycle. *Geochimica et Cosmochimica Acta*, 2008, 72(3), 780-792.
- Vigier, N., Gislason, S. R., Burton, K. W., Millot, R., Mokadem, F. The relationship between riverine lithium isotope composition and silicate weathering rates in Iceland. *Earth and Planetary Science Letters*, 2009, 287(3-4): 434–441.
- Vigier, N., Godderis, Y. A new approach for modeling Cenozoic oceanic lithium isotope paleo-variations: the key role of climate. *Climate of The Past*, 2015, 11(4), 635-645.
- Walker, J. C. G., Hays, P. B., Kasting, J. F. A negative feedback mechanism for the long-term stabilization of Earth's surface temperature. *Journal of Geophysical Research*. 1981, 86: 9776-9782.
- Wang, C., Bendle, J. A., Zhang, H., Yang, Y., Liu, D., Huang, J., Cui, J., Xie, S. Holocene temperature and hydrological changes reconstructed by bacterial 3-hydroxy fatty acids in a stalagmite from central China. *Quaternary Science Reviews*, 2018, 192, 97-105.

- Wang, H., Yang, Z., Wang, Y., Saito, Y., Liu, J. P. Reconstruction of sediment flux from the Changjiang (Yangtze River) to the sea since the 1860s. *Journal of Hydrology*, 2008, 349(3): 318-332.
- Wang, Q., Yang, S. Clay mineralogy indicates the Holocene monsoon climate in the Changjiang (Yangtze River) Catchment, China. *Applied Clay Science*, 2013, 74, 28-36.
- Wang, Q., Zhao, Z., Liu, C. New progress in lithium isotope environmental geochemistry. *Acta mineralogica Sinica*, 2006, 26(2): 196-202 (in Chinese with English abstract).
- Wang, Q. L., Chetelat, B., Zhao, Z. Q., Ding, H., Li, S. L., Wang, B. L., Li, J., Liu, X. L. Behavior of lithium isotopes in the Changjiang River system: Sources effects and response to weathering and erosion. *Geochimica et Cosmochimica Acta*, 2015, 151: 117-132.
- Wang, X., Yang, S. Y., Ran, X., Liu, X. M., Bataille, C. P., Su, N. Response of the Changjiang (Yangtze River) water chemistry to the impoundment of Three Gorges Dam during 2010–2011. *Chemical Geology*, 2018, 487: 1–11.
- Wang, Y., Fan, D. Provenance characteristics of the late Quaternary in the Yangtze River delta and its response to monsoon climate change. *Journal of Palaeogeography*, 2013, 15(6): 853-863. (in Chinese with English abstract)
- Wang, Z., Yang, S., Li, P., Li, C., Cai, J. Detrital mineral compositions of the Changjiang River sediments and their tracing implications. *Acta sedimentologica Sinica*, 2006, 24(4): 570-578 (in Chinese with English abstract).
- Wang, Z., Saito, Y., Zhan, Q., Nian, X., Pan, D., Wang, L., Chen, T., Xie, J., Li, X., Jiang, X. Three-dimensional evolution of the Yangtze River mouth, China during the Holocene: Impacts of sea level, climate and human activity. *Earth-Science Reviews*, 2018, 185: 938-955.
- Wang, Z.-L., Zhang, J., Liu, C.-Q. Strontium isotopic compositions of dissolved and suspended loads from the main channel of the Yangtze River. *Chemosphere*, 2007, 69(7): 1081–1088.
- Wang, Z., Saito, Y., Zhan, Q., Nian, X., Pan, D., Wang, L., Chen, T., Xie, J., Li, X., Jiang, X. Three-dimensional evolution of the Yangtze River mouth, China during the Holocene: Impacts of sea level, climate and human activity. *Earth-Science Reviews*, 2018, 185, 938-955.
- West, A. J., Galy, A., Bickle, M. Tectonic and climatic controls on silicate weathering. *Earth and Planetary Science Letters*, 2005, 235(1-2): 211–228.

- Weynell, M., Wiechert, U., Schuessler, J. A. Lithium isotopes and implications on chemical weathering in the catchment of Lake Donggi Cona, northeastern Tibetan Plateau. *Geochimica et Cosmochimica Acta*, 2017, 213, 155-177.
- Wimpenny, J., Gíslason, S. R., James, R. H., Gannoun, A., Von Strandmann, P. A. P., Burton, K. W. The behaviour of Li and Mg isotopes during primary phase dissolution and secondary mineral formation in basalt. *Geochimica et Cosmochimica Acta*, 2010a, 74(18): 5259–5279.
- Wimpenny, J., James, R. H., Burton, K. W., Gannoun, A., Mokadem, F., Gíslason, S. R. Glacial effects on weathering processes: new insights from the elemental and lithium isotopic composition of West Greenland rivers. *Earth and Planetary Science Letters*, 2010b, 290(3–4): 427–437.
- Wimpenny, J., Colla, C. A., Yu, P., Yin, Q. Z., Rustad, J. R., Casey, W. H. Lithium isotope fractionation during uptake by gibbsite. *Geochimica et Cosmochimica Acta*, 2015, 168: 133–150.
- Winnick, M. J., Maher, K. Relationships between CO₂, thermodynamic limits on silicate weathering, and the strength of the silicate weathering feedback. *Earth and Planetary Science Letters*, 2018, 485: 111-120.
- Wu, W., Yang, J., Xu, S., Yin, H. Geochemistry of the headwaters of the Yangtze River, Tongtian He and Jinsha Jiang: Silicate weathering and CO₂ consumption. *Applied Geochemistry*, 2008a, 23(12): 3712-3727.
- Wu, W., Xu, S., Yang, J., Yin, H. Silicate weathering and CO₂ consumption deduced from the seven Chinese rivers originating in the Qinghai-Tibet Plateau. *Chemical Geology*, 2008b, 249(3-4): 307-320.
- Wu, W., Xu, S., Lu, H., Yang, J., Yin, H., Liu, W. Mineralogy, minor and trace element geochemistry of riverbed sediments in the headwaters of the Yangtze, Tongtian River and Jinsha River. *Journal of Asian Earth Sciences*, 2011, 40: 611-621.
- Wu, Y., Fan, D., Wang, D., Yin, P. Increasing hypoxia in the Changjiang Estuary during the last three decades deciphered from sedimentary redox-sensitive elements. *Marine Geology*, 2020, 106044.
- Xiang, F., Zhu, L., Wang, C., Zhao, X., Chen, H., Yang, W. Quaternary sediment in the Yichang area: Implications for the formation of the Three Gorges of the Yangtze River. *Geomorphology*, 2007, 85(3–4): 249-258,

- Xu, K., Milliman, J. D. Seasonal variations of sediment discharge from the Yangtze River before and after impoundment of the Three Gorges Dam. *Geomorphology*, 2009, 104(3-4), 276-283.
- Yang, C., Yang, S., Gou, L., Wang, X., Li, Y. Lithium isotopes for tracing the supergene weathering and environmental evolution: review and prospective. *Bulletin of Mineralogy, Petrology and Geochemistry*. 2018, 37(5): 841-851. (in Chinese with English abstract)
- Yang, H., Yang, S. L., Xu, K. H., Milliman, J. D., Wang, H., Yang, Z., Chen, Z., Zhang, C. Y. Human impacts on sediment in the Yangtze River: a review and new perspectives. *Global and Planetary Change*, 2018, 162: 8-17.
- Yang, S. Y., Jung, H. S., Choi, M. S., Li, C. X. The rare earth element compositions of the Changjiang (Yangtze) and Huanghe (Yellow) river sediments. *Earth and Planetary Science Letters*, 2002, 201(2), 407-419.
- Yang, S. Y., Jung, H. S., Li, C. Two unique weathering regimes in the Changjiang and Huanghe drainage basins: geochemical evidence from river sediments. *Sedimentary Geology*, 2004, 164(1-2): 19-34.
- Yang, S. Y., Li, C. X., Yokoyama, K. Elemental compositions and monazite age patterns of core sediments in the Changjiang delta: Implications for sediment provenance and development history of the Changjiang river[J]. *Earth and Planetary Science Letters*, 2006, 245: 762-776.
- Yang, S., Jiang, S., Ling, H., Xia, X., Sun, M., Wang, D. Sr-Nd isotopic compositions of the Changjiang sediments: Implications for tracing sediment sources. *Science in China Series D: Earth Sciences*, 2007, 50(10), 1556-1565.
- Yang, S., Wang, Z., Guo, Y., Li, C., Cai, J. Heavy mineral compositions of the Changjiang (Yangtze River) sediments and their provenance-tracing implication. *Journal of Asian Earth Sciences*, 2009, 35(1): 56-65.
- Yang, S., Tang, M., Yim, W. W. S., Zong, Y., Huang, G., Switzer, A. D., Saito, Y. Burial of organic carbon in Holocene sediments of the Zhujiang (Pearl River) and Changjiang (Yangtze River) estuaries. *Marine Chemistry*, 2011, 123(1-4), 1-10.
- Yang, S., Li, C., Wang, Z., Wang, X., Shu, J. Heterogeneity of geochemical compositions of the changing sediments and provenance indication. *Quaternary Sciences*. 2013, 33(4): 645-655. (in Chinese with English abstract).

Yang, S., Wei, G., Shi, X. Geochemical approaches of tracing Source-to-Sink sediment processes and environmental changes at the East Asian continental margin. *Bulletin of Mineralogy, Petrology and Geochemistry*. 2015, 34(5): 901-909. (in Chinese with English abstract).

Yang, Z., Wang, H. J., Saito, Y., Milliman, J. D., Xu, K., Qiao, S., Shi, G. Dam impacts on the Changjiang (Yangtze) River sediment discharge to the sea: The past 55 years and after the Three Gorges Dam. *Water resources research*, 2006, 42(4).

Yao, F., Ma, C., Zhu, C., Li, J., Chen, G., Tang, L., Huang, M., Jia, T., Xu, J. Holocene climate change in the western part of Taihu Lake region, East China. *Palaeogeography, Palaeoclimatology, Palaeoecology*, 2017, 485, 963-973.

Yuan, D., Zhu, J., Li, C., Hu, D. Cross-shelf circulation in the Yellow and East China Seas indicated by MODIS satellite observations. *Journal of Marine Systems*, 2008, 70(1), 134-149.

Zachos J., Pagani, M., Sloan, L., Thomas, E., Billups, K., Smith, J. P., Uppenbrink, J. P. Trends, rhythms, and aberrations in global climate 65 Ma to present. *Science*, 2001, 292(5517), 686-693.

Zhao, Y., Zou, X., Gao, J., Wang, C., Li, Y., Yao, Y., Zhao, W., Xu, M. Clay mineralogy and source-to-sink transport processes of Changjiang River sediments in the estuarine and inner shelf areas of the East China Sea. *Journal of Asian Earth Sciences*, 2018, 152: 91-102.

Zhang, A., Zhang, J., Hu, J., Zhang, R., Zhang, G. Silicon isotopic chemistry in the Changjiang Estuary and coastal regions: Impacts of physical and biogeochemical processes on the transport of riverine dissolved silica. *Journal of Geophysical Research: Oceans*, 2015, 120, 6943-6957.

Zhang, E., Chang, J., Cao, Y., Sun, W., Shulmeister, J., Tang, H., Langdon, P., Yang, X., Shen, J. Holocene high-resolution quantitative summer temperature reconstruction based on subfossil chironomids from the southeast margin of the Qinghai-Tibetan Plateau. *Quaternary Science Reviews*, 2017a, 165, 1-12.

Zhang, E., Zhao, C., Xue, B., Liu, Z., Yu, Z., Chen, R., Shen, J. Millennial-scale hydroclimate variations in southwest China linked to tropical Indian Ocean since the Last Glacial Maximum. *Geology*, 2017b, 45(5), 435-438.

Zhang, G., Cheng, S., Guo, A., Dong, Y., Lai, S., Yao, A. Mianlue paleo-suture on the southern margin of the Central Orogenic System in Qinling-Dabie with a discussion of the

assembly of the main part of the continent of China. *Regional Geology of China*, 2004, 23(9): 846-853.

Zhang, H., Griffiths, M. L., Chiang, J. C., Kong, W., Wu, S., Atwood, A., Huang, J., Cheng, H., Ning, Y., Xie, S. East Asian hydroclimate modulated by the position of the westerlies during Termination I. *Science*, 2018, 362(6414), 580-583.

Zhang, H. F., Zhang, L., Harris, N., Jin, L., Yuan, H. U–Pb zircon ages, geochemical and isotopic compositions of granitoids in Songpan-Garze fold belt, eastern Tibetan Plateau: constraints on petrogenesis and tectonic evolution of the basement. *Contributions to Mineralogy and Petrology*, 2006, 152(1): 75-88.

Zhang, J., Huang, W., Liu, M., Zhou, Q. Drainage basin weathering and major element transport of two large Chinese rivers (Huanghe and Changjiang). *Journal of Geophysical Research*, 1990, 95: 13,277-13,288.

Zhang, L., Chan, L. H., Gieskes, J. M. Lithium isotope geochemistry of pore waters from Ocean Drilling Program Sites 918 and 919, Irminger Basin. *Geochimica et Cosmochimica Acta*, 1998, 62(14): 2437–2450.

Zhang, Z., Cao, Z., Grasse, P., Dai, M., Gao, L., Kuhnert, H., Gledhill, M., Chiessi, C., Doering, K., Frank, M. Dissolved silicon isotope dynamics in large river estuaries. *Geochimica et Cosmochimica Acta*, 2020, 367-382.

Zhao, B., Yao, P., Bianchi, T. S., Shields, M. R., Cui, X., Zhang, X., Huang, X., Schröder, C., Zhao, J., Yu, Z. The Role of Reactive Iron in the Preservation of Terrestrial Organic Carbon in Estuarine Sediments. *Journal of Geophysical Research*, 2018, 123(12), 3556-3569.

Zhang, Y., Gan, Y., Li, X., Liu, Y., Yu, K., Zhang, B. Water chemical characteristics and controlling factors of the Yangtze river in the wet season. *Resources and Environment in the Yangtze*, 2016, 25(4), 645 – 654. (in Chinese with English abstract)

Zheng, H., Clift, P., Wang, P., Tada, R., Jia, j., He, M., Jourdan, F. Pre-Miocene birth of the Yangtze River. *Proceedings of the National Academy of Sciences of the United States of America*, 2013, 110(19): 7556-7561.

Zhou, X., Li, A., Jiang, F., Lu, J. Effects of grain size distribution on mineralogical and chemical compositions: a case study from size-fractional sediments of the Huanghe (Yellow River) and Changjiang (Yangtze River). *Geological Journal*, 2015, 50(4): 414-433.

Zhu, X., Zhang, R., Wu, Y., Zhu, J., Bao, D., Zhang, J. The Remobilization and Removal of Fe in Estuary—A Case Study in the Changjiang Estuary, China. *Journal of Geophysical Research*, 2018, 123(4), 2539-2553.

Zong, Y., Wang, Z., Innes, J. B., Chen, Z. Holocene environmental change and Neolithic rice agriculture in the lower Yangtze region of China: A review. *The Holocene*, 2012, 22(6), 623-635.

Table des illustrations

Figure 1 : Sketch map showing global carbon cycle. This figure is modified after Sarmiento and Gruber, (2006), Frings, (2019) and Kasting, (2019). The processes of carbon consumption are presented with green arrows, while carbon releases are presented with black arrow. The flux of carbon consumption and release are presented with red font, and data cited from Gaillardet et al., 1999a and Frings, 2019	6
Figure 2 : Global deep-sea lithium and oxygen isotope records and atmospheric CO ₂ concentration over the past 60 Myr. Modified from Zachos et al. (2001); Pagani et al. (2009) and Misra and Froelich (2012). Seawater $\delta^7\text{Li}$ were estimated from measurements in planktonic foraminifera tests, assuming no isotope fractionation during their formation.	7
Figure 3 : Current and historical sediment flux of Asia's Mega rivers originated from the Tibetan Plateau. Modified after Kuehl et al. (2020)	10
Figure 4 : Sketch map showing monsoon systems in China and the tectonic units in the Changjiang basin. The Indian Summer Monsoon (ISM) dominates climate variation in the upper Changjiang basin, while the climate changes in the mid-lower basin are subject to East Asian Summer Monsoon (EASM). The line indicating modern summer monsoon limit is drawn according to precipitation (4 mm/day isochrone)	13
Figure 5 : (A) Sketch map showing the drainage and (B) the topography in the Changjiang basin. TGD means the Three Gorges Dam	14
Figure 6 : Sketch map showing the bedrock lithology in the Changjiang basin. Modified after Yang et al. (2009).....	15
Figure 7 : Simplified maps showing the development of the Changjiang River in response to tectonic evolution in East Asia. Modified after Zheng et al. (2013). (A) the Paleo-Changjiang River flowed into the South China Sea along the paleo-Red River channel at ~32 Ma suggested by Zheng et al. (2013). (B) the modern Changjiang River formed at least since the late Pleistocene (Yang et al., 2006). JHB: Jiangnan basin; SBSYB: Subei-South Yellow Sea Basin.....	17
Figure 8 : Schematic maps showing the major sources of sediments into the East China Sea determined by different methods. (A) sediment flux (Yang et al., 2006), (B) clay minerals (He et al., 2013), (C) detrital zircon U-Pb ages (He et al., 2014), (D) petrography and heavy minerals (Vezzoli et al., 2016).	19
Figure 9 : the water discharge (black line) and sediment flux (grey bars) transported by the Changjiang River into the East China Sea recorded at Datong gauging station. The data of water discharge and sediment flux were collected from the Changjiang Water Resources Commission website: http://www.cjw.com.cn/	20
Figure 10 : (A) model results showing the relationship between denudation and chemical weathering rate and (B) the relationship between regolith thickness and chemical weathering. Denudation rate is the sum of chemical weathering rate and physical erosion rate. After Gabet and Mudd (2009).	21
Figure 11 : Calculated contribution of different reservoirs to the cationic total dissolved solid for the Changjiang mainstream. The detailed method of calculation can refer to Chetelat et al. (2008). The graph is also modified after Chetelat et al. (2008).	22
Figure 12 : CO ₂ consumption by chemical weathering of silicates and carbonates in major world rivers. The data are mostly from Gaillardet et al. (1999a). The data in the Changjiang River are from Chetelat et al. (2008). The data in the Irramady River are from Manaka et al. (2015). This graph is modified after Manaka et al. (2015).	23

Figure 13 : Schematic diagram showing the location of Li in a 2:1 type phyllosilicate. Li⁺ can be incorporated into the octahedral site or pseudo-hexagonal sites in tetrahedral sheet, or be adsorbed onto the surface, interlayer sites. This diagram is modified from Vigier et al. (2008). 25

Figure 14 : (A) the Li concentration in river water and (B) in suspended particulate matter and (C) their Li isotope compositions. Data source: Kısakürek et al., 2005; Pogge von Strandmann et al., 2006, 2010, 2017; Vigier et al., 2009; Lemarchand et al., 2010; Millot et al., 2010; Wimpenny et al., 2010b; Bagard et al., 2015; Dellinger et al., 2014, 2015; Liu et al., 2015; Pogge von Strandmann and Henderson, 2015; Wang et al., 2015; HENCHIRI et al., 2016; Manaka et al., 2017; Bastian et al., 2019; Gou et al., 2019. The river and seawater lines are from Huh et al. (1998) and Chan and Edmond, (1988), and the upper continental crust line is from Teng et al. (2004). 27

Figure 15 : Dissolved Li isotope composition corrected from the composition of the bedrock ($\delta^7\text{Li}_{\text{diss}} - \delta^7\text{Li}_{\text{rock}}$) vs. silicate weathering intensity (W/D). W represents silicate weathering rate, and D is total denudation rate. Lithium isotope data are from Huh et al. (2001), Pogge von Strandmann et al. (2006, 2010), Vigier et al. (2009), Millot et al. (2010b), Wang et al. (2015), Ma et al. (2020). This graph is modified after Dellinger et al. (2015). 29

Figure 16 : Li isotope composition of fine-grained sediments corrected from the source rock ($\Delta\delta^7\text{Li}_{\text{fine-source}}$) vs. silicate weathering intensity (W/D). Modified after Dellinger et al. (2017). 30

Figure 17 : Sketch map showing location of all samples collected for this study. SPM means suspended particulate matters, and TGD represents the Three Gorges Dam. SPM samples were collected in water column with different depths. 31

Figure 18 : A photo showing all the members involved in the KECES cruise sampling the Changjiang Estuary. 35

Figure 19 : Sedimentary facies, sedimentation rate and depositional age of core CM97. The ¹⁴C ages are shown with a black arrow on the left (Hori et al., 2001). 36

Figure 20 : photos showing the instrument used for clay fraction separation..... 37

Figure 21 : A photo showing the rotating shaker used during the exchangeable phase extraction (2×1h). 38

Figure 22 : The measured ¹⁴³Nd/¹⁴⁴Nd ratios during my PhD for the international o basaltic reference BCR-2. The black line and grey bar represent the compiled data of BCR-2, with average of 0.512635±0.000029. 40

Figure 23 : Photos showing (A) the acid attack process and (B) resin columns used for Li purification. 41

Figure 24 : Li isotope compositions ($\delta^7\text{Li}$) of 7Li-N, BE-N, CM30.6, CM10.5 and CM20.7. The 7Li-N solution were analyzed without column chemistry. These materials were used to verify the analytical accuracy..... 42

Figure 25 : (a) Schematic map showing the Changjiang drainage basin and (b) a cartoon showing the relative position of tributaries, lakes and gauging stations. Red stars display sampling sites of this study, and circles represent sampling sites for data collected from literatures (Yang et al., 2004, 2013; Ding et al., 2014; He et al., 2015). 48

Figure 26 : The influence of 1M HCl pre-treatment on river suspended matter (SPM) and bed sands K/Si (a), Na/Si (b), Ca/Si (c) and Mg/Si (d), all reported as a function of Al/Si, considered as a proxy of grain size effects related to mineral sorting during transport (Lupker et al., 2012). 52

Figure 27 : Na/Si vs. Al/Si ratios measured for river bed sands and suspended particulate matter (SPM) of the Changjiang River (mainstream). Because there is a discrepancy for Na/Si ratios between different acid pre-treatment, only data of samples without acid pre-treatment are displayed here. 53

Figure 28 : K/Si vs. Al/Si ratios measured for bank sediments and suspended particulate matter of the Changjiang River (mainstream). Sediments collected from the upper reaches (in blue) display a distinct relationship from the mid-lower reaches (in red). The black square represents the average value of the source rock of the Upper Continental Crust (Rudnick and Gao, 2003). Major element data of bank sediments, fine-grained (< 63 μm) sediments and SPM are from Yang et al. (2004, 2013), He et al. (2015) and Ding et al. (2014), respectively. 54

Figure 29 : K/Si vs. Al/Si ratios measured for bank sediments and SPM sampled from the mid-lower Changjiang River (mainstream). (a) Between the time of the TGD operation and 2014, SPM and bank sediments from the mid-lower reaches (downstream of the Dam) display a progressive depletion in K (compared to Si). (b) K/Si vs Al/Si for SPM collected in the mid-lower reaches mainstream of the Changjiang Basin (Ding et al., 2014). The statistical test for SPM collected in 2005 is insignificant, and the best-fits line is not shown. 55

Figure 30 : (a) Water discharge and sediment flux as a function of time recorded at the Datong Gauging Station, located in the lower reaches (see Fig. 25). The sediment flux significantly decreased with time since the TGD operation, but the water discharge was little affected. (b) and (c) Relative contribution of the different sources of sediments to the total load. The data of water discharge and sediment flux were collected from the CWRC website: <http://www.cjw.com.cn/>. 58

Figure 31 : The variation of K/Si vs. Al/Si of samples collected in the mid-lower reaches tributaries (a), of Core LGZ samples collected in lower mainstream and best-fit lines for simulated riverbed sediments (b). The blue and red dash lines are drawn based on Figure 27. The K/Si vs. Al/Si ratios of mid-lower riverbed sediments are simulated by Monte-Carlo method..... 60

Figure 32 : Schematic drawing showing sediment-transport pattern changes before (a) and after (b) the TGD construction, and the possible mechanism for increased weathering signal after 2003. The width of arrow represents the amount of sediment flux, i.e. the wider arrow means larger sediment flux. The dark yellow represents the sediments experiencing stronger weathering during storage in floodplain and riverbed. 63

Figure 33 : Maps showing (A) the Changjiang estuary, sampling strategy, and (B) salinity variation during the sampling period. The blue color associated with isobath in (A) refer to water depth below the modern sea-level. 70

Figure 34 : Li concentrations of (A) the dissolved load, (B) exchangeable phase, (C)residual phase. The residue represents SPM samples after NH₄Cl saturation. 73

Figure 35 : Li isotope compositions of (A) the dissolved load, (B) exchangeable phase, (C) residual phase. The analytical uncertainty on δ⁷Li (2SD=0.4‰) is smaller than the symbol size of the dissolved load and exchangeable phase. 74

Figure 36 : The linear variation of dissolved Li concentrations as a function of salinity. The dash line represents the theoretical mixing line between seawater (26.1 μmol/l) and the Changjiang water (0.8 μmol/l). The light grey area displays related analytical uncertainties, with a 10% error for Li concentrations. 75

Figure 37 : The diagram for δ⁷Li_{diss.} vs. 1/[Li]_{diss.}. The x-axis is logarithmic. The dash lines represent conservative mixing lines, and the grey area represents analytical uncertainties of 0.4‰ (2SD) for Li isotope compositions. 76

Figure 38 : (A) SPM Li/Si ratio and (B) δ⁷Li variation as a function of corresponding Al/Si ratio. The linear correlation between Li/Si and Al/Si ratios are displayed with 95% confidence interval. The orange symbols represent data of Xuliujing SPM, and blue symbols represent data of estuarine SPM. 77

Figure 39 : δ⁷Li variation as a function of Li/Al ratio. The igneous rocks and shale end-members are modified after Dellinger et al. (2014). KECES SPM define a positive trend

between sampling site C1 (lowest $\delta^7\text{Li}$ data) and high salinity C9 site. This effect is best explained by a preferential removal by decantation of low $\delta^7\text{Li}$ clay minerals (probably kaolinite).....	78
Figure 40 : (A) Li isotope variation as a function of Li/(Na+K) ratios, and (B) isotope difference between the dissolved load and exchangeable phase ($\Delta_{\text{diss.-exc.}}$) versus water salinity. The geochemical compositions of samples C8B and C9S are likely contaminated by seawater. These SPM samples were not rinsed with Milli-Q in the laboratory, and seawater might be left on the membrane during filtration.....	80
Figure 41 : Schematic map showing (A) Asian monsoon regimes, and major tectonic blocks, (B) sampling sites, drainage basin and (C) topography in the Changjiang basin. (D) The sea level changes since 14 ka in the East China sea (Hori et al., 2001) and annual sediment mass deposited in the Changjiang estuarine and coastal areas (Wang et al., 2018). (E) Downcore variation of sedimentary facies and depositional age of CM97. The detailed description about sedimentary facies can refer to Hori et al. (2001).	87
Figure 42 : (A) Li and (B) Nd isotope compositions in the sediments from the modern Changjiang River and core CM97. $\delta^7\text{Li}$ values of suspended particulate matter (SPM) are from Wang et al. (2015). The $\delta^7\text{Li}$ values of mudstone, sandstone and shale in Lake Donggi Cona, northeastern Tibetan Plateau are from Weynell et al. (2017). The light and dark grey bars reflect the average $\delta^7\text{Li}$ values for the upper continental crust (UCC) published by Teng et al. (2004) and Sauz�at et al. (2015), respectively. The Nd isotope compositions of SPM and bank samples are from Yang et al. (2007) and He et al. (2015).....	90
Figure 43 : (A) Clay ϵ_{Nd} , (B) content ratios of kaolinite to illite, (C) ϵ_{Nd} values in bulk sediments, (D) mean grain size of bulk sediment, and (E) mean sedimentation rate for the core CM97. The postglacial sea-level changes in the East China Sea are also shown. Sea-level changes and mean grain size are from Hori et al. (2001) and Bi et al. (2017). Kaolinite and illite contents are from Wang and Yang (2013). The inverted triangles represent sampling positions of molluscan shells which were used for ^{14}C dating (Hori et al., 2001). The end-member ϵ_{Nd} values of the upper Changjiang basin, the Dongting and Poyang Lakes are estimated by averaging data analyzed in this study and those published by Yang et al. (2007) and He et al. (2015).	92
Figure 44 : (A) Na/Al ratios and (B) $\delta^7\text{Li}$ values as a function of Li/Al ($\times 1000$). The element concentrations of CM97 bulk sediments and suspended particulate matter (SPM) in the Changjiang basin are cited from Bi et al. (2017) and Wang et al. (2015). The end-members of igneous rocks and shales, and the mixing line with 95% confidence interval (grey) are cited from Dellinger et al. (2014).....	94
Figure 45 : Comparison of (A and C) clay Li-Nd isotopes and (B) kaolinite/illite ratios of CM97 with the temperature and rainfall records in the Changjiang basin. (D) Chironomid-inferred mean July temperature in Tiancai Lake, southeastern margin of the Tibetan Plateau (Zhang et al., 2017a). (E) Temperature reconstructed by branched fatty alcohol ratio (BNA ₁₅) in Dajiuhu peatland (Huang et al., 2013). (F) Grain size (<16 μm) fraction of lacustrine sediments in TCQH (Zhang et al., 2017b), indicating rainfall variation in the upper basin. (G) Mass accumulation of aerobic hopanoids in Dajiuhu peatland, reflecting rainfall variation in the middle Changjiang basin (Xie et al., 2013).	97
Figure 46 : Schematic map showing sampling sites that could be of interest in the near future.	104

Table des tableaux

Table 1: Basic information for the river bank samples collected and analyzed in this study ..	32
Table 2: Basic information corresponding to the suspended particulate matters (SPM) collected along depth profiles at the Xuliujing station.....	33
Table 3: Basic information of suspended particulate matters and water samples collected in the Changjiang Estuary	34
Table 4: parameters used to calculate velocity of particle deposition.....	37
Table 5: Major element concentrations of rock reference materials	39
Table 6: Major element concentrations of rock reference materials	41
Table 7: Water discharge and sediment flux for each end-member. The data were collected from the Changjiang Water Resources Commission website: http://www.cjw.com.cn/	57
Table 8: Parameters (Al/Si, K/Si and sediment flux proportion deduced from monitored fluxes and hydrological data) for each end-member used in the Monte-Carlo simulations	61
Table 9: The total dissolved K flux into the sea of the Changjiang (Yangtze) River	65
Table 10: Mineral compositions of SPM samples in the Changjiang Estuary.....	72

Résumé :

Au cours de ce travail, j'ai réalisé une série d'études dans le bassin du Changjiang (Yangtze), afin de mieux comprendre l'influence de ces effets.

Tout d'abord, l'exploitation du barrage des Trois Gorges (TGD) a modifié la composition géochimique des sédiments en aval. Depuis 2003, les sédiments venant des hauts bassins ont été en grande partie retenus en amont, tandis que les sédiments précédemment déposés dans le bassin moyen-inférieur ont été progressivement remis en suspension. Ces processus expliquent l'évolution géochimique des sédiments exportés vers la mer de Chine.

En deuxième partie, une étude systématique démontre que les compositions isotopiques en lithium des phases dissoutes et particulaires se comportent de façon conservative dans la zone de mélange de l'estuaire du Changjiang. Cependant, les phases échangeables ne représentent qu'une faible quantité de Li, ce qui explique son impact négligeable dans cette zone.

Troisièmement, Cette étude confirme que dans les grands bassins versants, l'altération chimique peut réagir rapidement à de grandes amplitudes climatiques. Ceci est particulièrement bien illustré, dans la carotte CM97, par la période du Younger Dryas. Depuis 2 000 ans, les $\delta^7\text{Li}$ des argiles s'accroissent clairement par rapport à la période précédente, à cause de l'érosion des sols de plaines induite par l'homme.

En résumé, ces résultats apportent de nouveaux éclairages sur l'interprétation des proxys et sur la réponse de l'altération chimique aux variations climatiques, ce qui est essentiel pour mieux quantifier l'impact de l'altération continentale sur les climats passés et futurs de notre planète.

Mots clés : altération chimique; barrage des Trois Gorges; le bassin du Changjiang (Yangtze); Isotopes Li et Nd; les fractions argileuses; Activités anthropiques; Processus estuaire

[Li isotope study of Yangtze River sediments: new constraints on climate, weathering and carbon cycle relationships]

Abstract :

In order to better understand the weathering-climate feedback, a series of studies was carried out in the Changjiang (Yangtze) Basin.

First, the operation of the Three Gorges Dam (TGD) changed downstream sediment geochemical compositions. Before 2003, large amounts of upstream-derived sediments deposited and experienced further weathering in the mid-lower basin. Since 2003, strong riverbed sediment resuspension changed the roles of the mid-lower reaches from important sinks to major sources of sediments delivered to the sea. As a consequence, an intensified weathering intensity of downstream sediment was observed.

Second, dissolved $\delta^7\text{Li}$ exhibit a conservative behavior in the Changjiang Estuary. During the process of SPM transported offshore, weathering product flocculated and deposited, while primary minerals resuspended. The combined effect resulted in the UCC-like SPM $\delta^7\text{Li}$ values. There is a Li isotope fractionation between the dissolved load and exchangeable phase. However, this process shows negligible impact on $\delta^7\text{Li}$ of dissolved load and particulates.

Third, weathering response to climate is complex in large river basins. During the Younger Dryas, the positive excursion of clay $\delta^7\text{Li}$ is consistent with enhanced incongruent weathering, in response to temperature cooling. The minor variation of clay $\delta^7\text{Li}$ at 11 – 2 ka likely indicate stable weathering and mild climate variation. Over the last 2 kyr, the fluctuation of clay $\delta^7\text{Li}$ is mostly caused by intensification of human activities.

In summary, this thesis sheds new lights on the weathering-climate feedback over geologic past, and provides perspectives on how human activities affect natural processes.

Keywords: Continental weathering; Three Gorges Dam; Changjiang (Yangtze River); Li and Nd isotopes; Clay; Paleoclimate; Anthropogenic activities; Estuary process

Chengfan Yang

Ph.D. Candidate, born in 1991, China

School of Ocean and Earth Science
Siping Road 1239, Tongji University
Shanghai 200092, P. R. China

Education Background

- ✧ 2017.11 – present
Joint Ph.D. student, **CNRS, Sorbonne University**, Villefranche-sur-Mer, France
- ✧ 2015.09 – present
Ph.D. candidate in Marine Science, **Tongji University**, Shanghai, China
- ✧ 2012.09 – 2015.03
M.S. in Quaternary Geology, **Tongji University**, Shanghai, China
- ✧ 2008.09 – 2012.07
B.S. in Geology, **Ocean University of China**, Qingdao, China

Publications during my Ph.D.

1. Li, C., Lian, E., **Yang, C.**, Deng, K., Qian, P., Xiao, S., Liu, Z., Yang, S. 2020. Seasonal variability of stable isotopes in the Changjiang (Yangtze) river water and its implications for natural climate and anthropogenic impacts. *Environmental Sciences Europe*, 32(1), 1-13.
2. **Yang, C.**, Yang, S., Song, J., Vigier, N. 2019. Progressive evolution of the Changjiang (Yangtze River) sediment weathering intensity since the Three Gorges Dam Operation. *Journal of Geophysical Research: Earth Surface*, 124, 2402–2416.
3. **Yang, C.**, Yang, S., Gou, L., Wang, X., Li, Y. 2018. Lithium Isotopes for Tracing the Supergene Weathering and Environmental Evolution: Review and Prospective. 37 (5), 841–851. (in Chinese with English abstract)
4. **Yang, C.**, Yang, S., Su, N. 2017. The hydrogen and oxygen isotopic compositions of hydroxyl in clay mineral from a weathering profile: New proxies for paleo-climate change? *Acta Geochimica*, 36(3), 370–373.
5. **Yang, C.**, Yang, S., Su, N. 2016. Stable hydrogen and oxygen isotopes in mineral-bound water and the indication for chemical weathering intensity. *Chemical Geology*, 441, 14–23.
6. **Yang, C.**, Yang, S., 2016. Using vacuum extraction-isotopic analysis technology to study hydrogen and oxygen isotopic compositions of water extracted from weathering profile sediments. *Rock and Mineral Analysis*, 35(1), 69–74. (in Chinese with English abstract)
7. Lian, E., Yang, S., Wu, H., **Yang, C.**, Li, C., Liu, J. 2016. Kuroshio subsurface water feeds the

wintertime Taiwan Warm Current on the inner East China Sea shelf. *Journal of Geophysical Research: Oceans*, 121(7), 4790–4803.

8. Li, C., Yang, S., Lian, E., **Yang, C.**, Deng, K., 2016. Damming effect on the Changjiang (Yangtze River) river water cycle based on stable hydrogen and oxygen isotopic records. *Journal of Geochemical Exploration*. 165: 125–133.
9. Deng, K., Yang, S., Lian, E., Li, C., **Yang, C.**, Wei, H., 2016. Three Gorges Dam alters the Changjiang (Yangtze) river water cycle in the dry seasons: evidence from H-O isotopes. *Science of The Total Environment*, 562, 89–97.
10. Su, N., Yang, S., Wang, X., Bi, L., **Yang, C.** 2015. Magnetic parameters indicate the intensity of chemical weathering developed on igneous rocks in China. *Catena*, 133, 328–341.

Patent

1. **Yang, C.**, Yang, S.Y., 2015. A vacuum instrument for sediment-water extraction (Patent number: ZL 201520491077.3, in Chinese)

Paper under review or in preparation

1. **Yang, C.**, Vigier, N., Yang, S., Revel, M., Bi, L. 2020. Clay Li and Nd isotope response to hydroclimate variations in the Changjiang basin over the past 14,000 years. (under review)
2. **Yang, C.**, Yang, S., Vigier, N., Lian, E., Lai, Z. 2020. Behavior of Li isotopes along a 2D transect in the Changjiang (Yangtze) Estuary. (in preparation)

Scholarship/Honor during my Ph.D.

1. 2017, supported by China Scholarship Council for two-years study in France
2. 2016, Excellent Doctor Scholarship, Tongji University
3. 2016, travel fee covered by the 26th Goldschmidt Conference Committee

Conference Participation during my Ph.D.

1. The 29th Goldschmidt Conference, August 17-August 24, 2019, Barcelona, Spain (**Poster**)
2. The 9th International Conference on Asian Marine Geology, October 10-October 12, 2018, Shanghai, China (**Poster**)
3. The 11th International Symposium on Geochemistry of the Earth's Surface, June 11-16, 2017, Guiyang, China (**Poster**)
4. The 16th annual seminar of China mineral rock geochemical society, April 18-21, 2017, Xi'an, China (**Poster**)
5. The 3rd Asian Clay Conference, November 17-20, 2016, Guangzhou, China (**Poster**)
6. The 4th Conference on Earth System Science, July 3-5, 2016, Shanghai, China (**Poster**)
7. The 26th Goldschmidt Conference, June 26-1 July, 2016, Yokohama, Japan (**Poster**)
8. Thirtieth anniversary of the founding of isotope geology professional committee, academic seminars and isotope geology application results, October 18-21, 2015, Ningbo, China (**Abstract**)

Field Work during my Ph.D.

- 2019.9, Summer cruise, Key Elements Cycling in the Changjiang-Estuary-Shelf Transect (KECES)
- 2016.3, Winter cruise. East China Sea inner-shelf mud wedge

YANG Chengfan – Thèse de doctorat - 2020

2016.1, Weathering profile sampling, Fujian Province

2015.8, Summer cruise, East China Sea inner-shelf